Hydrogel-Based Intranasal Drug Delivery Platforms

ENGINEERING STARCH NANOPARTICLE/CHITOSAN EMULSION-TEMPLATED NANOGELS AND IN SITU-GELLING HYDROGELS FOR THE INTRANASAL DELIVERY OF ANTI-PSYCHOTIC MEDICATION

By ALI BABAR, H.B.SC.

A Thesis Submitted to the School of Graduate Studies in Partial Fulfillment of the Requirements for the Degree of Master of Applied Science

MASTER OF APPLIED SCIENCE (2019)

School of Biomedical Engineering

McMaster University

Hamilton, Ontario, Canada

TITLE: Engineering Starch Nanoparticle/Chitosan Emulsion-Templated Nanogels and In Situ-Gelling Hydrogels for the Intranasal Delivery of Anti-psychotic Medication

AUTHOR: Ali Babar, H.B.Sc. (McMaster University)

SUPERVISOR: Dr. Todd Hoare

NUMBER of PAGES: 109

Abstract

Current strategies for oral or injectable antipsychotic drug delivery typically demonstrate low bioavailability to targeted brain regions, incentivizing the development of novel delivery strategies. Delivery via the nasal cavity circumvents multiple barriers to the reaching the brain: the blood-brain barrier, first-pass metabolism and gut degradation, but requires specific drug-carrier characteristics (e.g. pH, mucoadhesion) to be effective. Employing the use of nanoparticle drug carriers (~50nm in size) within this route can further improve efficacy, due to their enhanced tissue penetration abilities. Although existing intranasal delivery platforms have demonstrated great therapeutic value, there is a lack of controlled release features–an extremely valuable addition to this pathway.

Described in this thesis are biodegradable bulk hydrogels consisting of oxidized starch nanoparticles (SNPs) and carboxymethyl-chitosan (CMC) which allow for both intranasal mucosal adherence and functional controlled release of anti-psychotic drug (PAOPA) in an MK-801 pre-clinical model of schizophrenia. Results indicate that PAOPA-loaded SNP-CMC in-situ gelled hydrogels provide a sustained released profile such that they alleviate negative symptoms associated with schizophrenia (decreased social interaction time) for up to 72 hours at a decreased dosage (0.5mg/kg) when compared to acute symptom alleviation at a higher (1mg/kg) intra-peritoneal drug dosage. Also described is the formulation of nanoemulsion templated nanogels (~200nm) for eventual intranasal delivery applications. Nanogels (also consisting of SNP-CMC) demonstrated relevant degradation profiles resulting in SNP release, which may be employed for future tissue penetration applications within the nasal cavity. It is

anticipated the bulk hydrogel platform (and nanogel system, once further studied) will lower required drug doses and ultimately improve clinical outcomes in treating mental illness.

Acknowledgements

I would like to thank Dr. Todd Hoare for his constant support, encouragement, knowledge and guidance over the past two years. It was challenging to switch into the engineering department, however Dr. Hoare provided with me all the necessary resources to make my transition as smooth as possible. Dr. Mishra, thank you for all of your advice and honest opinions, I'm extremely grateful to have collaborated with you in the Psychiatry department. To Ashley, Judy and Brendan in the Mishra Lab, thank you for your constant knowledge impartment. A huge thank you to Michael Majcher, without whom this project would not have been possible. Thank you to both the Biomedical Engineering and Chemical Engineering departments for welcoming and supporting me through my time as a master's student. I would also like to thank Sarrah Lal, for giving me an opportunity to explore the healthcare commercialization realm.

To the members of the Hoare Lab, I could not have asked for a more diverse and encouraging group to spend my time with while navigating the research world. A special thank you to Ali A, Jon, Matt, Mitch, Kiki Yeetman, Maddi, Nicola, Eva, Nicole, Xiaoyun, Sophie and Richard, for all of your friendships, love and advice.

To my family, my parents and my sister, thank you for your constant support and endless positivity in my tenure as a graduate student. To the friends I have not named, you know your support was key in making this thesis a success.

Contents

List of Figures & Tables

List of Abbreviations & Symbols

aCSF	Aritificial cerebrospinal fluid
APD	Anti-psychotic drug
ATR-FTIR	Attenuated Total Reflectance Fourier Transform Infrared
BBB	Blood-brain barrier
°C	Degrees Celsius
CMC	Carboxymethyl Chitosan
DLS	Dynamic Light Scattering
DOPA	Dihydroxyphenylalanine
F-SNP-CHO	Aldehyde functionalized SNPs labelled with Alexaflour
HLB	Hydrophobicity lipophilicity
IN	Intranasal
IP	Intraperitoneal
MK-801	Dizocilpine (+)-MK 801 maleate
MQW	MilliQ water
NC	Nanocluster
nm	Nanometers

NTA	Nanosight Tracking Analysis
O/W	Oil-in-water
PAOPA	((3R)-2-Oxo-3-[[(2S)-2-PyrrolidinylcarbonylRamino]-1-pyrrolidineacetamide])
PBS	Phosphate buffered saline
PMMA	Poly(methyl methacrylate)
SNP	Starch nanoparticle
SNP-CHO	Starch nanoparticle with aldehyde functionality
TEM	Transmission Electron Microscopy
UV	Ultraviolet
W/O	Water-in-oil
Wt%	Weight percent
W/v%	Weight by volume percent

Declaration of Academic Achievement

The majority of the work described herein was conceived, conducted, analyzed and written by the author of this thesis, in consultation with Dr. Todd Hoare, with the following exception:

Chapter 2: Michael Majcher completed SNP-CHO functionalization optimization, as well as all associated characterization of said functionality. Ashlyn Leung assisted with hydrogel characterization and *in vitro* assays.

1. Introduction

1.1 Mental Health & Illness

“No health without mental health”, a statement endorsed at the World Health Organization (WHO) European Ministerial Conference in 2005 [1], accurately summarizes the importance of urgent and meaningful efforts towards mental health care. An estimated 7.4% of the world’s measurable burden of disease can be attributed to mental illness, with the impact on the surrounding communities greatly exceeding that value albeit impossible to accurately measure [1, 2]. Most mental disorders contribute to significant losses in quality of life and general functioning. Individuals suffering from different disorders may be physically incapacitated, deal with emotional instability, experience intense sensory overload, have severely altered behaviour, or any combination of these. Such hindrances introduced into patients’ lives often prevent them from participating in basic life activities such as maintaining healthy relationships, holding a job, or dealing with adversity on a daily basis. Lack of stable functioning can also ultimately affect societies and established workforces [3], negatively contributing to the well-being of all individuals. As a result, there is immense value in expanding treatment options and streamlining efforts towards initiatives to alleviate some of these burdens for both individuals affected by mental illness and the surrounding community.

1.2 Schizophrenia

As one of the more severe mental illnesses, schizophrenia is a primary target for the development of more efficient therapeutic delivery systems. The disease itself is characterized by a range of symptoms including delusions, hallucinations, social withdrawal, disorganized speech and disorganized behaviour and affects approximately

1% of the world's population [4]. Despite this relative rarity compared to other major diseases like cancer or heart disease, schizophrenia is the fifth leading cause of years lost to disability for men and sixth for women, emphasizing the necessity for improving clinical interventions [5]. Individuals affected by schizophrenia live with a severely decreased quality of life and often feel like they have "lost contact with reality", an extremely disorienting and distressing experience. Without proper intervention and support, an individual may develop depression that can in turn promote suicidal thoughts and tendencies. The burden is significant not only for patients, but also for caregivers and the larger community as a whole, with the economic weight of schizophrenia exceeding $60 billion USD annually in the US [6]. According to the WHO, the direct costs of schizophrenia in Western countries range from 1.6-2.6% of total healthcare expenditures [6]. Coupled with this financial stress is the social burden placed on communities, which struggle to provide meaningful support to those members affected by schizophrenia. As a result, it is necessary to continue in efforts towards finding effective treatments to help alleviate the burdens placed on those dealing with schizophrenia and the surrounding community.

1.2.1 - Symptomatology & Diagnosis

Providing effective treatment of schizophrenia requires an adequate understanding of the underlying symptomatology, which can be broken down into three main categories: positive symptoms, negative symptoms and cognitive dysfunction [7, 8].

Positive symptoms include behaviours which are present in individuals with schizophrenia but lacking in healthy populations. They are often a result of excess stimulation or sensory disruption and include delusions, hallucinations, disorganized

thought and disorganized behaviour [9]. Negative symptoms are behaviours lacking in those affected by schizophrenia but are normally present in healthy populations, including reduced motivation, loss of interest, social withdrawal, and reduced emotional expression [9]. These symptoms also tend to persist longer than positive symptoms, largely disrupting an individual's day-to-day activities.

Cognitive dysfunction resulting from schizophrenia includes the lack of ability to pay attention, poor memory retention, and difficulties in interpreting environments, making accurate judgements, processing information, engaging in meaningful social interactions, and self-expressing through language [10]. It is hypothesized this dysfunction is a result of hypoactivity in the cortex [11], where a few different neurotransmission pathways may be implicated. Decreased gamma-amino butyric acid (GABA) levels in the dorsolateral prefrontal cortex are theorized to impair pyramidal cell synchronization and contribute to deficits in working memory. Within the cholinergic system (where neurons innervate structures implicated in negative schizophrenic symptoms), reductions in alpha7 receptor levels in the prefrontal cortex may result in decreases in attention. M1 muscarinic receptor depletion in cortical areas has also been correlated with cognitive function impairment in verbal and working memory [11]. Unfortunately, no rigorous method of diagnosis exists for schizophrenia given that there is no one specific cause. Typically, a diagnosis is made by a clinician in partnership with psychologists and psychiatrists by examining a range of acquired patient data. There are no biological markers to pinpoint onset of the disease; however, some common physical characteristics such as an increase in ventrical size, an increase in striatal

dopamine storage and release, and a decrease in temporal lobe volume are observed across most schizophrenia patients [11].

1.2.2 - Epidemiology & Prognosis

Although schizophrenia affects both men and women, men are 40% more likely to develop the disease while also being more likely to be diagnosed earlier in life. Age of onset ranges between 18-25 for men and between 25-35 for women, with some supporting evidence that the prognosis for men is also worse [12]. Generally speaking, the disease progresses through three main phases: prodromal (beginning), active (acute) and residual (recovery), which then repeat sequentially in cycles throughout the duration of illness with varying lengths depending on the individual [9].

The prodromal phase is characterized by lack of interest in usual activities as well as social withdrawal from members close to the individual. Patients may start perceiving the world with abnormal views, have difficulty focusing, begin to seclude themselves, and obsess over specific topics or individuals (ex. historic figures, celebrities). The active phase presents psychotic symptoms, typically including hallucinations, delusions, and uncontrolled thoughts or feelings. In the residual phase, individuals may begin to regain control over their thoughts and behaviours and can conceptualize the illness affecting them.

1.3 Antipsychotic Medication

1.3.1 - Dopamine Pathways & the Dopamine Hypothesis

Dopamine is an organic catecholamine neurotransmitter that has several functions within the body [13]. Its primary role is to serve as a signalling molecule for multiple pathways that modulate memory, emotion, movement, and the reward system. Outside of the nervous system, it plays a role in cardiovascular function modulation, hormone secretion, vascular tone, gastrointestinal motility, and renal function [14]. The most common method of dopamine synthesis within the brain (and the adrenal grand) uses the amino acid tyrosine as the starting material, using tyrosine hydroxylase to convert tyrosine into dihydroxyphenylalanine (DOPA) and then further into dopamine by DOPA decarboxylase [15]. Dopamine is then stored in synaptic vesicles using vesicular monoamine transporter (VMAT). Upon release, dopamine has the ability to act on 5 postsynaptic receptors (D1-D5) [16].

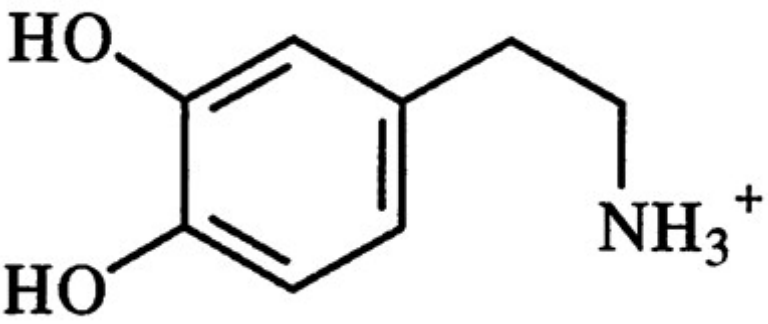

Figure 1-1.Chemical structure of dopamine.

Dopamine deficiency can be implicated in the development of Parkinson's disease, a degenerative motor condition; however, altered dopamine levels are also suspected to

correlate with the onset of schizophrenic symptoms [17]. The dopamine hypothesis of schizophrenia postulates that hyperactive dopamine transmission results in schizophrenic symptoms [13]. This hypothesis dates back to the 1960's, when use of amphetamine to increase dopamine levels was demonstrated to result in psychotic symptomatology while the use of reserpine (an adrenergic uptake inhibitor) to deplete dopamine levels alleviated these symptoms [18].

An understanding of the biochemistry related to the dopamine hypothesis requires comprehension of dopamine transmission pathways in the brain. Within the brain there are four major neuronal pathways relevant to dopamine neurotransmission: mesolimbic (positive symptoms), mesocortical (negative symptoms), nigrostriatal (extrapyramidal symptoms) and tuberoinfundibular (TI) [13, 19]. The mesolimbic pathway projects from the ventral tegmental area (VTA) to the nucleus accumbens (NAc) in the limbic system and is thought to provide key contributions in emotional regulation, motivation, and the reward system. Hyperactivity of dopamine in this pathway has also been shown to contribute to positive symptomatology in schizophrenia [15]. The mesocortical pathway projects from the VTA to the prefrontal cortex, where the dorsolateral component regulates cognitive and executive functioning and the ventromedial component regulates emotions and affect [15, 19]. Hypoactivity of dopamine in this pathway is theorized to contribute to the negative symptoms of schizophrenia along with depression [8, 19]. The nigrostriatal pathway projects from dopaminergic neurons in the substantia nigra (SN) to the basal ganglia, where this pathway mediates motor movements. Here, D2 receptor inhibition may contribute to Parkinsonian symptoms and dystonia, with sustained D2 blockages in the SN can lead to tardive dyskinesia. Lastly,

the tuberoinfundibular pathway projects from the hypothalamus to the anterior pituitary, where D2 receptor blockage has been implicated in sexual dysfunction. A combination of these 4 pathways results in the complex symptomatology presented in schizophrenia, explaining the difficulties that exist in identifying a universally-effective medical treatment. However, the dopamine hypothesis is not without its limitations; in particular, there are varying opinions on whether dopamine level elevation or depletion provides the most effective negative symptom alleviation [20]. Recent research also suggests that approximately one third of individuals fail to respond to commonly prescribed antipsychotic drugs (see section 1.3.2) likely on the basis of their symptomatology failing to be solely explained by dysfunction of dopaminergic pathways. Thus, while action on dopamine pathways is an imperfect target to address all aspects of schizophrenic symptoms, it remains a leading and useful target for suppressing the symptoms of schizophrenia.

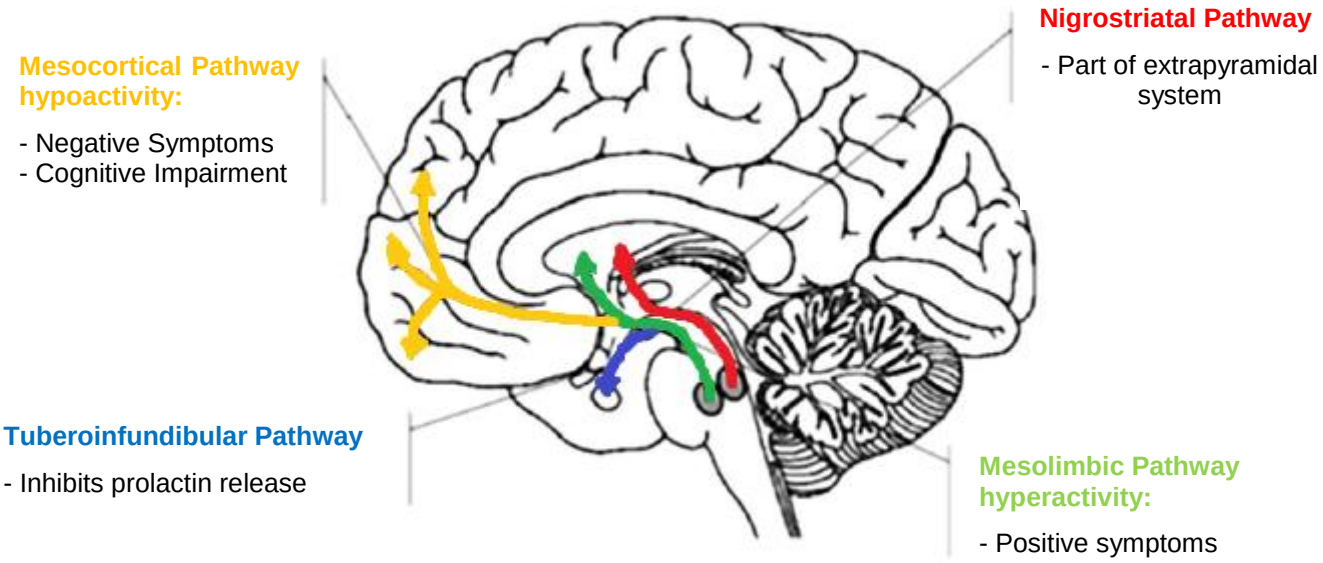

Figure 1-2. Major neuronal pathways for dopamine in the brain. There are four pathways relevant to dopamine transmission in the brain: (1) mesolimbic; (2) mesocortical; (3) nigrostriatal; and (4) tuberoinfundibular. Adapted from Yong et al., (2015).

1.3.2 - APD Functionality

Although schizophrenia lacks a precise cure, antipsychotic drugs (APDs) serve as the first line of defence in combating symptoms and are often used in conjunction with other medication such as mood stabilizers and antidepressants [9]. APDs help relieve the debilitating symptomatology of schizophrenia, leading to overall improvement in quality of life despite not directly tackling the underlying causes of the disease. Most APDs function as dopamine D2 receptor antagonists, competing with endogenous dopamine with the goal of dopamine reduction in the mesolimbic tract or, more specifically, the striatum [21-23].

APDs may be separated into three categories: first generation (typical), second generation (atypical), and third generation (atypical). Some first generation APDs commonly used include haloperidol, loxapine, chlorpromazine and perphenazine [24]. The primary method of action of these hydrophobic APDs involves exclusive interaction with dopamine D2 receptors, competing with dopamine as antagonists [25]. However, while often effective in treating positive symptoms of schizophrenia, typical APDs fail to relieve negative symptoms (ex. social withdrawal) and cognitive dysfunction. Second generation APDs include clozapine, olanzapine, risperidone, lurasidone, and ziprasidone, among others [26]. This generation of APDs focuses on targeting the negative symptoms of schizophrenia, with the initially developed wave of drugs acting on dopamine D2 receptors and serotonin 5-HT_{2A}antagonistically and the second wave acting on D2/D3 receptors with non-specific binding capacities [27]. The second wave is considered more efficacious in modulating negative and cognitive dysfunction because of their broad binding spectrum [28]. The latest atypical APDs belong to the third generation, with the leading drug aripiprazole functioning as a partial D2 agonist. It is considered a “dopamine stabilizer” due to this property, as it may compete with dopamine in high concentration environments as an antagonist, or conversely supply dopamine signalling via receptor binding in dopamine deficient environments [28] .

1.3.3 - Side Effects & Limitations

APDs have several side effects that have stimulated the continued development of next-generation medication. The use of first generation APDs can cause the appearance of cognitive impairment and extrapyramidal symptoms such as movement disorders similar to Parkinson's symptomatology [29], thus reducing patient adherence. Chronic use of typical APDs may produce tardive dyskinesia, which is characterized by involuntary repetitive moments stimulated by D2 receptor blockage in the nigrostriatal pathway. Second generation APDs have been shown to introduce serious metabolic side effects including weight gain, elevated cholesterol, changes in glucose utilization, and sedation [30], all of which can lead to a predisposition for cardiovascular disease and type 2 diabetes mellitus [30]. The third generation drug aripiprazole has also been implicated in minor weight gain and some movement disorder induction, although maintaining a significantly lower incidence rate of both side-effects compared to first and second generation APDs [31].

1.3.4 - Allosteric Modulators

Traditionally, drugs are designed for direct binding to the primary active sites (orthosteric sites) from which a therapeutic chemical cascade begins. However, a secondary class of drugs, allosteric modulators, has gained great traction in medical practice for their altered mechanism of action. Allosteric modulators are ligands which bind to receptors on a biological target that are separate from orthosteric sites, also known as allosteric (regulatory) sites [32]. Once bound, they induce conformational changes to target active sites (ex. proteins), which then affects further binding of orthosteric ligands and overall site activity [33]. Such agents may act as either positive

allosteric modulators (PAMs), which enhance the binding affinity of ligands to active sites and further increase active site signals, or negative allosteric modulators (NAMs), which inhibit ligand binding to active sites and decrease signalling [34]. Allosteric modulators have high specificity for target sites and do not compete with endogenous ligands, adding to their therapeutic value. That being said, the effects allosteric modulators produce also have an upper limit as they are able to saturate their own binding sites, thus resulting in a finite effect [35]. As a result, higher allosteric modulator doses are more tolerable, de-risking the prescription process and offering alternative medication to orthosteric compounds [32]. These characteristics combined make allosteric modulators valuable treatment tools for complicated mental illnesses.

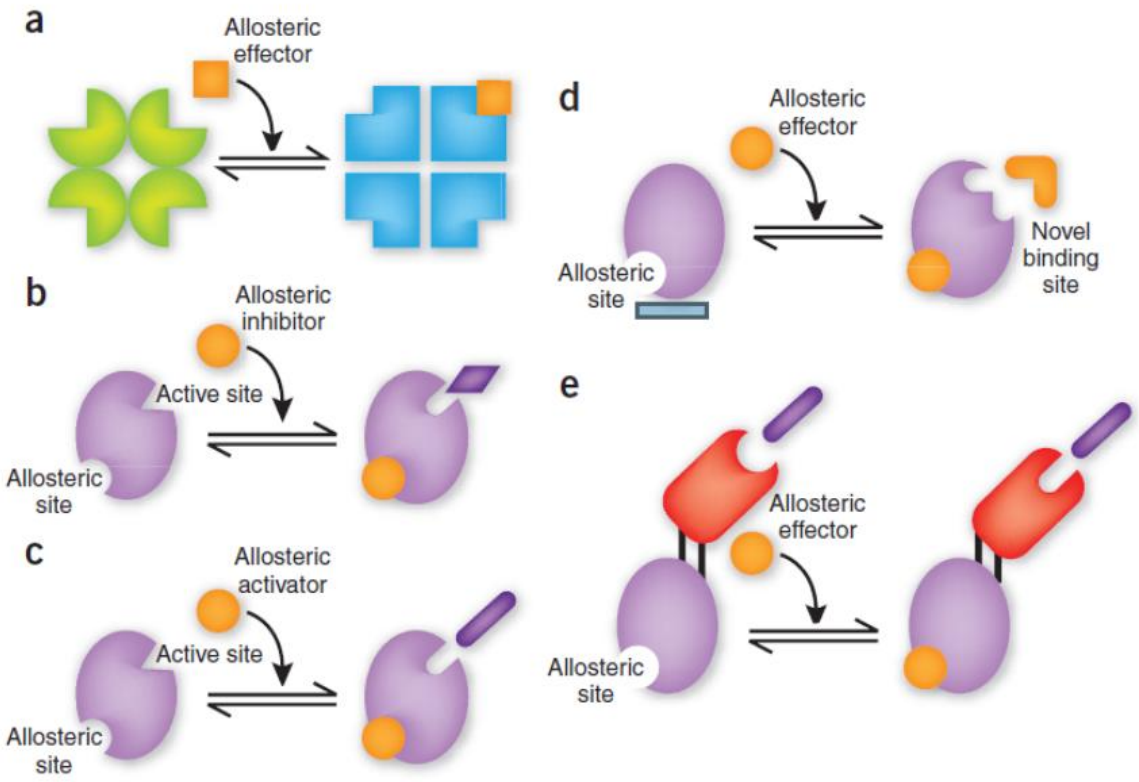

Figure 1-3. Different modes of allosteric modulation. (a) Cooperativity: a symmetric, multi-unit protein can exist in one of two different conformational states, active and inactive; (b) Monomeric allosteric inhibition: an allosteric inhibitor decreases active site binding; (c) Monomeric allosteric activation: an allosteric effector increases active site binding affinity; (d) Active site formation via allosteric effector: binding of an effector may introduce a new binding site to the complex, which upon ligand binding could change active site geometry; (e) Enzyme-protein fusion: an allosteric effector controls enzyme activity. Adapted from Goodey et al., (2008).

1.4 PAOPA for Schizophrenia Treatment

Of particular interest for schizophrenia treatment is the precursor drug prolyl-leucyl-glycinamide (PLG), a tripeptide cleaved from the dopamine allosteric modulator oxytocin that has demonstrated therapeutic value in pre-clinical studies involving major depressive disorder [36]. Derived from PLG is a promising potent analogue, 3(R)-[(2(S)-

pyrrolidinylcarbonyl) amino]-2-oxo-1-pyrrolidineacetamide also known as PAOPA (Fig. 1-4), which provides positive allosteric modulation of dopamine D2 receptors without inducing an effect on antagonist binding [37]. This method of action may allow for symptom alleviation of biochemical and behavioural abnormalities that result in positive and negative symptoms of schizophrenia. In particular, there is evidence that PAOPA therapy increases dopaminergic sensitivity in the nigrostriatal pathway, potentially preventing induced extrapyrimidial symptoms such as movement disorders [38, 39]. PAOPA has also been previously demonstrated to prevent and reverse and negative behavioural symptoms, particularly social withdrawal [40]. Although the exact physiological mechanism which by PAOPA is able to attenuate social interaction deficits is yet to be fully elucidated, a host of literature provides strength for this claim [40, 41].

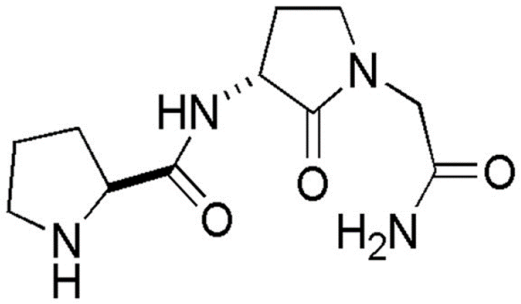

Figure 1-4. Chemical structure for PAOPA.

1.5 Intranasal Drug Delivery

Traditional methods of APD delivery include oral administration or intraperitoneal (IP) injections. However, these traditional methods are limited by several complicating factors. First, orally ingested medication is challenged by “first pass” metabolism which

sequesters and degrades a large amount of drug [42]. Although this effect may occur in various tissues, the liver is primarily responsible for most drug absorption [43]. When drugs are absorbed in the gastrointestinal (GI) tract, they are shuttled to the liver via the hepatic portal vein and then subsequently metabolized by enzymes. As a result, the majority of the active drug components fails to exit the liver and reach systemic circulation [44]. Second, there is growing evidence supporting the interference and modulation of drug efficacy due to the gut microbiome, as gut bacteria may break down or inhibit active drug constituents and thus limit the quantity of (active) drug reaching systematic circulation [45]. Third, and most challenging in terms of obstacles to oral delivery, is the blood-brain barrier (BBB), a highly selective barrier that excludes a majority of molecules (~98%) from the central nervous system (CNS) [46]. The BBB is composed of endothelial cells that form a wall of capillaries [47], tight junctions, an enzymatic surveillance system, and complicated structures made of pericytes and astrocytes [46]. These barriers limit the BBB penetration of most large or polar molecules, allowing only small non-polar molecules (e.g. hormones) through [47]. The combination of the aforementioned complicating factors associated with traditional delivery methods results in extremely low bioavailability of most APDs, with only ~5% of administered drug dosages typically reaching the brain [48]. Lowered bioavailability forces the use of higher drug doses that are not only costly but run the risk of increasing severe side effects.

Intranasal (IN) delivery provides an alternative non-invasive route of APD administration that is increasingly attracting interest in terms of minimizing side-effects and dosages of schizophrenia drug therapies. Relative to oral or IP delivery, IN administration offers a

more direct pathway to the brain through the olfactory and/or trigeminal nerves. It is important to note that IN delivery is a combination of several pathways which assist in CNS targeting. Drugs may be transported via neuronal connections through either intracellular or extracellular pathways [49]. The intracellular pathway allows for endocytosis of drugs into terminal regions of the olfactory and trigeminal axons located in the nasal cavity followed by transport into the brain (bypassing the BBB) via the nervous tissue; the extracellular pathway facilitates drug transport alongside olfactory or trigeminal nerves by general bulk flow processes [49]. Other pathways shuttle drugs through supporting cells and tight junctions, also bypassing the BBB. The net consequence of these different delivery pathways is that drugs administered into the nasal cavity are readily absorbed directly into systemic circulation, thus circumventing first pass hepatic metabolism, gut microbiome degradation, and even the BBB. This allows for increases in bioavailability, quicker therapeutic effects, and decreased dosages while maintaining drug efficacy. Ease of nasal cavity access also allows for straightforward IN drug administration in easy-to-handle dosage forms such as nasal drips or sprays [50].

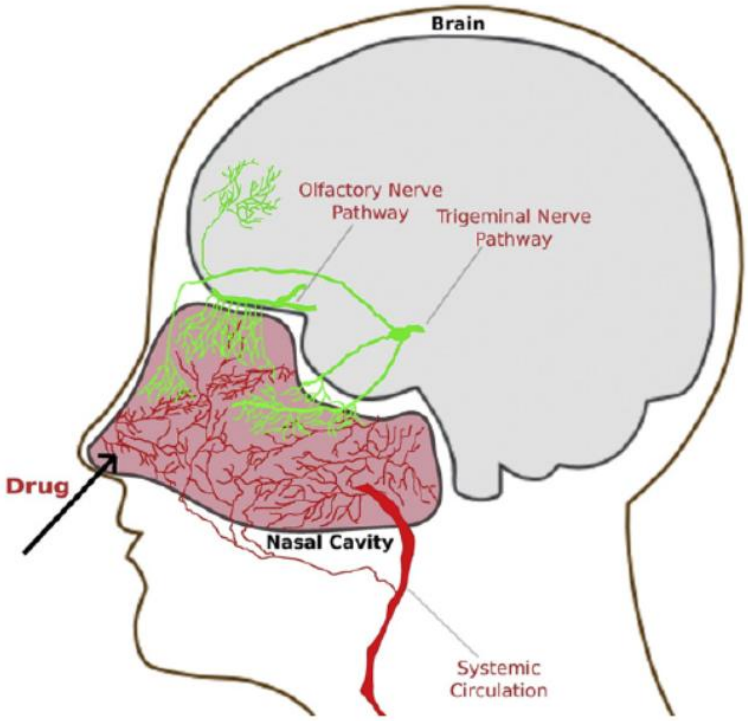

Figure 1-5. The different pathways for intranasal drug transport to the brain and systemic circulation. Nerve endings are depicted in green. Adapted from Katare *et al*., (2016).

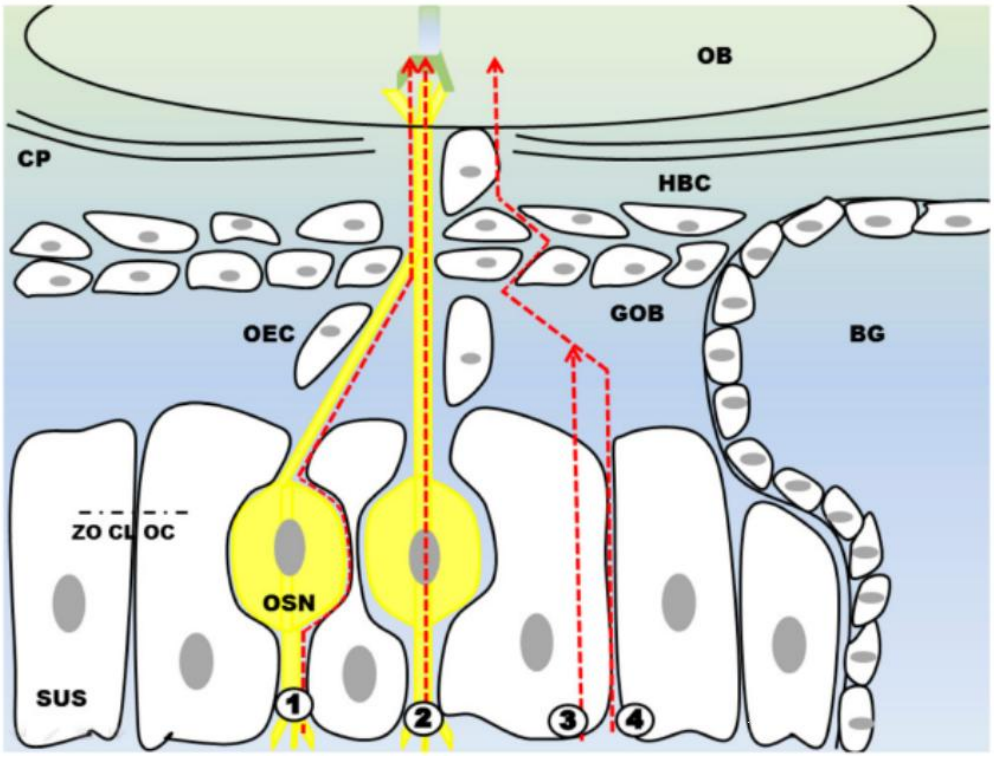

Figure 1-6. Four different pathways for intranasal delivery through the BBB. (1) The extracellular pathway: bulk flow processes alongside the olfactory sensory neuron (OSN) or trigeminal nerve (not pictured). (2) The intracellular pathway: drugs are endocytosed and travel to the CNS through the cell body. (3, 4) Alternate pathways including shuttling via tight junctions and through or alongside other cells. Adapted from Ganger *et al*., (2018).

1.6 Hydrogels

Hydrogels can be described as three-dimensional cross-linked polymer networks capable of imbibing substantial volumes of water [51]. Hydrogels can be formed using a

range of different water-soluble polymers and can be formed in various sizes and structures to provide different functions, including bulk hydrogels, thin films, coatings, microparticles, and nanoparticles [52]. In the specific context of drug delivery, hydrogels offer several attractive properties that promote spatial and/or temporal control over therapeutic release [53]. Due to their porous network structure, diffusion-based drug loading and release can readily be achieved and controlled by manipulating cross-link densities. The extremely high water content observed in most hydrogels (70-99%), coupled with physiochemical properties of hydrogels (e.g. mechanics) that mimic those of native biological tissues, promote good cytocompatibility and tissue compatibility in preclinical and clinical use [51, 54]. The soft, rubbery, and deformable nature of hydrogels is also valuable for biological applications, allowing such materials to conform to the shape of the application site [54].

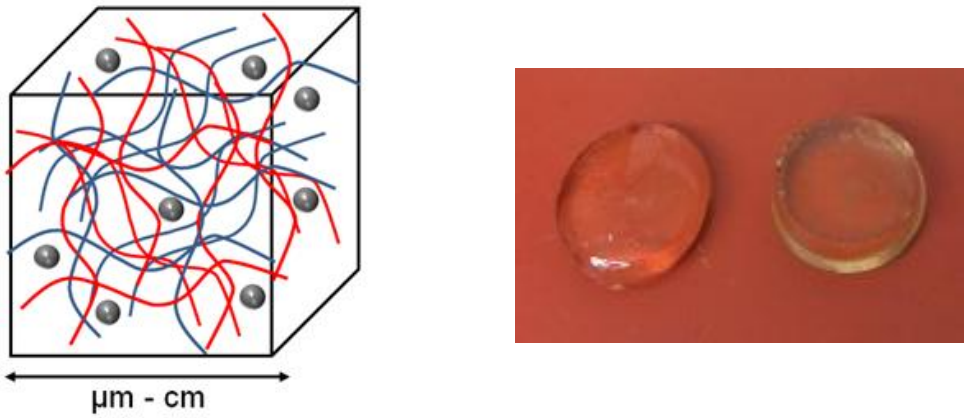

Figure 1-7. General structure and properties of hydrogels. (Left) Schematic of a theoretical 3D hydrogel matrix, with polymers in red and blue. (Right) Picture of a hydrogel after formation, as the polymer cross-links strengthen and set.

1.6.1 - Cross-Linking

Hydrogel networks may be formed using a variety of approaches, including both physical and covalent cross-links [55]. Of particular interest in the context of intranasal drug delivery are *in situ*-gelling hydrogels that can spontaneously form upon spraying or flow-based administration into the nose. Utilizing physical and chemical cross-linking chemistries, such hydrogels can be prepared in a multitude of approaches [51, 53, 55]. Physically cross-linked gels can be formed using a host of environmental triggers (temperature, pH, ionic strength) and an array of physiochemical interactions (hydrophobic interactions, hydrogen bonding, charge interactions). A common technique for gelation through hydrophobic interactions makes use of hydrophobes grafted to water soluble polymers which can be modulated by temperature changes (ex. increasing temperature results in hydrophobe aggregation) to form a gel, with gelation temperature depending on polymer concentration [55]. Charge interactions may also be exploited for cross-linking *in situ* polymers, where interactions between two polymers or polymers and small molecules of opposite charge induce gelation.

Alternately, covalently *in situ* chemically cross-linked gels can be formed through substitution or condensation reactions between a nucleophile-functionalized polymer and an electrophile-functionalized polymer [53, 56]. For use in the body, reactions that are spontaneous and fast at physiological conditions are ideal for *in situ* gel formation. Multiple chemistries exist for such reactions, all of which have benefits and drawbacks. First, Michael-type addition cross-linking involves addition of a nucleophile to the β position of an α,β-unsaturated carbonyl compound such as an aldehyde or ketone. This chemistry can occur spontaneously under physiological conditions but is somewhat

slower than some alternatives (i.e. a few minutes to tens of minutes), which can be undesirable for certain applications. The slightly basic conditions used to drive the reaction may also cause biocompatibility issues in pH sensitive environments. Second, disulfide cross-linking involves the reaction of two thiol groups (unprotonated and nonreactive in their reduced state) to form an S-S bond in an oxidizing environment (ex. extracellular space). At physiological pH however, they present low gelation rates (tens of minutes to hours) when lacking an oxidizing agent, limiting their application to locations in the body where longer residence times exist [57].

Third, hydrazone Schiff base crosslinking (condensation of a primary amine and aldehyde/ketone, further discussed in section 2.1.2) can be utilized to form imine (nucleophilic addition of a nitrogen from an amine to a carbonyl group) or hydrazone bonds (nucleophilic addition of a nitrogen from a hydrazine group to a carbonyl group), both resulting in water elimination [58]. Both imine and hydrazone crosslinking both occur fairly rapidly, however the former is generally more hydrolytically labile; the type of nucleophile (amine or hydrazide) affects the stability of the bond and thus the degradation rate. If faster degradation is desired, an imine bond should be selected, while a hydrazone bond may be selected if slower degradation is required. Gels formed with hydrazones have demonstrated good biocompatibility when compared to other injectable hydrogel chemistries, however some have concerns have been raised surrounding cross-reactivity of aldehyde groups with native tissue and storage stability [57]. Matching the benefits/drawbacks of a particular covalent in situ-gelling chemistry with the needs of a particular application is essential for the practical use of such materials.

1.7 Nanoparticle Nanocomposite Hydrogels

Nanoparticle-based therapeutic delivery systems hold great promise in the field of drug delivery. Nanomaterials can be defined as materials between 1-1000nm in size [59] and have unique properties according to their significantly higher surface area-to-mass ratio when compared with other larger particles, allowing for increased binding/adsorption, specific drug loading regimens, and differential biological transport mechanisms that can be leveraged in various biomedical applications [60]. In particular, smaller nanoparticles have greater tissue-penetration abilities, an increased residence time in the circulatory system, and decreased inflammatory responses which facilitates easy drug uptake by target cell and tissue regions [59]. However, the high mobility of nanoparticles can also cause challenges in treating local conditions, such as brain delivery. Significant emerging research has thus been focused in either physically entrapping various types of nanoparticles inside hydrogels or using nanoparticles themselves as the building block for fabricating a hydrogel [61]. In this context, the hydrogel can immobilize the nanoparticle at the desired active site (at least until a programmed degradation event releases the nanoparticle) to improve the localization of nanoparticle drug therapy as well as leverage the biphasic nature of the delivery vehicle to engineer release kinetics, often with much longer kinetic profiles than achieved with hydrogels alone [62].

There are several examples in the literature of nanocomposite hydrogel materials in which an assortment of nano- and micron-sized drug carriers such liposomes, polymer nano/microparticles, and microgels have been physically entrapped or covalently crosslinked within hydrogels and utilized for drug delivery. Polymeric nanoparticles with

dendritic components offer a multitude of surface functional groups, which can be utilized to incorporate nanoparticles into hydrogel networks through covalent or non-covalent bonding [61]. Using these highly branched structures, bioactives (drugs, peptides) can be readily encapsulated either within or conjugated on the periphery of the nanoparticles. Release from these polymeric nanocomposite hydrogels can be controlled through time-based systems (i.e. drug carriers released as bulk gel degrades degrades/dissolves), thermo- or pH-sensitive means (i.e. the materials undergo triggered degradation/de-crosslinking under certain environmental conditions), the relative swelling/de-swelling of both the carriers and bulk gel (resulting in dynamic free volume generation at the interface between the filler and the gel), and/or by manipulating the affinity towards drugs for either of the two phases to control release via partitioning [63, 64].

One specific example of passive drug release via a nanocomposite hydrogel system is by the delivery of the anti-inflammatory drug methylprednisolone (MP) by loaded the drug into pol(lactic-co-glycolic acid (PLGA) nanoparticles and embedding the nanoparticles within an agarose hydrogel. Continuous release of MP was observed for up to 6 days as opposed to a few hours via traditional delivery means [62]. Another example highlights stimuli-based controlled release of melanin nanoparticles dispersed within heat degradable hydrogel networks physically cross-linked by amphiphilic PLGA-PEG-PLGA copolymers. Following UV irradiation, the hydrogel was observed to degrade, releasing the encapsulated nanoparticles on demand [62]. Other examples make use of microgels embedded within hydrogels, forming a soft nanocomposite system. Physical entrapment of microgels within an in-situ gelling hydrogel network

cross-linked via hydrazide-aldehyde chemistry has previously been demonstrated to facilitate drug release for up to 60 days, compared to release from a hydrogel or microgel alone (<1 week) [63]. Covalent attachment of microgels to hydrogels via dynamic hydrazone chemistry has also been shown, exhibiting a decrease in drug release in contrast to physical microgel incorporation [56]. Gel nanoparticles offer several benefits when utilized as a building block for a hydrogel matrix. They are easily chemically modified to incorporate a variety of ligands, which further allows for relatively straightforward cross-linking [65]. Due to their “soft” nature, they can match target tissue properties once released, increasing their potential to penetrate biological barriers. Their size also allows for them to respond rapidly to environmental changes such as pH and temperature. Lastly, they are capable of great drug loading capacity, prolonging active agent activity in biological environments, ultimately making them excellent candidates for drug delivery purposes [66]

1.8 Starch

Starch is an extremely abundant polymer that is low in cost, easily produced and stored, and is non-cytotoxic, making it one of the most extensively used biopolymers in drug delivery [67-69]. Starch consists of glucose monomers attached together by α-[1,4]-glycosidic linkages. Multiple repeats of these monomers in a linear chain structure may be classified as amylose, while branched monomers via α-[1,6]-glycosidic linkages result in crystalline regions referred to as amylopectin [70]. However, native starch has very high viscosity due to its tightly bound structures (preventing water dissolution), high polydispersity, and a highly crystalline structure (complicating chemical modification) [69].

Starch nanoparticles (SNPs) are emerging alternatives to conventional starch as drug carriers that can circumvent some of these aforementioned issues. In contrast to “soluble” starch, SNPs are highly hygroscopic (akin to nanogels), amorphous in structure (enabling facile functionalization), and can be produced via an extrusion-based process with sizes in the range of 20-50nm, a size range not easily achieved with other types of nano-formulations but highly beneficial in drug delivery applications in which high tissue penetration is desired [71]. SNPs have also been shown to demonstrate sustained release profiles of drugs over the course of multiple days [72], suggesting their potential to mediate both the release kinetics and transport of water-soluble therapeutics such as peptides like PAOPA.

1.9 Thesis Objectives

The aim of this thesis was to investigate the synthesis, properties, and applications of starch nanoparticle-carboxymethyl chitosan hydrogel drug delivery platforms for the intranasal delivery of hydrophilic therapeutics to alleviate schizophrenic symptoms. Drug delivery to the brain has inherent limitations following traditional oral or IV-based administration, an issue the intranasal route can circumvent. Furthermore, developing a controlled release vehicle that is both mucoadhesive (via the use of carboxymethyl chitosan) and promoting of tissue penetration (via the use of small and soft starch nanoparticles is hypothesized to provide a valuable platform for APD delivery. To capitalize on the advantages provided by SNPs and the IN route, we aim to create formulations which are: (1) easily sprayable within the nose; (2) mucoadhesive to the mucus layer; (3) release nanoparticles over time to promote mucosal tissue penetration; and (4) slow releasing to provide sustained symptom alleviation following one dose.

Successful platform development would allow for a reduction in overall drug administration and thus minimization of bodily side-effects associated with constant drug use, with modification of the platform possible to extend the benefits of the platform to other hydrophilic APDs.

Chapter 2 discusses the development and application of PAOPA-loaded bulk hydrogels for the alleviation of negative symptoms of schizophrenia. SNPs were functionalized with aldehyde groups and cross-linked via imine crosslinking with carboxymethyl chitosan to form fully characterized hydrogels. Hydrogels demonstrated rapid gelation and relevant degradation and spray profiles. IN administration demonstrated retention of the formulation in the nose and functional controlled release of PAOPA in induced-schizophrenia in vivo models. Symptom alleviation over the period of 3 days was observed with a lower drug dose than used in conventional intraperitoneal injections.

Chapter 3 discusses the development of nanocluster nanogel drug carriers (~200nm) using the same carboxymethyl chitosan/starch nanoparticle chemistry but by performing the crosslinking inside an inverse emulsion template. Emulsion optimization parameters are described, followed by characterization of the template-based nanocluster formation. Nanogels were further characterized for stability and degradation in organic and aqueous phases, demonstrating long-term organic phase stability (30 days) and relevant degradation profiles in water (over the period of 4 days). Future applications of such nanocluster delivery vehicles are envisioned for IN delivery.

Chapter 4 highlights the key conclusions from the work and suggests future recommendations to continue the development of these hydrogel drug delivery platforms.

1.10 References

[1] A. E. Becker and A. Kleinman, "Mental health and the global agenda," *N Engl J Med,* vol. 369, no. 1, pp. 66-73, Jul 4 2013, doi: 10.1056/NEJMra1110827.

[2] C. J. L. Murray *et al.*, "Disability-adjusted life years (DALYs) for 291 diseases and injuries in 21 regions, 1990–2010: a systematic analysis for the Global Burden of Disease Study 2010," *The Lancet,* vol. 380, no. 9859, pp. 2197-2223, 2012, doi: 10.1016/s0140-6736(12)61689-4.

[3] "Depression and other Common Mental Disorders: Global Health Estimates," *Geneva: World Health Organization,* 2017.

[4] S. Saha, D. Chant, J. Welham, and J. McGrath, "A systematic review of the prevalence of schizophrenia," *PLoS Med,* vol. 2, no. 5, p. e141, May 2005, doi: 10.1371/journal.pmed.0020141.

[5] H. A. Whiteford, A. J. Ferrari, L. Degenhardt, V. Feigin, and T. Vos, "The global burden of mental, neurological and substance use disorders: an analysis from the Global Burden of Disease Study 2010," *PLoS One,* vol. 10, no. 2, p. e0116820, 2015, doi: 10.1371/journal.pone.0116820.

[6] H. Y. Chong, S. L. Teoh, D. B. Wu, S. Kotirum, C. F. Chiou, and N. Chaiyakunapruk, "Global economic burden of schizophrenia: a systematic review," *Neuropsychiatr Dis Treat,* vol. 12, pp. 357-73, 2016, doi: 10.2147/NDT.S96649.

[7] T. J. Crow, "Positive and Negative Schizophrenic Symptoms and the Role of Dopamine," *The British Journal of Psychiatry,* vol. 137, no. 4, pp. 383-385, 1980.

[8] J. V. Os and S. Kapur, "Schizophrenia," *Lancet,* vol. 374, pp. 635-645, 2009.

[9] D. Ernest, O. Vuksic, A. Shepard-Smith, and E. Webb, "Schizphrenia: An Information Guide," *Centre for Addiction and Mental Health,* 2017.

[10] K. H. Nuechterlein, D. M. Barch, J. M. Gold, T. E. Goldberg, M. F. Green, and R. K. Heaton, "Identification of separable cognitive factors in schizophrenia," *Schizophr Res,* vol. 72, no. 1, pp. 29-39, Dec 15 2004, doi: 10.1016/j.schres.2004.09.007.

[11] C. Karam *et al.*, "Signaling pathways in schizophrenia:emerging targets and therapeutic strategies," *Trends in Pharmacological Science,* vol. 21, no. 8, pp. 381-390, 2010.

[12] A. P. Association. *Diagnostic and Statistical Manual, Fourth Edition Text Revision (DSM-IV TR)*, American Psychiatric Publishing, 2000.

[13] R. Brisch *et al.*, "The role of dopamine in schizophrenia from a neurobiological and evolutionary perspective: old fashioned, but still in vogue," *Front Psychiatry,* vol. 5, p. 47, 2014, doi: 10.3389/fpsyt.2014.00047.

[14] C. Missale, S. R. Nash, S. W. Robinson, M. Jaber, and M. G. Caron, "Dopamine Receptors: From Structure to Function," *Physiological Reviews,* vol. 78, no. 1, pp. 189-212, 1998.

[15] S. Rege. "The Dopamine Hypothesis of Schizophrenia – Advances in Neurobiology and Clinical Application." https://psychscenehub.com/psychinsights/the-dopamine-hypothesis-of-schizophrenia/ (accessed September 17, 2019).

[16] N. Miyake, J. Thompson, M. Skinbjerg, and A. Abi-Dargham, "Presynaptic dopamine in schizophrenia," *CNS Neurosci Ther,* vol. 17, no. 2, pp. 104-9, Apr 2011, doi: 10.1111/j.1755-5949.2010.00230.x.

[17] J. J. Weinstein, M. O. Chohan, M. Slifstein, L. S. Kegeles, H. Moore, and A. Abi-Dargham, "Pathway-Specific Dopamine Abnormalities in Schizophrenia," *Biol Psychiatry,* vol. 81, no. 1, pp. 31-42, Jan 1 2017, doi: 10.1016/j.biopsych.2016.03.2104.

[18] O. D. Howes and S. Kapur, "The dopamine hypothesis of schizophrenia: version III--the final common pathway," *Schizophr Bull,* vol. 35, no. 3, pp. 549-62, May 2009, doi: 10.1093/schbul/sbp006.

[19] Y. T. Kwak, Y. Yang, and H.-r. Jang, "Understanding of Antipsychotics in Elderly Patients with Dementia," *Dementia and Neurocognitive Disorders,* vol. 14, no. 2, 2015, doi: 10.12779/dnd.2015.14.2.53.

[20] O. Howes, R. McCutcheon, and J. Stone, "Glutamate and dopamine in schizophrenia: an update for the 21st century," *J Psychopharmacol,* vol. 29, no. 2, pp. 97-115, Feb 2015, doi: 10.1177/0269881114563634.

[21] B. A. Fischer and R. W. Robert W Buchanan. "Schizophrenia in adults: Epidemiology and pathogenesis." https://www.uptodate.com/contents/schizophrenia-in-adults-epidemiology-and-pathogenesis (accessed September 17, 2019).

[22] H. Y. Meltzer, "The Mechanism of Novel Antipsychotic Drugs," *Schizophrenia Bulletin,* vol. 7, no. 2, pp. 265-287, 1991.

[23] J. Mukherjee, "Evaluation of Dopamine D-2 Receptor Occupancy by Clozapine, Risperidone, and Haloperidol In Vivo in the Rodent and Nonhuman Primate Brain Using 18F-Fallypride," *Neuropsychopharmacology,* vol. 25, no. 4, pp. 476-488, 2001, doi: 10.1016/s0893-133x(01)00251-2.

[24] A. M. Abou-Setta, S. S. Mousavi, and C. Spooner, *First- Generation Versus Second-Generation Antipsychotics in Adults: Comparative Effectiveness*. Rockville (MD): Agency for Healthcare Research and Quality (US), Rockville (MD): Agency for Healthcare Research and Quality 2012.

[25] S. H. Schutlz, S. W. North, and C. G. Shields, "Schizophrenia: A Review," *American Family Physician,* vol. 75, no. 12, 2007.

[26] L. Koster, M. Carbon, and C. U. Correll, "Emerging drugs for schizophrenia: an update," *Expert Opinion: Emerging Drugs,* vol. 19, no. 4, pp. 1-21.

[27] H. Y. Meltzer, "What's atypical about atypical antipsychotic drugs?," *Current Opinion in Pharmacology,* vol. 4, no. 1, pp. 53-57, 2004.

[28] R. B. Mailman and V. Murthy, "Third generation antipsychotic drugs: partial agonism or receptor functional selectivity?," *Current Pharmaceutical Design,* vol. 16, no. 5, pp. 488-501, 2010.
[29] A. Serretti, D. De Ronchi, C. Lorenzi, and D. Berardi, "New antipsychotics and schizophrenia: a review on efficacy and side effects," *Curr Med Chem,* vol. 11, no. 3, pp. 343-58, Feb 2004, doi: 10.2174/0929867043456043.
[30] C. Rummel-Kluge *et al.*, "Head-to-head comparisons of metabolic side effects of second generation antipsychotics in the treatment of schizophrenia: a systematic review and meta-analysis," *Schizophr Res,* vol. 123, no. 2-3, pp. 225-33, Nov 2010, doi: 10.1016/j.schres.2010.07.012.
[31] P. J. Goodnick and J. M. Jerry, "Aripiprazole: profile on efficacy and safety," *Expert Opin Pharmacother,* vol. 3, no. 12, pp. 1773-81, Dec 2002, doi: 10.1517/14656566.3.12.1773.
[32] A. F. Abdel-Magid, "Allosteric modulators: an emerging concept in drug discovery," *ACS Med Chem Lett,* vol. 6, no. 2, pp. 104-7, Feb 12 2015, doi: 10.1021/ml5005365.
[33] E. Vavers, L. Zvejniece, T. Maurice, and M. Dambrova, "Allosteric Modulators of Sigma-1 Receptor: A Review," *Front Pharmacol,* vol. 10, p. 223, 2019, doi: 10.3389/fphar.2019.00223.
[34] N. M. Goodey and S. J. Benkovic, "Allosteric regulation and catalysis emerge via a common route," *Nat Chem Biol,* vol. 4, no. 8, pp. 474-82, Aug 2008, doi: 10.1038/nchembio.98.
[35] T. Kenakin, "Allosteric Theory: Taking Therapeutic Advantage of the Malleable Nature of GPCRs," *Current Neuropharmacology,* vol. 5, no. 3, pp. 149-156, 2007.
[36] R. S. Khan *et al.*, "Brain Activation by Peptide Pro-Leu-Gly-NH(2) (MIF-1)," *International Journal of Peptides,* vol. 2010, 2010.
[37] R. K. Mishra, L. K. Srivastava, and R. L. Johnson, "Modulation of high-affinity CNS dopamine D2 receptor by l-pro-l-leu-glycinamide (PLG) analogue," *Progress in Neuro-Psychopharmacology and Biological Psychiatry,* vol. 14, no. 5, 1990.
[38] E. R. Marcotte, A. C. Chugh, R. K. Mishra, and R. L. Johnson, "Protection Against MPTP Treatment by an Analog of Pro-Leu-Gly-NH2 (PLG, MIF-1)," *Peptides,* vol. 19, no. 2, pp. 403-406, 1998.
[39] S. Sharma *et al.*, "Pro-Leu-glycinamide and its peptidomimetic, PAOPA, attenuate haloperidol induced vacuous chewing movements in rat: A model of human tardive dyskinesia," *Peptides,* vol. 24, no. 2, pp. 313-319, 2003.
[40] M. G. Beyaert, R. P. Daya, B. A. Dyck, R. L. Johnson, and R. K. Mishra, "PAOPA, a potent dopamine D2 receptor allosteric modulator, prevents and reverses behavioral and biochemical abnormalities in an amphetamine-sensitized preclinical animal model of schizophrenia," *Eur Neuropsychopharmacol,* vol. 23, no. 3, pp. 253-62, Mar 2013, doi: 10.1016/j.euroneuro.2012.04.010.
[41] B. Dyck, K. Guest, C. Sookram, D. Basu, R. Johnson, and R. K. Mishra, "PAOPA, a potent analogue of Pro-Leu-glycinamide and allosteric modulator of the dopamine D2 receptor, prevents NMDA receptor antagonist (MK-801)-induced deficits in social interaction in the rat: implications for the treatment of

negative symptoms in schizophrenia," *Schizophr Res,* vol. 125, no. 1, pp. 88-92, Jan 2011, doi: 10.1016/j.schres.2010.09.025.
[42] S. M. Pond and T. N. Tozer, "First-Pass Elimination Basic Concepts and Clinical Consequences," *Clinical Pharmacokinetics,* vol. 9, 1, pp. 1-25, 1984.
[43] V. Rodighiero, "Effects of Liver Disease on Pharmacokinetics," *Clinical Pharmacokinetics,* vol. 37, no. 5, pp. 399-431, 1999.
[44] L. Sultatos, "First-Pass Effect," in *xPharm: The Comprehensive Pharmacology Reference*, 2007, pp. 1-2.
[45] S. P. van Kessel *et al.*, "Gut bacterial tyrosine decarboxylases restrict levels of levodopa in the treatment of Parkinson's disease," *Nat Commun,* vol. 10, no. 1, p. 310, Jan 18 2019, doi: 10.1038/s41467-019-08294-y.
[46] Y. K. Katare *et al.*, "Intranasal delivery of antipsychotic drugs," *Schizophr Res,* vol. 184, pp. 2-13, Jun 2017, doi: 10.1016/j.schres.2016.11.027.
[47] N. J. Abbott, A. A. Patabendige, D. E. Dolman, S. R. Yusof, and D. J. Begley, "Structure and function of the blood-brain barrier," *Neurobiol Dis,* vol. 37, no. 1, pp. 13-25, Jan 2010, doi: 10.1016/j.nbd.2009.07.030.
[48] C. Saraiva, C. Praca, R. Ferreira, T. Santos, L. Ferreira, and L. Bernardino, "Nanoparticle-mediated brain drug delivery: Overcoming blood-brain barrier to treat neurodegenerative diseases," *J Control Release,* vol. 235, pp. 34-47, Aug 10 2016, doi: 10.1016/j.jconrel.2016.05.044.
[49] S. Ganger and K. Schindowski, "Tailoring Formulations for Intranasal Nose-to-Brain Delivery: A Review on Architecture, Physico-Chemical Characteristics and Mucociliary Clearance of the Nasal Olfactory Mucosa," *Pharmaceutics,* vol. 10, no. 3, Aug 3 2018, doi: 10.3390/pharmaceutics10030116.
[50] M. U. Ghori, M. H. Mahdi, A. M. Smith, and B. R. Conway, "Nasal Drug Delivery Systems: An Overview," *American Journal of Pharmacological Sciences,* vol. 3, no. 5, 2015, doi: 10.12691/ajps-3-5-2.
[51] J. Maitra and V. K. Shukla, "Cross-linking in Hydrogels - A Review," *American Journal of Polymer Science,* vol. 4, no. 2, pp. 25-31, 2014, doi: 10.5923/j.ajps.20140402.01.
[52] J. Li and D. J. Mooney, "Designing hydrogels for controlled drug delivery," *Nat Rev Mater,* vol. 1, no. 12, Dec 2016, doi: 10.1038/natrevmats.2016.71.
[53] S. M. Bindu, A. Chatterjee, and V. Ashok, "As A Review on Hydrogels as Drug Delivery in the Pharmaceutical Field," *international Journal of Pharmceutical and Chemical Sciences,* vol. 1, no. 2, pp. 642-661, 2012.
[54] N. A. Peppas, "Hydrogels and drug delivery," *Current Opinion in Colloid & Interface Science,* pp. 531-537, 1997.
[55] T. R. Hoare and D. S. Kohane, "Hydrogels in drug delivery: Progress and challenges," *Polymer,* vol. 49, no. 8, pp. 1993-2007, 2008, doi: 10.1016/j.polymer.2008.01.027.
[56] D. Sivakumaran, D. Maitland, T. Oszustowicz, and T. Hoare, "Tuning drug release from smart microgel-hydrogel composites via cross-linking," *J Colloid Interface Sci,* vol. 392, pp. 422-430, Feb 15 2013, doi: 10.1016/j.jcis.2012.07.096.

[57] M. Patenaude, N. M. Smeets, and T. Hoare, "Designing injectable, covalently cross-linked hydrogels for biomedical applications," *Macromol Rapid Commun,* vol. 35, no. 6, pp. 598-617, Mar 2014, doi: 10.1002/marc.201300818.

[58] E. Bakaic, N. M. Smeets, and T. Hoare, "Injectable hydrogels based on poly(ethylene glycol) and derivatives as functional biomaterials," *RSC Advances,* vol. 5, pp. 35469-35486, 2015.

[59] J. K. Patra *et al.*, "Nano based drug delivery systems: recent developments and future prospects," *J Nanobiotechnology,* vol. 16, no. 1, p. 71, Sep 19 2018, doi: 10.1186/s12951-018-0392-8.

[60] W. H. Jong and P. J. Borm, "Drug delivery and nanoparticles: Applications and hazards," *International Journal of Nanomedicine,* vol. 3, no. 2, pp. 133-149, 2008.

[61] A. K. Gaharwar, N. A. Peppas, and A. Khademhosseini, "Nanocomposite hydrogels for biomedical applications," *Biotechnol Bioeng,* vol. 111, no. 3, pp. 441-53, Mar 2014, doi: 10.1002/bit.25160.

[62] W. Gao, Y. Zhang, Q. Zhang, and L. Zhang, "Nanoparticle-Hydrogel: A Hybrid Biomaterial System for Localized Drug Delivery," *Ann Biomed Eng,* vol. 44, no. 6, pp. 2049-61, Jun 2016, doi: 10.1007/s10439-016-1583-9.

[63] D. Sivakumaran, D. Maitland, and T. Hoare, "Injectable microgel-hydrogel composites for prolonged small-molecule drug delivery," *Biomacromolecules,* vol. 12, no. 11, pp. 4112-20, Nov 14 2011, doi: 10.1021/bm201170h.

[64] Sonia Merino, † Cristina Martı´n,† Kostas Kostarelos,‡ Maurizio Prato,*,§ and Ester Va´ zquez*,†, S. Merino, C. Martin, K. Kostarelos, M. Prato, and E. Vazquez, "Nanocomposite Hydrogels: 3D Polymer-Nanoparticle Synergies for On-Demand Drug Delivery," *Americal Chemical Society Nano,* vol. 9, no. 5, pp. 4686–4697, 2015.

[65] G. Soni and K. S. Yadav, "Nanogels as potential nanomedicine carrier for treatment of cancer: A mini review of the state of the art," *Saudi Pharm J,* vol. 24, no. 2, pp. 133-9, Mar 2016, doi: 10.1016/j.jsps.2014.04.001.

[66] K. H. Bae, H. Mok, and G. T. Park, "Synthesis, characterization, and intracellular delivery of reducible heparin nanogels for apoptotic cell death," *Biomaterials,* vol. 29, no. 23, pp. 3376-3383, 2008.

[67] A. K. Bajpai and S. Bhanu, "Dynamics of controlled release of heparin from swellable crosslinked starch microspheres," *Journal of Materials Science: Materials in Medicine,* vol. 18, no. 8, pp. 1613-1621, 2007.

[68] E. T. Baran, J. F. Mano, and R. L. Reis, "Starch–chitosan hydrogels prepared by reductive alkylation cross-linking," *Journal of Materials Science: Materials in Medicine,* vol. 15, no. 7, pp. 759-765, 2004.

[69] P. F. Builders and M. I. Arhewoh, "Pharmaceutical applications of native starch in conventional drug delivery," *Starch - Stärke,* vol. 68, no. 9-10, pp. 864-873, 2016, doi: 10.1002/star.201500337.

[70] M. G. Sajilata, R. S. Singhal, and P. R. Kulkarni, "Resistant Starch— A Review," *Comprehensive Reviews in Food Science and Food Safety,* vol. 5, pp. 1-17, 2006.

[71] L. Messager *et al.*, "Photochemical crosslinking of hyaluronic acid confined in nanoemulsions: towards nanogels with a controlled structure," *Journal of Materials Chemistry B,* vol. 1, no. 27, 2013, doi: 10.1039/c3tb20300j.

[72] S. Bloembergen, "Aptamer Bioconjugate Drug Delivery Device," United States, 2012.

2. In Situ-Gelling Hydrogels for Intranasal Delivery of PAOPA for Schizophrenia Treatment

2.1 Introduction

2.1.1 - Mucoadhesive In Situ Gels for Intranasal Delivery

In situ-gelling hydrogels for IN delivery of therapeutics have recently gained great traction. Traditional IN delivery methods include use of suspension/solution sprays, nasal drops, emulsions, powders, ointments, liposomes, microspheres and nanoparticles [1]. Typically, these non-mucoadhesive formulations undergo rapid removal from the nasal cavity due to mucociliary clearance, leading to a half-life of clearance of 15-30 minutes for liquid or powder formulations. As a result, drug absorption time is limited and bioavailability to the brain is low [2, 3]. Mucoadhesive formulations, including in situ hydrogels, offer a viable solution to this issue given that their ability to adhere to nasal mucosa increases nasal cavity residence time [4]. The increase in contact time and consequently surface area facilitates increased drug absorption and bioavailability. Additionally, mucoadhesive in situ gels may reduce post-nasal drip at the back of the throat, further minimizing drug loss [5]. These gels may also provide increased retention within the nose, with further engineering of pore size and drug affinity of the gel promoting controlled release of drugs.

Mucoadhesion can be defined as the adhesion between a mucosal surface and another material. Multiple theories of mucoadhesion exist to help explain commonly observed phenomena in the adhesion process. The longest standing theory is the wetting theory, which states the adhesion process undergoes a wetting (initial contact) and subsequent consolidation phase [6]. A mucoadhesive surface contacts a mucosal membrane

(intimate wetting) and is then consolidated via physiochemical interactions to strengthen the adhesive joint (chemical bonding; ionic, covalent, hydrogen bonding, etc.) The electrostatic theory of mucoadhesion states that if a substrate and adhesive possess opposite charges, they will experience an attractive electrostatic force which creates a double layer of equal yet opposite charges on both surfaces [7, 8].The diffusion theory states that interpenetration and entanglement of both polymer and mucin drives mucoadhesion, a process which is dependent on chain flexibility and adequate surface area contact [7, 9]. Mucoadhesive polymers often contain hydrophilic functional groups (hydroxyls, carboxyls, amides, etc) that cause polymers to swell in aqueous conditions, thus exposing the maximum number of adhesive sites [10].

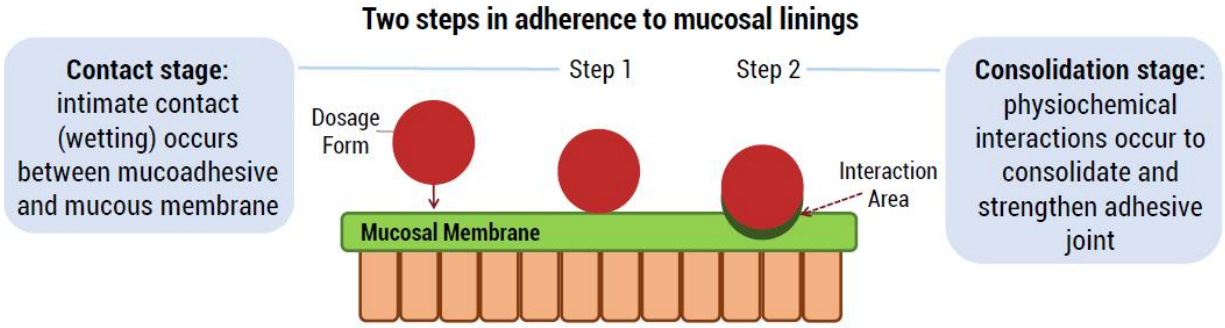

Figure 2-1. Schematic of mucoadhesion depicting the wetting theory, in which dosage forms contact a mucosal membrane and subsequently consolidate through physiochemical interactions.

O-Carboxymethyl Chitosan

A commonly used mucoadhesive polymer in the biomedical realm is chitosan, which is derived from chitin, a natural polysaccharide found in the shells of crustaceans (shrimps, crabs, lobsters, etc). Chitin has a linear structure composed of 2-acetamide-2-deoxy-d-glucopyranose units linked by β (1–4) bonds, while chitosan is a copolymer of

2-amino-2-deoxy-d-glucopyranose and 2-acetamide-2-deoxy-d-glucopyranose units [11]. Chitosan's generally low cytotoxicity has made it widely applicable in a range of biomedical applications including tissue engineering, wound healing and drug delivery [12]. However, chitosan is generally insoluble in aqueous conditions, requiring further chemical modification for use in non-acidic conditions [13]. A common modification is carboxymethylation, which not only enhances hydrophilicity but also increases cytocompatibility and biodegradability [11]. The modification involves substitution of some of the –OH groups by $–CH_2COOH$ groups, leaving –COOH and $–NH_2$ groups available for further bonding (e.g. crosslinking or mucoadhesion) (Fig. 2-2) [14]. Indeed, the O-carboxymethyl chitosan (CMC) derived from such a reaction has been demonstrated to maintain good mucoadhesion [15, 16] through strong adherence between the positive charges on CMC to the negative charges on the nasal membrane, in particular sialic acid residues on mucin [16, 17].

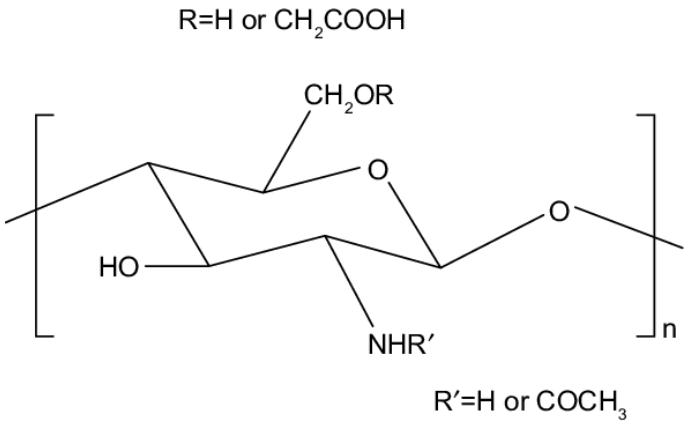

Figure 2-2. Chemical structure of o-carboxymethyl chitosan.

2.1.2 - Schiff Base Hydrogels

In addition to promoting mucoadhesion, the amine groups in CMC can enable chemical cross-linking and, in some cases, *in situ* chemical crosslinking to formulate an injectable or potentially sprayable hydrogel vehicle. One such method of hydrogel formation is imine bonding between two different water soluble polymers. An imine, or Schiff base, is a reversible bond formed via nucleophilic addition of a nitrogen from an amine to the carbonyl group of an aldehyde through a condensation reaction (Fig. 2-3) [18]. These bonds offer rapid and tunable kinetics and may be easily reversed through hydrolysis. Typical Schiff base formation offers limited hydrolytic stability which results in quick (hours-days) hydrogel degradation, a potentially advantageous characteristic when developing a drug delivery carrier. The extent of degradation can be further tuned by varying the concentrations of polymers and the aldehyde/amine functionality of the polymers. Imine-based hydrogels also typically demonstrate good cytocompatibility [19], exhibiting minimal in vitro and in vivo cytotoxicity when cross-linked in situ [20]. The combination of these factors makes Schiff base hydrogels valuable for drug delivery in addition to a variety of other biological applications including cell scaffolding, tissue engineering, and wound dressings [18, 21, 22]

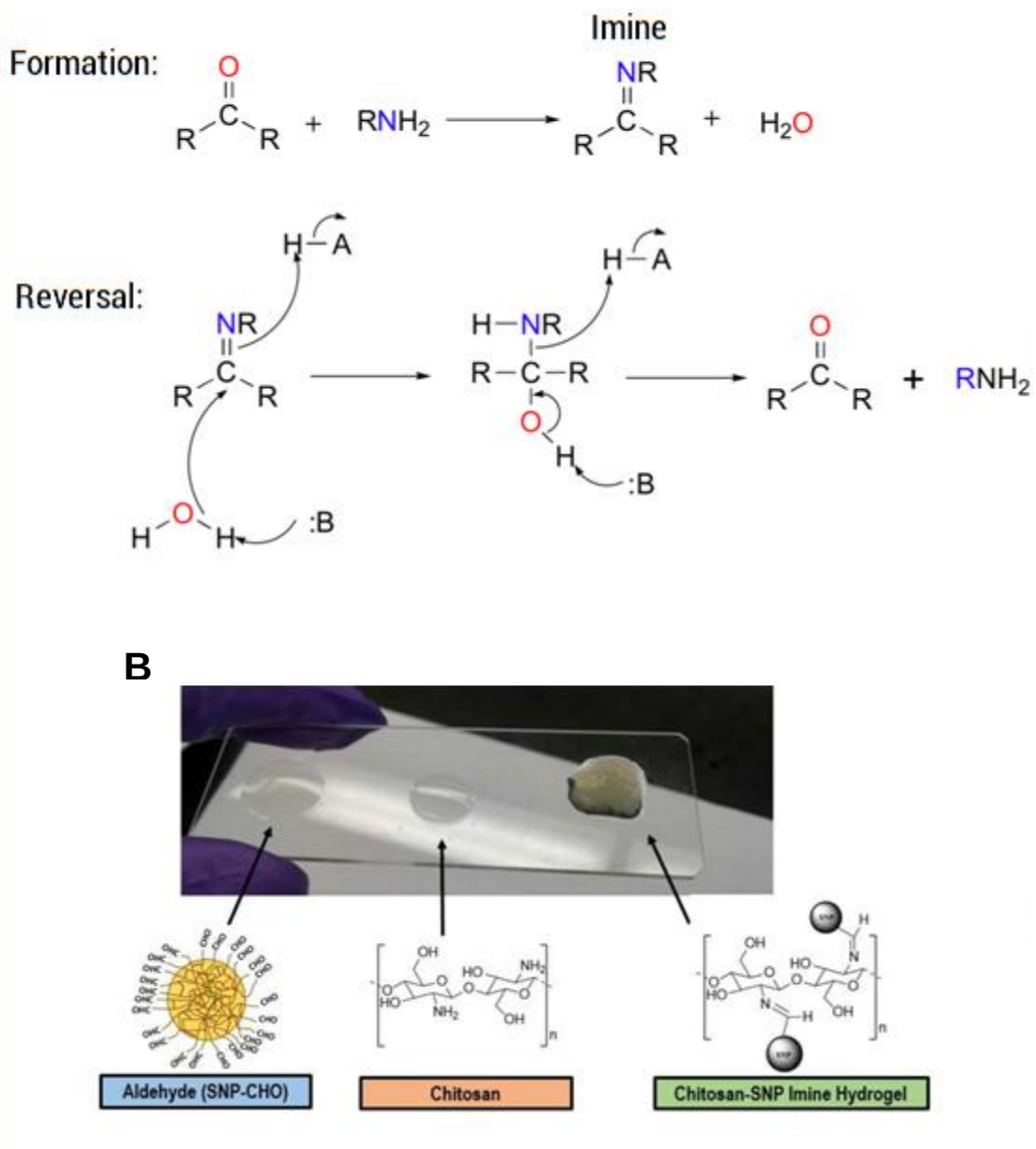

Figure 2-3. (A) Formation and reversal of an imine bond. (B) Depiction of the precursors and cross-linking process for imine gel formation; (left) aldehyde-functionalized starch nanoparticles (SNP-CHO); (middle) CMC; (right) SNP-CHO + CMC imine cross-linked hydrogel.

2.1.3 - PAOPA for Schizophrenia Treatment

One of the key potential applications of mucoadhesive hydrogels is intranasal drug delivery, with antipsychotic drugs particularly useful targets to take advantage of the enhanced bioavailability of therapeutics delivered through the nose rather than through the oral or intraperitoneal (IP) route. Of particular interest for schizophrenia treatment is, PAOPA, as discussed in section 1.4.

2.1.4 - Dizocilpine (MK-801) Schizophrenia Knockdown

N-methyl-D-aspartate (NMDA) receptor antagonists generate widely acknowledged pre-clinical models of positive, negative and general cognitive deficits observed in schizophrenia [23]. Dizocilpine ((+)-MK 801 maleate) or MK-801, is one of the most potent non-competitive NMDA antagonists, which functions via binding to sites located within ion channels of the NMDA receptor complex to block cation flow [24]. The MK-801 model allows for tracking of the efficacy of a delivered drug by monitoring social interaction withdrawal, a negative symptom often associated with schizophrenia in which individuals have a decreased tendency to engage in meaningful social interactions with others thought to be primarily related to the hypoactivity of dopamine in the mesocortical pathway [25]. The use of NMDA receptor antagonists (such as MK-801) is accepted to accurately model this withdrawal and is generally considered reliable and easy to induce, making it commonly used to examine therapeutic value of potential drug candidates in treatment of schizophrenia [26, 27]. MK-801 is typically administered in concentration ranges of 0.1mg/kg-0.4mg/kg via an intraperitoneal injection (IP), with 0.3mg/kg most commonly used in the literature to induce the model. MK-801 is utilized in both acute and chronic models of schizophrenia; however for the

purposes of this chapter MK-801 is used to induce social withdrawal at an acute time point (symptom induction 30 minutes after IP injection, lasting ~2 hours) [24, 28].

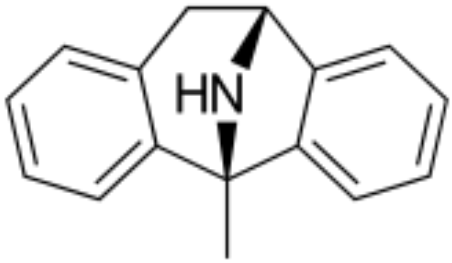

Figure 2-4. Chemical structure for MK-801 (right).

2.2 Experimental Objectives

The objective of this chapter was to develop drug-carrying bulk hydrogels for the controlled and sustained delivery of PAOPA through the intranasal route. Although in situ-hydrogels for IN delivery of APDs have been explored, there exists a need for controlled release vehicles to further decrease dosages and simplify administration for patients. Such a formulation would ideally be: (1) sprayable to enable facile administration; (2) mucoadhesive and/or in situ-gelling to promote immobilization of the formulation (and thus the drug) to the mucus layer upon administration; (3) transportable (ideally via active transport mechanisms) across the nasal epithelium and subsequently to the olfactory and/or trigeminal nerve(s); and (4) slow releasing to facilitate extended efficacy following a single dose, reducing the need for frequent administrations that can reduce schizophrenic patient compliance.

In this chapter we explore the development and application of PAOPA-loaded bulk imine hydrogels for alleviation of the negative schizophrenic symptom of social withdrawal. Chemical modification of SNPs, cross-linking with CMC to form hydrogels, and the resulting properties of hydrogels (swelling, gelation kinetics, degradation, and nebulization) are all investigated. Following, IN administration of in situ-gels is discussed and mucosal adherence of gels and functional controlled release of PAOPA is examined in an induced-schizophrenia in vivo model. We aim to decrease the typical IP dosage of PAOPA (1mg/kg) while increasing hydrogel nasal residence time for extended symptom alleviation.

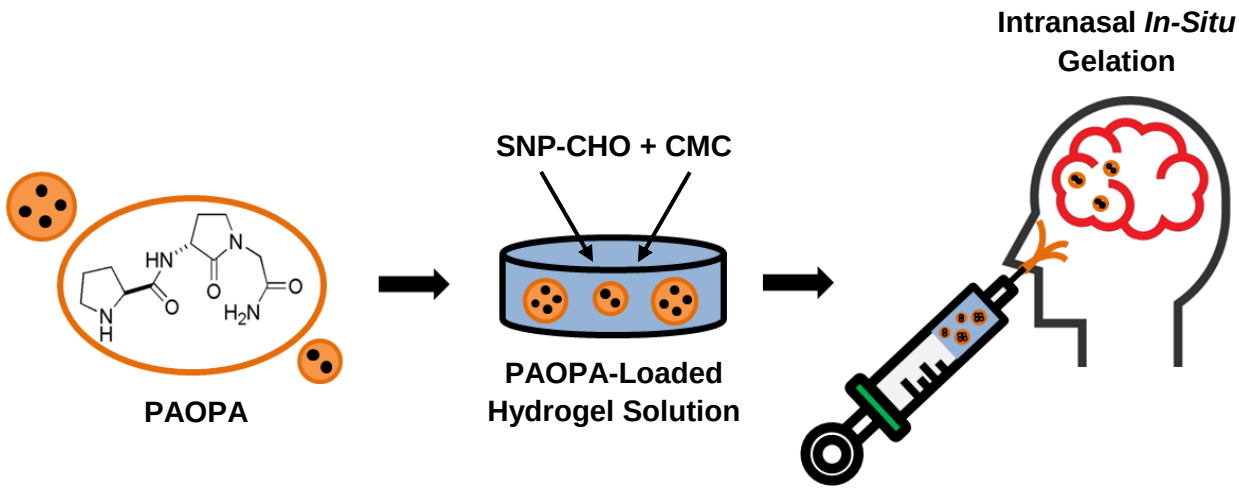

Figure 2-5. Schematic depicting the overarching process of IN delivery of PAOPA via in situ-gelation.

2.3 Materials

Experimental grade starch nanoparticles (SNPs) were supplied by EcoSynthetix Inc. [Burlington, ON, Canada] and used as received. O-carboxymethyl chitosan (CMC) was obtained from Bonding Chemical [Katy, TX, USA] and used as received.

Sodium periodate ($NaIO_4$), 99% from AK Scientific [California, USA], and diethylene glycol from MilliporeSigma [Oakville, ON, Canada], were used as received.

For all experiments, Millipore Milli-Q grade distilled de-ionized water (MQW, 18.2 MΩ/cm resistivity) was used.

Phosphate buffered saline tablets (PBS, 0.01 M phosphate buffer, 0.0027 M potassium chloride and 0.137 M sodium chloride, pH 7.4, at 25 °C) [MilliporeSigma, Oakville, ON, Canada] were dissolved in 200 mL/tablet of MQW to achieve the desired concentrations. The pH of the buffer was confirmed using a pH probe.

PAOPA ((3R)-2-Oxo-3-[[(2S)-2-Pyrrolidinylcarbonyl]amino]-1-pyrrolidineacetamide]) was purchased from Tocris Bioscience [Oakville, ON, Canada]. (+)-MK-801 ((+)-5-methyl-10,11-dihydro-5H-dibenzo [a,d]cyclohepten-5,10-imine maleate salt) was purchased from Sigma-Aldrich [Oakville, ON, Canada].

SHSY-5Y human neuroblastoma cells were obtained from American Type Culture Collection (ATCC). Dulbecco's Modified Eagle Medium: Nutrient Mixture (DMEM:F12) media (supplemented with heat inactivate bovine serum [10%v/v], L-glutamine [1%v/v] and penicillin streptomycin [1%v/v] at 37 C in 5% CO2) were both obtained from Thermo Fisher Scientific [Burlington, ON, Canada]. Resazurin dye solution (In Vitro

Toxicology Assay Kit, Resazurin Based) was obtained from Sigma-Aldrich [Oakvile, ON, Canada]

LMA MAD nasal intranasal mucosal atomization devices were obtained from Equipment Medical Rive Nord (EMRN) [Montreal, QC, Canada], and used in conjunction with a double barrel syringe (L-series) [MEDMIX, Rotkreux, Switzerland].

Male Sprague-Dawley rats were obtained from Charles River (CR) at 250-300 grams in weight [St. Constant, QC, Canada]. Isoflurane was obtained from CDMV, Saint-Hyacinthe, QC, Canada.

Artificial cerebrospinal fluid (aCSF) was prepared by sequentially dissolving the following in 100mL of MQW: 701mg of 120mM NaCl, 36mg of 4.8mM KCl, 16mgof 1.2mM KH2PO4, 30mg of 1.2 mMMgSO4, 37mg of 25mM NaHCO3, 211mg of 2.5mM CaCl2, and 180mg of 10mM D-glucose.

2.4 Methodology

2.4.1 - Aldehyde Functionalization of Starch Nanoparticles (SNP-CHO)

Sodium periodate oxidation was used to introduce dialdehydes on the anhydrous glucose unit (AGU) repeat units of SNPs [29]. 10 g of dry SNPs were dispersed in 400 mL Milli-Q water (MQW) and the pH was adjusted to pH 7. A second solution was then made in which the respective amount of sodium periodate (corresponding to molar equivalents of 0.25 and 0.5 fold of the number of anhydrous glucose units in the SNPs) was dissolved in 100 mL of MQW and subsequently added to the SNP dispersion in a darkened flask in order to minimize radical formation. The mixture was then allowed to react at room temperature for 4h. Following, the reaction was stopped by adding an

equimolar amount of ethylene glycol to quench residual sodium periodate. The reaction was stirred overnight, and the product was dialyzed using a 3.5 kDa MWCO membrane for 6 cycles (6 hours each) against MQW. The product was then lyophilized and stored at room temperature in the dark as a dry powder. The samples were denoted as “SNP-CHO-x”, where x was the molar equivalent of sodium periodate added for the oxidation reaction.

2.4.2 - Hydrogel Characterization

2.4.2.1 - Formation

CMC was dissolved in MQW at 2, 4, or 6 w/v% while SNP-CHOs were dispersed in MQW at 35, 25, or 10 w/v%. For degradation testing, each component was placed into separate barrels of a double barrel syringe (2.5 mL) and a 16 gauge needle was attached to the mixing end of the syringe. The gels were expelled into 400 µL silicone rubber moulds (diameter 6.35 mm) for degradation kinetics measurements. Gelation was allowed to proceed for 16 hours prior to subsequent testing to ensure equilibrium crosslink formation.

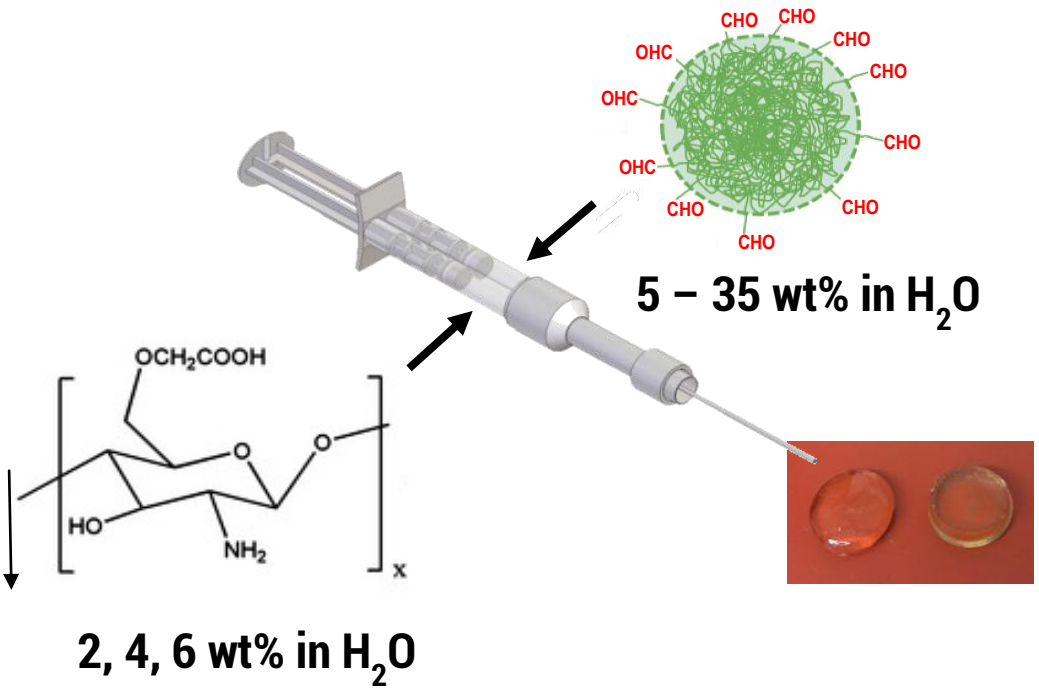

Figure 2-6. Schematic depicting the hydrogel formation process. A double barrel syringe is loaded with CMC and SNP-CHO in separate chambers, and then co-extruded into silicone moulds and removed prior to characterization.

2.4.2.2 - Gelation kinetics

In a 1.5 mL Eppendorf centrifuge tube, 100 µL of both CMC (2-6 wt%) and SNP-CHO (5-35 wt%) were added and regularly inverted whilst agitating by hand during the testing period. The vial was inverted every 2 seconds, with the gelation time (t_{gel}) recorded as the time at which no flow was observed within 1 second after sample inversion. All gel combinations were run in triplicate (n=3).

2.4.2.3 - Swelling and Degradation

Hydrogel disks were fabricated in silicone moulds (4 mm thick, 6.35 mm diameter) using the double barrel syringe delivery strategy described in section 2.4.2.1 and allowed to equilibrate overnight (16 hours) prior to testing. The formed gels were then loaded into pre-weighed transwell inserts to allow for free diffusion of water and immersed fully in 10 mM PBS (0.01 M phosphate buffer, pH 7.4, at 25 °C) using a 6-well plate. At predetermined time intervals (every half hour for the first hour, every hour for the next 4 hours and then twice a day for two weeks), the transwell inserts were removed, excess water was wicked away using a Kimwipe, the sample mass was weighed, and the inserts were returned to the tray. Wells were topped up to 10mL of 10mM PBS solution to keep gels completely submerged in PBS throughout the experiment.

2.4.2.4 - Nebulization

For assessment of spray-based delivery, LMA MAD nasal intranasal mucosal atomization devices (EMRN, Montreal, QC) were attached to the end of the double barrel syringe and sprayed on a vertical sheet of paper from distances of 5, 10 and 15 cm, with the upper limit selected based on the distance between the nostril and the nasopharynx (the posterior of the nasal cavity [30]). Blue and yellow food coloring was used to visualize the spray field, which was subsequently imaged and analyzed (using ImageJ) for total surface area deposition.

2.4.3 - In Vitro Cytotoxicity

SH SY5Y human neuroblastoma cells were cultured in DMEM:F12 media to ~70% confluency. Following trypsin addition and centrifugation, 50 µL of a 200,000 cells/mL cell suspension (corresponding to 10,000 cells/well) were plated in a 96 well plate and incubated for 24 hours. Polymer solutions were prepared in sterile 10 mM PBS, filtered through a 0.2 µm syringe filter (SNP-CHO) or 0.8 µm syringe filter (CMC, accounting for the higher viscosity of this solution), and added to the wells at concentrations between 0.1-10 mg/mL. After 24 hours of incubation, 50 µL of resazurin dye was added to each well. After another 24 hours of incubation, plates were read using an Infinite 200 Pro plate reader using excitation and emission wavelengths of 560nm and 590nm respectively.

2.4.4 - In Vivo Behavioural Testing

Age-matched male Sprague-Dawley rats (250-300 g, Charles River Canada, St. Constant, QC, Canada) received care that complied with protocols approved by the Animal Research Ethics Board at McMaster University and the guidelines of the Canadian Council on Animal Care. Animals were housed individually in standard cages on a reverse 12 h light cycle. Upon arrival, animals were habituated to their holding room for 1 week, followed by a week of handling (touching and petting for 5 minutes each, every other day) prior to any testing. Animals were handled regularly throughout the duration of all experimentation (2-3 times per week) and housed in a room maintained at 22°C with 50% humidity and access to food and water ad libitum.

2.4.5 - Social Interaction Paradigms

Rats were assessed for social interaction with and without MK-801 and drug/formulation administration following published methods. Animals were habituated alone in the social interaction arena, a black polyvinyl open box (100 x 100 x 40 cm) placed on black polyvinyl floor, prior to testing. On the day of testing, two unfamiliar (no prior social interaction) rats were clearly marked with a non-toxic biodegradable paint on their back (allowing clear identification) and were placed in opposite corners of the social interaction arena. A ceiling-mounted video camera was located above the arena to track interactions during a 5 min tracking time (during which the experimenter was absent from the room), with half of the room lights remaining switched on during the testing period (Fig. 2-7). Total time spent in interaction was recorded for each rat and further divided into active interaction (sniffing, following, crawling over/under, grooming, and any aggressive behaviour) or passive interaction (close proximity). Recordings were analyzed by blinded observers, with the interaction times as assessed by each observer averaged. No animal pairing was repeated (i.e. each rat pair represented a novel social interaction), and the arena was thoroughly cleaned with 75% ethanol between each social interaction recording.

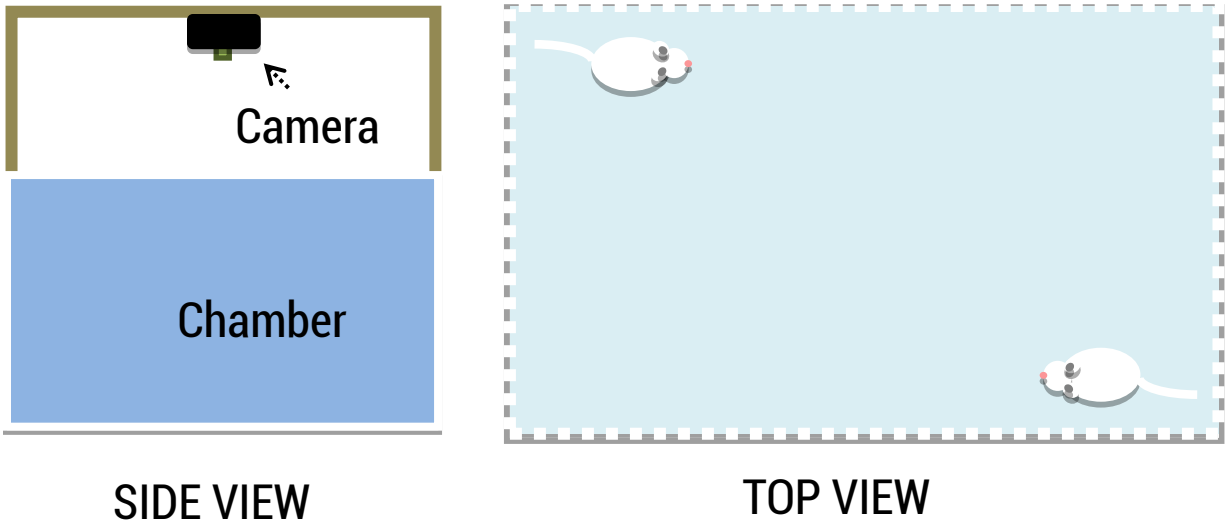

Figure 2-7. Schematic of the social interaction chamber. Side view (left) shows the camera mounting position, top view (right) shows the initial animal placement at the start of the behavioural test.

2.4.6 - Intranasal Administration

The total nasal cavity volume of adult rats is ~250mm^3 [31, 32]. Working under this limit, 120uL is the maximum solution volume that can be administered IN. Animals were anaesthetized using isoflurane, and 30uL of solution was pipetted into each nasal cavity, with a 1 minute break between each pair of nostrils to allow for deposition within the cavity. Animals were placed into recovery chambers for 5 minutes and subsequently tested. For controls, animals received either no solution, aCSF, or free PAOPA. For experimental gel groups, precursor solutions of SNP-CHO and CMC (either with or without PAOPA), were mixed immediately prior to IN administration.

2.4.7 - PAOPA Loading

PAOPA was passively loaded into precursor solutions of SNP-CHO and CMC overnight (16 hours) prior to behavioural testing. As SNPs swell, PAOPA may be physically encapsulated within the interior as water is imbibed into the particles. Upon formation of gels, PAOPA may be either trapped within the SNPs or suspended within the polymer matrix of the hydrogel, allowing for full drug retention within this carrier upon gelation.

2.4.8 - PAOPA Dosage Trials

Due to a lack of existing data, intranasal PAOPA dosage trials were conducted in order to elucidate an appropriate drug concentration prior to hydrogel-loaded release studies. A range of doses (0.1, 0.25, 0.5 and 1mg/kg of PAOPA via IN administration) were tested using the social interaction paradigm.

2.4.9 - PAOPA-Loaded Hydrogel Delivery

All drugs were dissolved in aCSF solution formulated in-lab. PAOPA (with or without hydrogel formulation) was administered at a concentration of 0.5mg/kg intranasally, selected based on the most effective concentrations observed in the PAOPA dosage trials (section 2.4.8). After 30 minutes, MK-801 was administered at 0.3 mg/kg via IP injection (Fig. 2-14). Six experimental groups were tested at different PAOPA and gel concentrations (n=4 per experimental group): A) No drug, no gel, no MK-801 (blank control); B) Drug, no gel, no MK-801 (drug-only control); C) Gels, no drug, no MK-801 (material-only control); D) No drug, no gel, MK-801 (negative behavioural control); E) Drug, no gel, MK-801 (drug-induced symptom alleviation); F) Drug, gel, MK-801 (formulation-induced symptom alleviation). All behavioural tests were conducted 30

minutes following MK-801 administration. Note that the MK-801 model induction lasted a duration of 2 hours, consistent with other reported studies [33].

2.4.10 - In Vivo Biodistribution Assay

To track the transport and residence time of the gel formulation, SNP-CHO were fluorescently tagged (F-SNP-CHO) with AlexaFluor Hydrazide 657 by adding 1 mg of AlexaFluor to 700 mg of SNPs in aCSF and stirring at room temperature for 1 h. Following, sodium cyanoborohydride (2x molar excess to the amount of aldehyde groups) was added to the solution and the flask was allowed to stir overnight to reduce the hydrazone bond. The particles were then dialyzed against MQW (6 x 6 hour cycles, 3.5kkDa MWCO membrane) and lyophilized. Following, F-SNP-CHO were re-dispersed in a 35 wt% dispersion and gelled with 2 or 4 wt% CMC directly within the animal nose using the method described in section 2.4.6. At t = 24hrs (1 day) and t = 72hrs (3 days), the animals were sacrificed and the whole brain (with separate sections of the cerebellum and olfactory bulb), liver, lung, kidney, spleen, and nasal tissue were removed. The tissues were washed using saline and then frozen in an aluminum foil-wrapped container. Following, the tissue samples were homogenized in saline, and the fluorescence of the resulting mixtures was analyzed using an Infinite 200 Pro plate reader (λex = 633 nm, λem = 683 nm). The concentration of F-SNP-CHO in each organ was then estimated based on a standard curve of F-SNP-CHO in saline suspension.

2.5 Statistical Analysis

For behavioural tests, the data was collected and processed using a one-way analysis of variance (ANOVA) with an alpha value of 0.05 along with a Tukey's post-hoc test in order to determine specific groups with statistical differences.

2.6 Results & Discussion

2.6.1 - Characterization of SNP-CHO

Aldehyde functionalization of SNPs was directly adopted from existing techniques within our lab group, with previous confirmation of functionality. Oxidation of the C2/C3 *cis*-diol groups on the anhydrous glucose unit of starch to form two aldehyde groups can be confirmed qualitatively via ATR-FTIR spectroscopy, with an expected aldehyde peak at 1800 cm^{-1}appearing following the oxidation reaction. Transmission electron microscopy confirmed the average size of the SNP-CHO particles as being between 20-40 nm and the shape to be largely spherical, with any observed shape deformation likely attributable to the drying of a soft gel-like nanoparticle in the presence of the hard anti-film forming PMMA latex (visible as the lighter larger particles in the background of the TEM image). Further characterization techniques were not pursued for the purposes of this chapter, as gelation was readily observed when SNPs were cross-linked with CMC. In summary, sodium periodate oxidation can successfully produce aldehyde-functionalized SNPs with controllable aldehyde contents while preserving the small but well-defined nanoparticle morphology of native SNPs hypothesized to be useful for penetration through the nasal epithelium and transport of drug into the brain.

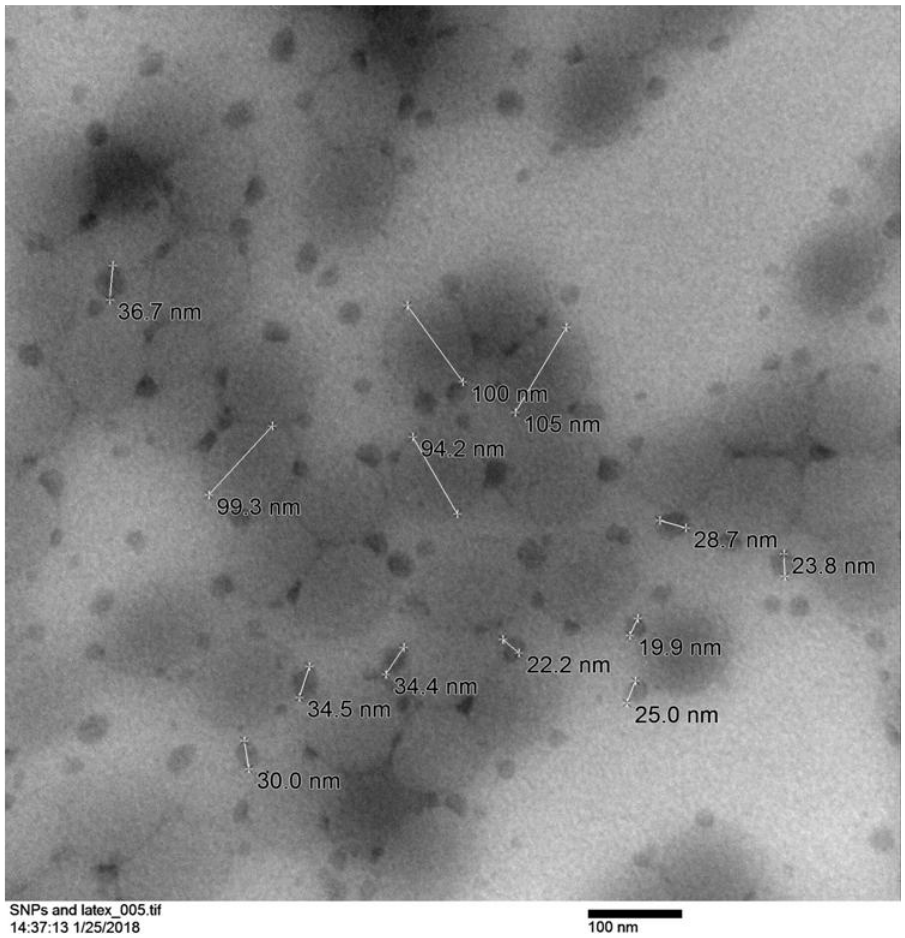

Figure 2-8. Representative transmission electron microscopy image of SNP-CHO-0.25 in the presence of background PMMA nanoparticles used to prevent SNP-CHO film formation during drying (100 nm scale bar).

2.6.2 - Physical Characterization of CMC/SNP-CHO Hydrogels

2.6.2.1 - Gelation Kinetics

The gelation times observed following mixing of various concentrations of O-carboxymethyl chitosan (2-6 wt%, the upper limit corresponding to the highest wt% at which CMC remained an injectable solution) with various concentrations and degrees of oxidation of SNP-CHO are shown in Figure 2-9. Note that the y-axis scales and the SNP concentrations tested for each degree of oxidation of SNP tested are significantly different, corresponding to the different concentrations of SNP required to make gels in each case and the different gelation times that result from those formulations.

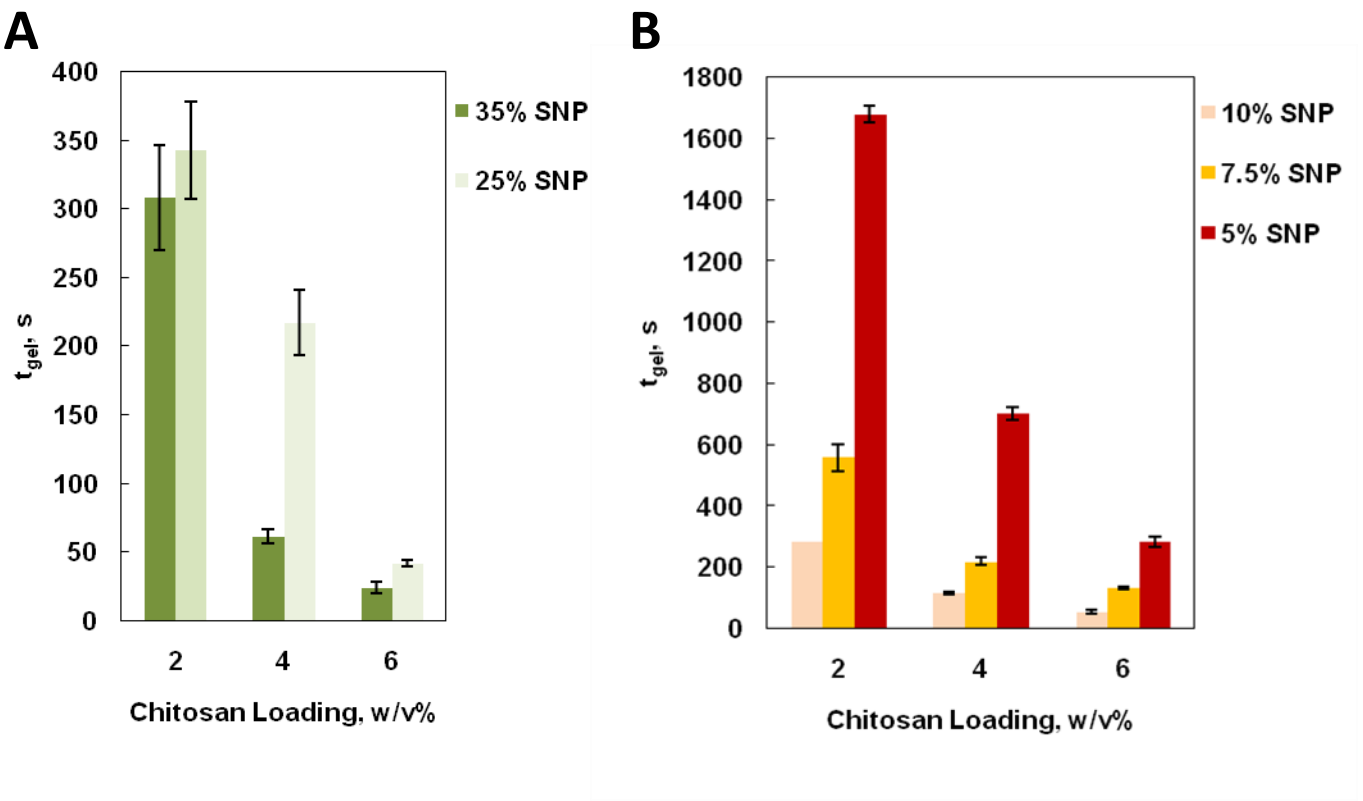

Functionalization	t_{gel} range (s)
0.25 mol	41 - >1800
0.5 mol	54 - 1680

Figure 2-9. Gelation times (via vial inversion) for CMCS/SNP-CHO hydrogels prepared using various CMC and SNP-CHO concentrations: (A) SNP-CHO-0.25-based hydrogels; (B) SNP-CHO-0.50-based hydrogels. Numerical values are provided in the table below the graphs.

As the weight/volume percent (w/v%) of SNP-CHO or CMC increased, gelation time decreased; correspondingly, increasing the functionality of SNP-CHO resulted in decreased gelation times. This result is consistent with the proposed Schiff base-induced crosslinking mechanism, in which the presence of more aldehyde and/or amine groups should result in more crosslinking and thus faster gel formation. Hydrogels prepared with SNP-CHO-0.25 required at least 25 mol% SNPs to fabricate gels, while increasing the degree of oxidation of the SNPs (SNP-CHO-0.50) resulted in gel formation within the <10 minute timeframe for SNP concentrations as low as 5 wt%. Given the practical considerations around performing in situ gelation in the nose, for which gelation times on the order of a few minutes are anticipated to be ideal to enable facile injection/spray but still promote good retention of the gel on the nasal mucosa, formulations based on SNP-CHO-0.25 appear to be most attractive, with the very high potential SNP loading particularly useful from a drug delivery perspective if the SNPs can be used as drug carriers.

2.6.2.2 - Swelling & Degradation

To assess the hydrolytic stability of the resulting labile Schiff base crosslinked hydrogels, the mass of the gels was tracked over time to gravimetrically assess the swelling and ultimate degradation of the hydrogel (Fig. 2-10). Note that the lifetime of the gel in vivo is expected to be somewhat different based on the less fully hydrated conditions in the nasal cavity coupled with the presence of enzymes and esterases in rat mucosa and interstitial fluids; however, the comparisons in Fig. 2-10 provide effective relative comparisons of gel swelling and stability.

Hydrogels with higher CMC contents tended to exhibit substantial swelling upon incubation in PBS, with the 6 wt% CMC/35 wt% SNP-CHO-0.25 hydrogel in particular exhibiting swelling ratios up to 6.5x its original mass prior to the onset of mass loss due to degradation. Lower (ideally near zero) swelling hydrogels would be preferred for nasal administration to ensure a thin film (or a thin array/droplets) is deposited on the nasal mucosa as opposed to a thicker gel layer. Hydrogels were observed to fully degrade between 4 to 6.5 days (100-150 h) in PBS, with hydrogels prepared with lower SNP-CHO and CMC contents showing predictably faster degradation times compared to higher wt% hydrogels.

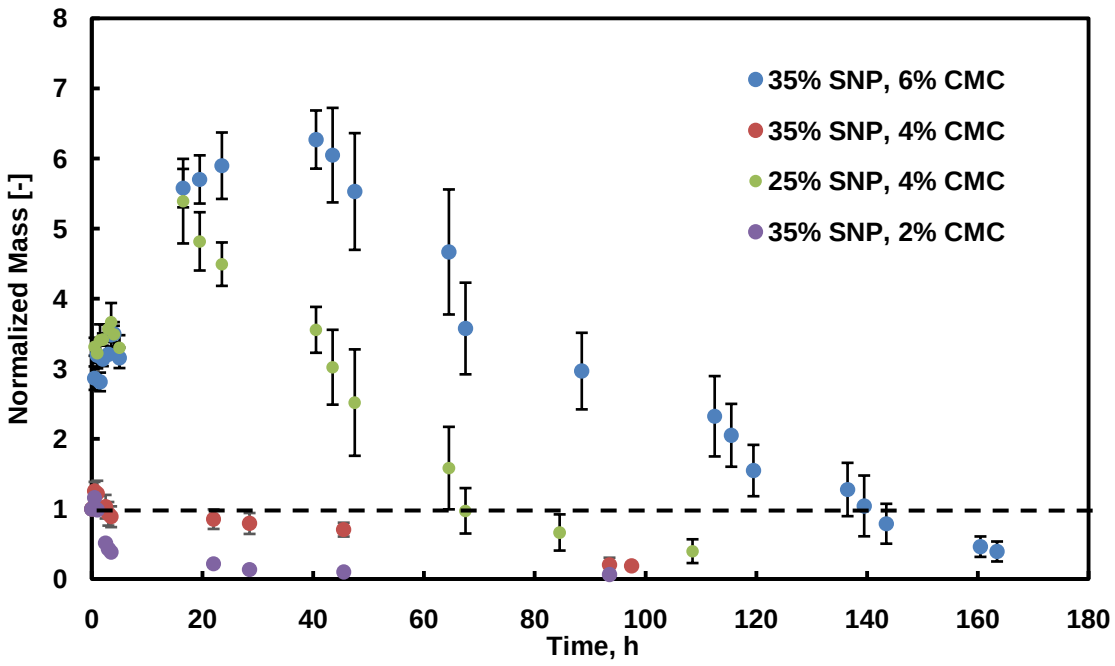

Figure 2-10. Gravimetric in vitro swelling/degradation profiles in 10 mM PBS at 37 ˚C for CMCS/SNP-CHO hydrogels based on SNP-CHO-0.25.

2.6.2.3 - Nebulization/Aerosolization Testing

To confirm the ease of spray-based administration of the selected optimal formulations for intranasal delivery, the potential of the formulations to be nebulized was assessed using a MAD nasal intranasal mucosal atomization device. Figure 2-11 shows the average spray areas achieved as a function of the spray distance to a vertically-mounted paper substrate, with the maximum tested 15 cm distance corresponding to the approximate maximum typical distance between the human nostril and nasopharynx [34].

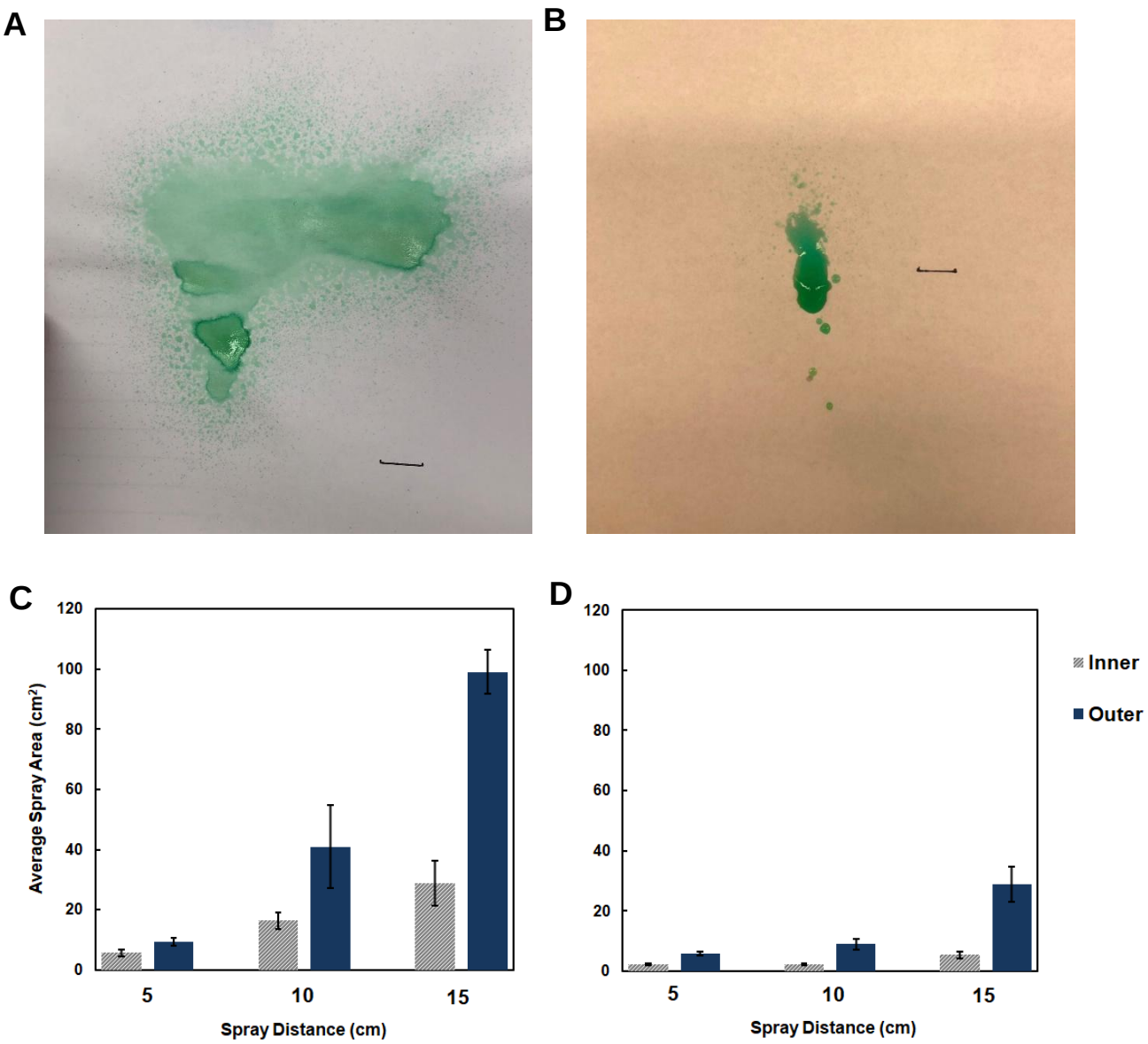

Figure 2-11. Depiction of a spray field of a nebulized hydrogel for (A) 2wt% CMC/35wt% SNO-SNP-0.25 hydrogel at 15cm and (B) 4 wt% CMC/35 wt% SNP-CHO-0.25 hydrogel. CMC was dyed with blue food colouring, SNP-CHO was dyed with yellow food colouring, and both were loaded into a double barrel syringe and co-extruded through an atomizer tip onto a vertically-mounted paper substrate. Average gel spray area (cm^2) was then quantified from the images for (C) 2 wt% CMC/35 wt% SNP-CHO-0.25 and (D) 4 wt% CMC/35 wt% SNP-CHO-0.25 hydrogels. The inner series corresponds to the focused spray area in which most droplets are deposited, while the outer series corresponds to the maximum diameter impacted by the atomization.

In both cases, an inner (thicker) and outer (thinner) layer was observed, with the former representing the focus of the spray and the latter representing the total potentially impacted surface following spray (Fig. 2-11 A, B.). At a distance of 5 cm, both the inner and outer profiles were relatively close, covering 6-10 cm^2; these areas diverged at larger distances, with inner areas of ~30 cm^2 and outer areas of up to ~100 cm^2 observed at a 15 cm spray distance for 2 wt% CMC/35 wt% SNP-CHO-0.25 (Fig. 2-11 C). These areas are consistent with the surface area of the human intranasal cavity (~80-160cm^2) [30, 34, 35], suggesting the potential for effective spray-based delivery of this formulation. The higher viscosity of the 4 wt% CMC/35 wt% SNP-CHO-0.25 formulation resulted in smaller overall spray distances and less uniform nebulization (Fig. 2-11 D), although the formulation could still be delivered via spray-based administration to form a thin film hydrogel over a somewhat smaller surface area.

2.6.3 - In Vitro Cytotoxicity

The cytotoxicity of CMC and various functionalized SNP-CHO gel precursor materials to SH-SY5Y neuroblastoma cells was assessed using a resazurin assay, the results of which are shown in Figure 2-12.

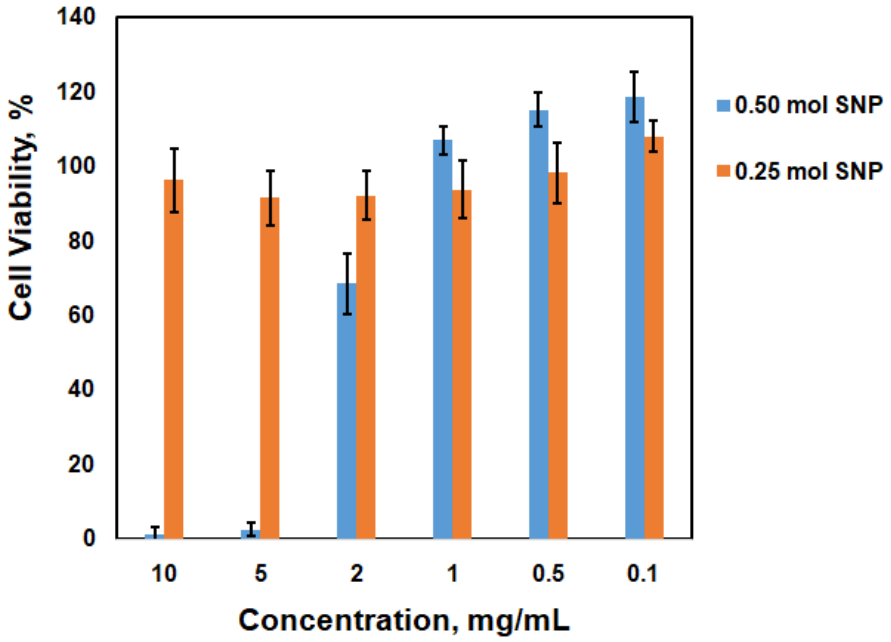

Figure 2-12. Cell viability resazurin assay for SNO-CHO-0.25 (orange) and SNP-CHO-0.50 (blue) with SH-SY5Y neuroblastoma cells.

At higher concentrations of SNP-CHO-0.5 (2, 5 and 10mg/mL), we observe decreased cell viability in comparison to SNP-CHO-0.25, which maintained high viability levels through the entire concentration range tested. This further informed our decision to choose SNP-CHO-0.25 to apply within the in vivo experiments.

2.6.4 - In Vivo Behavioural Studies

2.6.4.1 - PAOPA Dosage Trials

Schizophrenic behaviour was mimicked in Sprague-Dawley rats via IP injection of MK-801, as outlined in section 2.1.4. First, given that there are no previous reports of intranasal delivery of PAOPA, the potential of various IN doses of PAOPA to effectively alleviate MK-801 induced schizophrenic symptoms was first investigated. Animals were dosed with 0.1, 0.25, 0.5, and 1 mg/kg PAOPA via IN administration and tested for total social interaction time, the results of which are shown in Fig. 2-13.

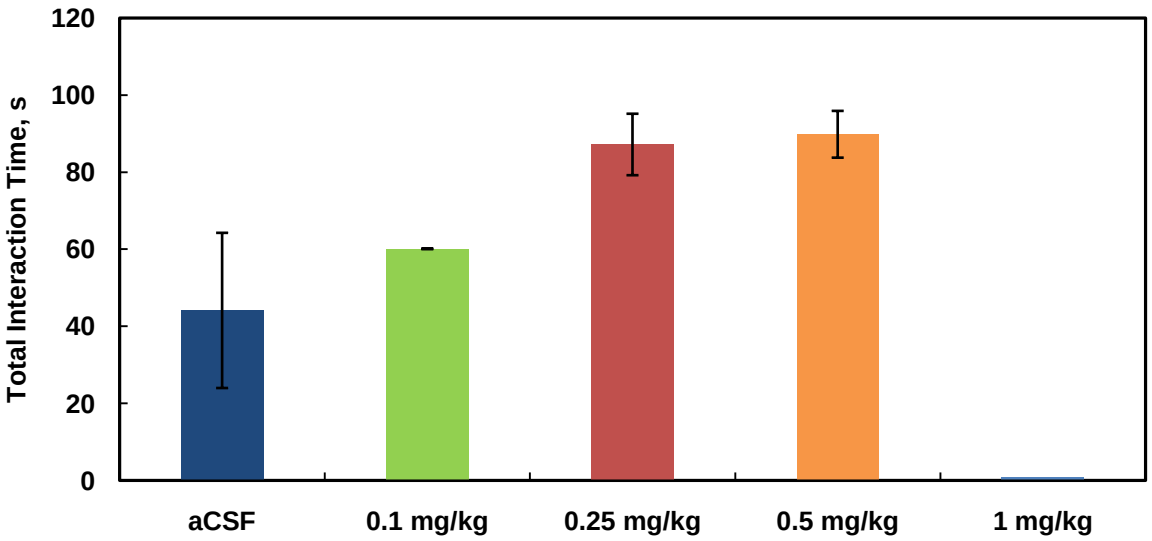

Figure 2-13. Total social interaction time following MK-801 knockdown of rats treated with various IN doses of PAOPA.

Dosing 0.1 mg/kg PAOPA does not significantly increase social interaction time versus the aCSF-only IN administration; yet, substantial increases in social interaction time were achieved with PAOPA doses as low as 0.25 mg/kg. However, further increasing the dose to 1 mg/kg PAOPA (the same concentration administered for efficacy via the

IP route) resulted in a substantial decrease in total interaction time far below the aCSF control. We hypothesize that the higher efficacy of IN versus IP delivery of PAOPA results in PAOPA receptor internalization, which in effect makes the rat function worse and thus leads to zero social interaction amongst the rats. As such, 0.5 mg/kg was used as the base PAOPA loading for the gel formulations.

2.6.4.2 - PAOPA-Loaded 7 Day Study

Changes in total social interaction time for various treatment groups are shown in Figure 2-14. In the absence of MK-801 knockdown (panel A), groups treated via IN of PAOPA only (0.5 mg/kg) or unloaded hydrogel formulations (2wt% CMC/35wt% SNP-CHO-0.25 or 4wt% CMC/35wt% SNP-CHO-0.25) showed neither increased nor decreased total interaction times relative to the negative control rat that received no treatment. The PAOPA result is consistent with the literature, in which delivery of PAOPA at 1 mg/kg via IP did not affect social interaction time [33]. When MK-801 was administered (panel B), injection with aCSF only resulted in significant decreases in total interaction times ($F(5,19) = 38.85$, $p<0.00001$; post hoc, $^{*}p<0.01$).

Administration of PAOPA (0.5 mg/kg) at an acute time point 30 minutes before MK-801 challenge demonstrated the expected attenuation of social interaction deficits when assessed 30 minutes post-MK-801 administration ($F(5,19) = 38.85$, $p<0.00001$; post hoc, $^{**}p<0.05$); however, when groups treated with PAOPA were challenged with MK-801 24 hours later without further drug administration, the benefits of PAOPA were no longer observed ($F(5,19) = 38.85$, $p<0.00001$; post hoc, $^{*}p<0.01$ comparing 1 hr and 24 hr PAOPA-only treatments), indicating rapid clearance of PAOPA and mandating repeated administrations of PAOPA for any observed clinical benefit. In contrast, when

the same 0.5 mg/kg dose of PAOPA was delivered in the 2wt% CMC/35wt% SNP-CHO-0.25 hydrogel (panel C), full symptom alleviation relative to the negative controls (panel A) was observed for as long as 3 days post-administration, with significant decreases in social interaction time not observed until t=120 h (5 days)($F(6,22) = 27.39$, $p<0.00001$; post hoc, $^*p<0.01$). The 4 wt% CMC/35 wt% SNP-CHO-0.25 hydrogel (panel D) also exhibits positive effects relative to the controls but only achieves comparable social interaction times to negative control results at the 24 hour time point, with an apparent induction time at shorter time points and a tailing off of drug efficacy at longer time points($F(6,23) = 35.49$, $p<0.00001$; post hoc, $^*p<0.01$). We speculate that the higher viscosity, and longer degradation time (Fig. 2-11), corresponding to slower release of the SNP-CHO carriers from the hydrogel film) of the 4wt% CMC/35wt% SNP-CHO-0.25 hydrogels all result in slower release of PAOPA, resulting in sub-clinical doses at both shorter release times and longer release times. In addition, the higher viscosity of the 4wt% CMC formulation likely results in more patchy deposition upon injection (consistent with the spray results, Fig. 2-12.A,B), creating larger gel structures that offer both longer diffusional path lengths for PAOPA release and an increased likelihood of being sloughed off of the nasal mucosa. Over the course of 7 days (168 hours), both groups presented social interaction times comparable to the aCSF controls, indicating either full degradation of gels or depletion of PAOPA in the gels to a sub-clinical dose.

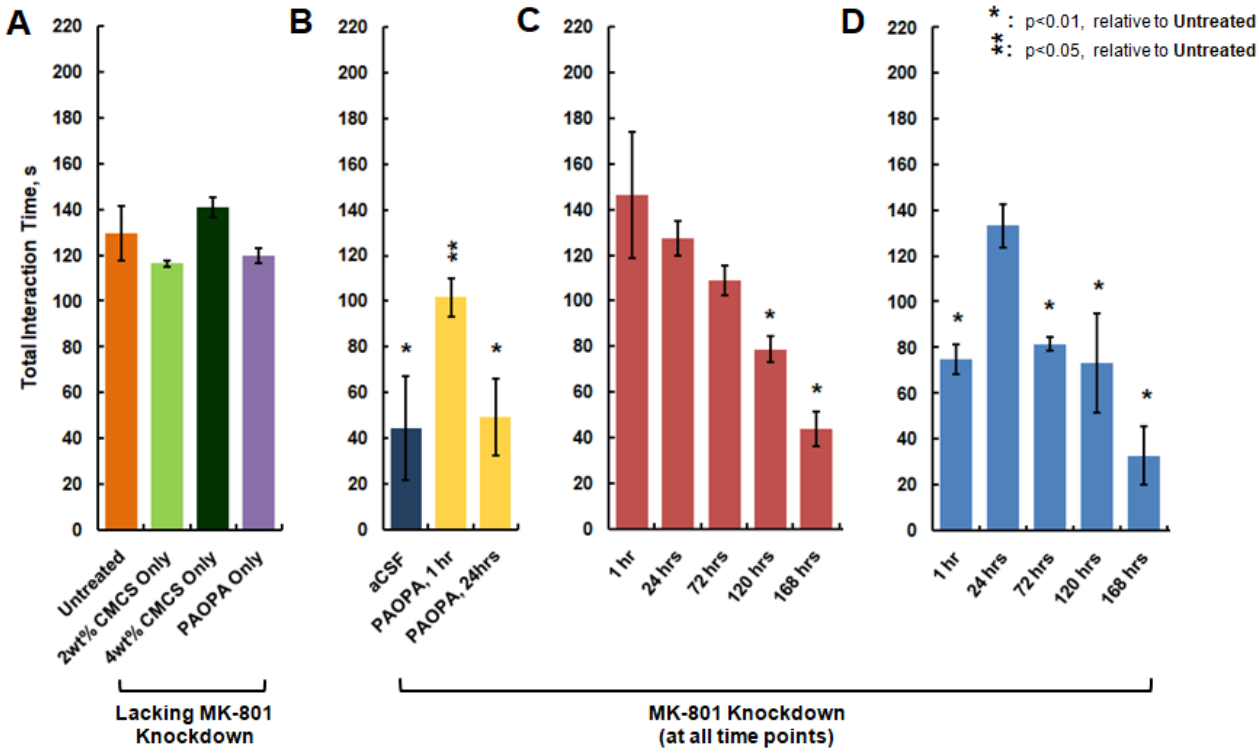

Figure 2-14. Total time spent in social interaction for all control and experimental groups. Groups in panel A did not receive any MK-801 knockdown. Groups in panels B-D received MK-801 at all time points tested. Groups that received PAOPA (free or with gel-carrier) did only so at the 0 hour timepoint. Measurements were taken 1-hour post intranasal administration, with the knockdown model receiving MK-801 30 minutes prior to testing. (A) The light green and dark green bars represent 2 and 4 wt% CMC/35% SNP-CHO-0.25 hydrogels with no loaded PAOPA, demonstrating that the presence of gel in the nasal cavity alone does not lead to a change in social behaviour. Free drug alone (purple, negative control) at 0.5mg/kg also did not alter social behaviour. (B) Administration of MK-801 with aCSF (dark blue, positive control) resulted in a decrease of total social interaction time. The yellow bars represent administration of free PAOPA (0.5 mg/kg) tested at 1 hour and 24 hours later, demonstrating both the efficacy of PAOPA for acute symptom alleviation as well as its fast clearance. (C) 2wt% CMCS/35wt% SNP-CHO-0.25 hydrogel can sustain the effect of PAOPA in preserving social interaction for at least 3 days, with positive effects persisting over 5 days; (D) 4wt% CMCS/35wt% SNP-CHO-0.25 hydrogel can sustain some positive effects of PAOPA for up to 5 days but does not fully achieve the control interaction times and appears to also have an induction time at shorter testing intervals. n=4 for all test groups; statistical comparisons at different confidence intervals are shown by different symbols on the graphs.

2.6.5 - In Vivo Biodistribution Studies

To correlate the observed efficacy in prolonged PAOPA delivery to the brain to the distribution of the SNP-CHO-0.25 nanoparticles hypothesized to be the primary carriers of PAOPA, a biodistribution study was performed by formulating sprayable hydrogels using AlexaFluor 647-labeled SNPs. The accumulation of SNP-derived fluorescence in major clearance organs, the nose, and the brain (separated assayed from within the cerebellum, the olfactory bulb, and the remainder of the brain) at 1 (24h) and 3 (72 h) day observation times post-IN administration is shown in Figure 2-15. Note that the auto-fluorescence of the untreated tissues was subtracted from each of the F-SNP-CHO-0.25 results to ensure the fluorescence is attributable to the nanoparticles present.

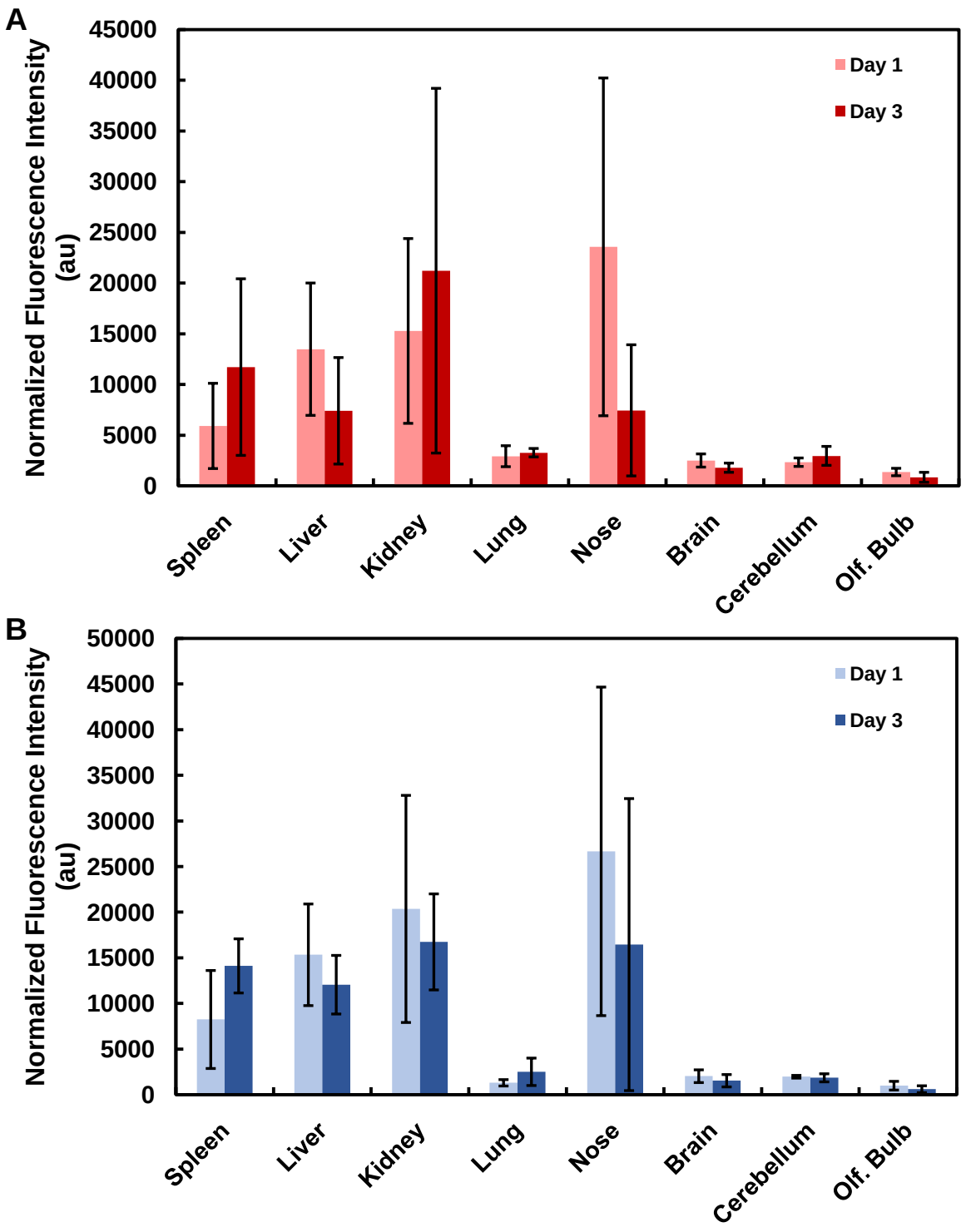

Figure 2-15. Biodistribution of SNP-CHO particles normalized to background fluorescence and tissue-concentration corrected for each organ 1 day (light series) or 3 days (dark series) after IN administration for (A) 2wt% CMCS/35wt% SNP-CHO-0.25 hydrogel and (B) 4wt% CMCS/35wt% SNP-CHO-0.25 hydrogel

On day 1, for both the 2 wt% and 4 wt% CMCS/35 wt% SNP-CHO-0.25 gels, the largest fluorescence intensity was detected in the nose, with significant but lower fluorescence detected in typical nanoparticle clearance organs (e.g. spleen, liver, kidney) and very low fractions present in the lung. This result suggests relatively good retention of the administered formulation in the nasal cavity, accounting for the effective longer-term behavioral benefits observed with the gel delivery vehicles. Note that the larger error bars associated with the nose readings are associated with the very small volume of the nasal cavity collected and thus more animal-to-animal sampling errors in isolating only the nasal cavity tissue, although the nose retention for the slower degrading 4 wt% CMC hydrogels is on average higher (albeit not statistically significantly so) consistent with the slower degradation of this formulation. While fluorescence in the different collected brain regions was lower than that observed in clearance organs, substantial signals related to the presence of the SNPs throughout the brain are still measured that clearly demonstrate transport of SNPs to the brain. On day 3, similar overall patterns in biodistribution were observed, albeit with lower concentrations (although again not statistically significant given the large error bars) in the nose, corresponding similar or slightly lower (but still significant) concentrations in most brain regions, and slightly higher concentrations in clearance organs. Thus, the *in situ* gelling hydrogel is demonstrated to be both effectively retained in the nose over several days and enable the transport of the SNP component at least into the brain, as desired for effective antipsychotic delivery.

2.7 Conclusions

This chapter highlights the development and application of a hydrophilic drug-carrying in situ-bulk gel for the delivery of PAOPA intranasally. Aldehyde functionalization of SNPs did not alter the desirable size and morphology of native SNPs (20-40nm, spherical) that gives them valuable tissue penetration and ultimately drug delivery characteristics [36]. Varying degrees of aldehyde functionalized SNPs (0.25 and 0.5 molar equivalence of oxidation) were synthesized in order to elucidate an ideal functionality for formation of bulk hydrogels which may be delivered intranasally. Bulk hydrogels were formed via imine cross-linking between SNP-CHO and CMC, and further characterized for gelation speed, swelling, and degradation for the purpose of identifying gel parameters that would allow for optimal IN sprayability and mucoadhesion. SNP-CHO-0.25 gels (with varying concentrations of CMC) allowed for higher polymer wt% utilization compared to SNP-CHO-0.5 gels at relevant IN administration gelation times (<5 mins). In vitro cytotoxicity tests revealed greater cell viability with SH-SY5Y neuroblastoma cells at higher polymer concentrations for SNP-CHO-0.25 as opposed to SNP-CHO-0.5. SNP-CHO-0.25 gels further demonstrated relevant degradation profiles (~5 days) for use as an in-nose sustained release vehicle. Nebulization tests for these gels revealed the differing spray profiles exhibited by varying polymer concentrations (2wt% or 4wt% CMC), with sprays under certain conditions achieving total surface areas of ~100cm^2 or greater consistent with the area of the human nasal cavity. The lower concentration 2wt% CMC/35wt% SNP-CHO-0.25 gel had superior performance relative to the substantially more viscous4wt% CMC/35wt% SNP-CHO-0.25 gel in sprayability,

reaching ~100cm^2 in surface area covered at a distance of 15cm from nebulizer to substrate.

Optimal IN dosage administration of PAOPA was examined via a dosage trial wherein a range of PAOPA doses (0.1mg/kg-1mg/kg) were tested using a social interaction paradigm in which animals were induced with social withdrawal symptoms that were alleviated through use of IN administration of PAOPA. Dosages of 0.5mg/kg performed best, while the 1.0mg/kg dosage used for IP injections resulted in zero social interaction due to PAOPA receptor internalization. The 0.5mg/kg PAOPA concentration was subsequently used for a 7 day release study, whereby both 2wt% and 4wt% CMC (with 35wt% SNP-CHO-0.25) PAOPA loaded gels were formed in situ intranasally and studied for symptom alleviation of social withdrawal over time. The 2wt% CMC gels were shown to have better performance, with full symptom alleviation for up to 3 days and general efficacy up to 5 days following a single spray administration. The 4wt% CMC gels demonstrated significant but less substantial symptom alleviation over 5 days, with only the measured alleviation at a 24 hour time point matching the healthy rat controls. Both gels failed to produce symptom alleviation at the final 7 day time point, indicating either intranasal gel clearance or depletion of PAOPA. Nasal tissue and brain penetration were examined through use of fluorescently tagged (F-)SNP-CHO-0.25 particles. A biodistribution assay revealed that F-SNP nasal cavity residence was greater than any other collected tissue 1 day (24 h) post IN gelation, while still maintaining high fluorescence at 3 days (72 h) post gelation for both 2wt% and 4wt% CMC gels. F-SNPs were also located throughout the brain at both time points, confirming the aforementioned ability of the small and soft SNPs to penetrate the brain.

Overall, the results of this study clearly indicate the potential benefits of using a hydrolytically-labile in situ-gelling hydrogel formulation based on nanoparticle building blocks for delivering PAOPA to the brain. We expect that very similar benefits may be observed with any other antipsychotic peptide, given that the same Schiff base interactions could be achieved between any amine-terminated peptide and the SNP-CHO building blocks. In principle, other nanoparticle vehicles could also be physically entrapped inside the gel to enable the delivery of more conventional antipsychotic drugs loaded into more hydrophobic nanocarriers using a similar strategy; co-delivery of precise doses of combination therapies could also be envisioned in the same manner by simply mixing different nanoparticle delivery vehicles and co-entrapping them in the in situ-gelling hydrogel. The components of the delivery vehicle are all carbohydrates with an established record of safe use in vivo [37], while the sprayability of the formulation (Fig. 2-11) also indicates that such delivery vehicles could be administered via existing delivery technologies to patients. The longer-term (sustained) efficacy of these formulations, coupled with the lowered total drug dosage thus required for effective therapy, has great potential to decrease the frequency of APD administration for patients, reducing the likelihood of patient non-compliance with drug formulations, reducing the impact of high drug costs for individuals and communities, and adding immense benefits to patient quality of life.

2.8 References

[1] M. M. Ban, V. R. Chakote, G. N. Dhembre, J. R. Rajguru, and D. A. Joshi, "Situ Gels for Nasal Delivery Ban," *International Journal of Development Research,* vol. 8, no. 2, pp. 18763-18769, 2018.

[2] Y. Chugh, P. Kapoor, and A. K. Kapoor, "Intranasal drug delivery: a novel approach," *Indian J Otolaryngol Head Neck Surg,* vol. 61, no. 2, pp. 90-4, Jun 2009, doi: 10.1007/s12070-009-0044-2.

[3] P. Arora, S. Sharma, and S. Garg, "Permeability issues in nasal drug delivery," *Drug Discovery Today,* vol. 7, no. 18, pp. 967-975, 2002.

[4] N. G. N. Swamya and Z. Abbas, "Mucoadhesive in situ gels as nasal drug delivery systems: An overview," *Asian Journal of Pharmaceutical Sciences* vol. 7, no. 3, pp. 168-180, 2012.

[5] A. Pires, A. Fortuna, G. Gilberto Alves, and F. Amílcar, "Intranasal Drug Delivery: How, Why and What for?," *Journal of Pharmaceutical Sci,* vol. 12, no. 3, pp. 288 - 311, 2009.

[6] J. W. McBain and D. G. Hopkins, "On Adhesives and Adhesive Action," pp. 188-205, 1925.

[7] A. Alexander Amit, S. Sharma Sharad, Ajazuddin, and K. M. Junaid, "Theories and Factors affecting Mucoadhesive Drug Delivery Systems: A Review," *International Journal of Research in Ayurveda and Pharmacy,* vol. 2, no. 4, pp. 1155-1161, 2011.

[8] V. Simpson, "Fundamental studies of adhesion," Department of Materials Engineering, University of Wollongong, 1997.

[9] M. R. Jiménez-castellanos, H. Zia, and C. T. Rhodes, "Mucoadhesive Drug Delivery Systems," *Drug Development and Industrial Pharmacy,* vol. 19, no. 1-2, pp. 143-194, 2008, doi: 10.3109/03639049309038765.

[10] X. Z. Yang and J. R. Robinson, "Bioadhesion in Mucosal Drug Delivery," *Biorelated Polymers and Gels,* 1999.

[11] A. Anitha *et al.*, "Synthesis, characterization, cytotoxicity and antibacterial studies of chitosan, O-carboxymethyl and N,O-carboxymethyl chitosan nanoparticles," *Carbohydrate Polymers,* vol. 78, no. 4, pp. 672-677, 2009, doi: 10.1016/j.carbpol.2009.05.028.

[12] S. Islam, M. A. R. Bhuiyan, and M. N. Islam, "Chitin and Chitosan: Structure, Properties and Applications in Biomedical Engineering," *Journal of Polymers and the Environment,* vol. 25, no. 3, pp. 854-866, 2016, doi: 10.1007/s10924-016-0865-5.

[13] F. S. Kittura, K. V. Harish Prashantha, K. U. Sankarb, and R. N. Tharanathana, "Characterization of chitin, chitosan and their carboxymethyl derivatives by differential scanning calorimetry," *Carbohydrate Polymers* vol. 49, pp. 185-193, 2002.

[14] R. K. Farag and R. R. Mohamed, "Synthesis and characterization of carboxymethyl chitosan nanogels for swelling studies and antimicrobial activity," *Molecules,* vol. 18, no. 1, pp. 190-203, Dec 24 2012, doi: 10.3390/molecules18010190.

[15] S. Chopra, S. Mahdi, J. Kaur, Z. Iqbal, S. Talegaonkar, and F. J. Ahmad, "Advances and potential applications of chitosan derivatives as mucoadhesive biomaterials in modern drug delivery," *J Pharm Pharmacol,* vol. 58, no. 8, pp. 1021-32, Aug 2006, doi: 10.1211/jpp.58.8.0002.

[16] M. R. Saboktakin, R. M. Tabatabaie, A. Maharramov, and M. A. Ramazanov, "Development and in vitro evaluation of thiolated chitosan--Poly(methacrylic acid) nanoparticles as a local mucoadhesive delivery system," *Int J Biol Macromol,* vol. 48, no. 3, pp. 403-7, Apr 1 2011, doi: 10.1016/j.ijbiomac.2010.12.014.

[17] R. S. Khan *et al.*, "Brain Activation by Peptide Pro-Leu-Gly-NH(2) (MIF-1)," *International Journal of Peptides,* vol. 2010, 2010.

[18] E. Bakaic, N. M. Smeets, and T. Hoare, "Injectable hydrogels based on poly(ethylene glycol) and derivatives as functional biomaterials," *RSC Advances,* vol. 5, pp. 35469-35486, 2015.

[19] A. M. Olaru, L. Marin, S. Morariu, G. Pricope, M. Pinteala, and L. Tartau-Mititelu, "Biocompatible chitosan based hydrogels for potential application in local tumour therapy," *Carbohydr Polym,* vol. 179, pp. 59-70, Jan 1 2018, doi: 10.1016/j.carbpol.2017.09.066.

[20] Y. Yang *et al.*, "Tissue-Integratable and Biocompatible Photogelation by the Imine Crosslinking Reaction," *Adv Mater,* vol. 28, no. 14, pp. 2724-30, Apr 13 2016, doi: 10.1002/adma.201505336.

[21] T. R. Hoare and D. S. Kohane, "Hydrogels in drug delivery: Progress and challenges," *Polymer,* vol. 49, no. 8, pp. 1993-2007, 2008, doi: 10.1016/j.polymer.2008.01.027.

[22] N. Boehnke, C. Cam, E. Bat, T. Segura, and H. D. Maynard, "Imine Hydrogels with Tunable Degradability for Tissue Engineering," *Biomacromolecules,* vol. 16, no. 7, pp. 2101-8, Jul 13 2015, doi: 10.1021/acs.biomac.5b00519.

[23] J. C. Neill *et al.*, "Animal models of cognitive dysfunction and negative symptoms of schizophrenia: focus on NMDA receptor antagonism," *Pharmacol Ther,* vol. 128, no. 3, pp. 419-32, Dec 2010, doi: 10.1016/j.pharmthera.2010.07.004.

[24] J. P. Rung, A. Carlsson, K. Ryden Markinhuhta, and M. L. Carlsson, "(+)-MK-801 induced social withdrawal in rats; a model for negative symptoms of schizophrenia," *Prog Neuropsychopharmacol Biol Psychiatry,* vol. 29, no. 5, pp. 827-32, Jun 2005, doi: 10.1016/j.pnpbp.2005.03.004.

[25] Y. T. Kwak, Y. Yang, and H.-r. Jang, "Understanding of Antipsychotics in Elderly Patients with Dementia," *Dementia and Neurocognitive Disorders,* vol. 14, no. 2, 2015, doi: 10.12779/dnd.2015.14.2.53.

[26] R. P. Daya *et al.*, "The Dopamine Allosteric Agent, PAOPA, Demonstrates Therapeutic Potential in the Phencyclidine NMDA Pre-clinical Rat Model of Schizophrenia," *Front Behav Neurosci,* vol. 12, p. 302, 2018, doi: 10.3389/fnbeh.2018.00302.

[27] Z. Rogoz, A. Wasik, and E. Lorenc-Koci, "Combined treatment with aripiprazole and antidepressants reversed some MK-801-induced schizophrenia-like symptoms in mice," *Pharmacol Rep,* vol. 70, no. 4, pp. 623-630, Aug 2018, doi: 10.1016/j.pharep.2018.02.022.

[28] F. Sams-Dodd, "(MK-801 and Phencyclidine Induced Neurotoxicity do Not Cause Enduring Behaviours Resembling the Positive and Negative Symptoms of

Schizophrenia in the Rat," *Basic & Clinical Pharmacology & Toxicology,* vol. 95, pp. 241–246., 2004.

[29] J. Maia, R. A. Carvalho, J. F. J. Coelho, P. N. Simões, and M. H. Gil, "Insight on the periodate oxidation of dextran and its structural vicissitudes," *Polymer,* vol. 52, no. 2, pp. 258-265, 2011, doi: 10.1016/j.polymer.2010.11.058.

[30] J. R. Harkema, S. A. Carey, and J. G. Wagner, "The nose revisited: a brief review of the comparative structure, function, and toxicologic pathology of the nasal epithelium," *Toxicol Pathol,* vol. 34, no. 3, pp. 252-69, 2006, doi: 10.1080/01926230600713475.

[31] E. A. Gross, J. A. Swenberg, S. Fields, and J. A. Popp, "Comparative morphometry of the nasal cavity in rats and mice," *Journal of Anatomy,* vol. 135, no. 1, 1982.

[32] R. D. Alvites, A. R. Caseiro, S. S. Pedrosa, M. E. Branquinho, A. S. P. Varejao, and A. C. Mauricio, "The Nasal Cavity of the Rat and Mouse-Source of Mesenchymal Stem Cells for Treatment of Peripheral Nerve Injury," *Anat Rec (Hoboken),* vol. 301, no. 10, pp. 1678-1689, Oct 2018, doi: 10.1002/ar.23844.

[33] B. Dyck, K. Guest, C. Sookram, D. Basu, R. Johnson, and R. K. Mishra, "PAOPA, a potent analogue of Pro-Leu-glycinamide and allosteric modulator of the dopamine D2 receptor, prevents NMDA receptor antagonist (MK-801)-induced deficits in social interaction in the rat: implications for the treatment of negative symptoms in schizophrenia," *Schizophr Res,* vol. 125, no. 1, pp. 88-92, Jan 2011, doi: 10.1016/j.schres.2010.09.025.

[34] G. K. Reznik, "Comparative Anatomy, Physiology, and Function of the Upper Respiratory Tract," *Environmental Health Perspectives,* vol. 85, pp. 171-176, 1990.

[35] Y. Liu, M. R. Johnson, E. A. Matida, S. Kherani, and J. Marsan, "Creation of a standardized geometry of the human nasal cavity," *J Appl Physiol (1985),* vol. 106, no. 3, pp. 784-95, Mar 2009, doi: 10.1152/japplphysiol.90376.2008.

[36] J. K. Patra *et al.*, "Nano based drug delivery systems: recent developments and future prospects," *J Nanobiotechnology,* vol. 16, no. 1, p. 71, Sep 19 2018, doi: 10.1186/s12951-018-0392-8.

[37] L. Zhang, J. Pan, S. Dong, and Z. Li, "The application of polysaccharide-based nanogels in peptides/proteins and anticancer drugs delivery," *J Drug Target,* vol. 25, no. 8, pp. 673-684, Sep 2017, doi: 10.1080/1061186X.2017.1326123.

3. Fabrication of Emulsion-templated Nanogels for Brain Penetration

3.1 Introduction

3.1.1 - Emulsions

An emulsion can be defined as a mixture of two or more immiscible liquids (usually oil and water), one of which is dispersed as spherical droplets (dispersed phase) in the other (continuous phase) [1]. Typically, emulsions are categorized as either oil-in-water (O/W) or water-in-oil (W/O, or inverse emulsion), with the former more commonly studied and utilized. Emulsions can be further characterized by droplet size range and thermodynamic stability: macroemulsions (1-100 μm, thermodynamically unstable), microemulsions (1-1000nm, thermodynamically stable), and nanoemulsions (1-1000nm, thermodynamically unstable) [2, 3]. The unique properties associated with emulsions provide immense value in a variety of industries including cosmetics (creams, lotions, ointments, topical applicants), agriculture (agrochemical encapsulation), food (ingredient encapsulation, thinners, spreads), and pharmaceutical/biomedical (capsules, drug-delivery platforms) [4-6].

Of particular relevance in the biomedical and pharmaceutical fields are nanoemulsions given their ability to encapsulate an assortment of bio-actives and drugs into materials with sizes appropriate for biological transport and penetration [7]. Nanoemulsions are easily formulated into multiple dosage forms such as gels, creams, liquids and sprays, allowing for simple administration through intravenous, intraperitoneal, oral, or intranasal routes [8]. Their nanosized morphology also provides them with greater surface area and improved particle dispersion when formulated using stabilizing agents compared against macro-sized formulations with larger droplet sizes, a valuable

characteristic in drug delivery [9]. Nanoemulsions have been employed to resolve issues surrounding drug stability (oxidation, enzymatic degradation, hydrolysis in physiological conditions) and solubility, furthering the case for their biomedical application [10].

Multiple methods of emulsion preparation exist, including high pressure homogenization, microfluidization, phase inversion, solvent displacement and membrane emulsification [11, 12]. Both macro and micro emulsions require low-energy inputs for formation, with macroemulsions being visually opaque and microemulsions translucent. Nanoemulsions are also optically translucent but require high-energy input methods for formation, often via mechanical shear (e.g. homogenization, sonication) [3, 13]. To develop and maintain stable emulsions, emulsifiers–also known as surfactants–are incorporated within the mixture. Emulsifiers, amphiphilic molecules that can stabilize oil-water interfaces, reduce the interfacial tension between the two phases to maintain smaller particle sizes than would otherwise be possible [14]. Emulsifier selection, coupled with the relative volumes between the two phases, controls the type of emulsion that is formed (O/W or W/O). According to Bancroft's rule, the liquid in which the stabilizer (emulsifier) has a higher solubility forms the continuous phase [15]. Generally speaking, the selection of an emulsifier which has greater solubility in water (aqueous) phases will result in O/W emulsions while the use of oil (organic) soluble emulsifiers will result in W/O emulsions.

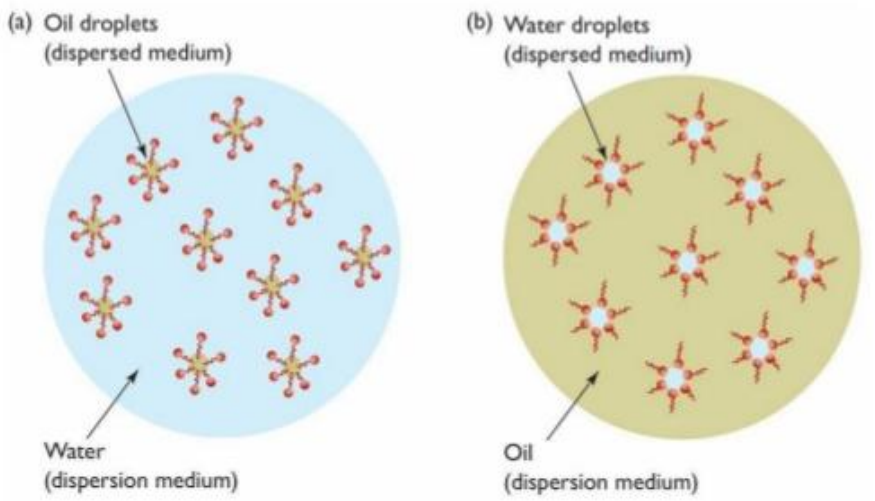

Figure 3-1. Schematic depicting **(A)** O/W emulsions, and **(B)** W/O emulsions. Emulsions are stabilized by surfactants, which are depicted here with hydrophilic heads (circles) and lipophilic tails (lines attached to circles). Adapted from Singhania, (2016).

Surfactant selection is aided by the hydrophobicity lipophilicity balance (HLB) system. The HLB system assesses the expected activity of any given surfactant interacting with a mixture. A numerical value (between 1-50, but usually between 1-20) is associated with surfactants, known as the HLB takes into account the ratio of hydrophilic to hydrophobic moieties in a surfactant [16] (Fig. 3-2). Surfactants with low HLB values are considered lipophilic (W/O emulsifiers, HLB 3-6) while high HLB values indicate more hydrophilic surfactants (O/W emulsifiers, HLB 8-18). Individual organic phases also have associated “required” HLB values for promoting stable emulsion formation; matching the HLB value to the desired emulsion type (O/W or W/O) results in an ideal emulsion environment [17]. A blend of surfactants may be employed to reach a target HLB value, a common practice that can be used to customize the interfacial stability in a given emulsion. To calculate the HLB of a blend of surfactants, the following formula may be used: (%Surfactant A* HLB of Surfactant A) + (%Surfactant B * HLB of

Surfactant B) = HLB of blend. Examples of frequently used surfactants include non-ionic sorbitan fatty acid esters (the Span series of surfactants) and polyxoethylene sorbitan fatty acid esters (the Tween series of surfactants), which when combined together are able to stabilize a range of emulsion types [18]. Span 80 (sorbitan monooleate, HLB = 4.3) in particular is a well-documented emulsifier for creating W/O emulsions with extensive applications in the food, cosmetic and pharmaceutical industry [19]. PGPR (polyglycerol polyricinoleate, HLB = 1.5-2) is another widely used emulsifier with a particularly low HLB value that is capable of providing long term stability for nano-scale emulsions, with a major industrial use as a thinner to reduce viscosity in chocolate products [19-21]. Combinations of these two surfactants have been previously reported to enable stable W/O emulsion formation over a range of different droplet sizes [19, 22].

Table 3-1. The hydrophilic–lipophilic balance (HLB) scale correlated with the emulsions best stabilized by each HLB range, including common surfactants in each category.

Surfactant Solubility	HLB Range	Application	Common Surfactants
No dispersability in water	0-2	W/O stabilizer	Oleic acid, PGPR
Poor dispersability	4-6	W/O emulsifier	Sorbitantristearate (Span 65), Sorbitan monooleate (Span 80)
Milky dispersion, unstable	7-9	Wetting agent	Sorbitan monolaurate (Span 20)
Milky dispersion, stable	8-10	O/W emulsifier	Polyoxyethylenesorbitan monooleate (Tween 81)
Translucent, stable	11-14	O/W emulsifier, detergent	Polyoxyethylenesorbitan Trioleate (Tween 85)
Clear, stable	15-18	Solubilizer	Polyethylene glycol sorbitan monooleate (Tween 80)

Given the kinetic stability of most emulsions, over time the quality of an emulsion typically deteriorates via some combination of aggregation (flocculation, coalescence), phase separation (creaming, sedimentation), phase inversion, or Ostwald ripening (smaller disperse phase globules being absorbed by larger globules) [23, 24]. Most of these phenomena (except for aggregation events) are however specific to the dispersed phase remaining a liquid, such that solidification/gelation of the dispersed phase to create nanoparticles/nanogels can improve the long-term stability of the nanophases produced.

3.1.1.1 - Nanoemulsion Hydrogel Templating

Nanoemulsion templating utilizes the suspended dispersed phase as a template for formation of nanogels. An aqueous “pre-gel” solution can be dispersed in the organic phase of a W/O emulsion (or vice versa) and subsequently undergo a crosslinking reaction to produce a nanogel templated by each emulsified droplet [25]. For the purposes of this project, homogenous cross-linking is pursued such that the entirety of

each nanodroplet forms a gel, a previously documented process [26]. The emulsion formation process may be pursued through traditional (shear-based) methods or through microfluidic and membrane-based techniques. Following emulsification, hydrogel crosslinking has previously been achieved in a variety of ways, with three most commonly reported: thermally-initiated free radical polymerization of unsaturated monomers formation (polymerization of monomers in the presence of crosslinkers to form networks) [27], UV photocrosslinking using a photoinitiator of unsaturated monomers (ultraviolet radiation activation of a photo-initiator, the cross-linker, which attacks the polymer backbone forming a network) [28], and thermal gelation of a thermoresponsive precursor (transition from a polymer precursor solution to a gel upon temperature change, altering polymer solubility resulting in gelation), to name a few. [29]. Nanoemulsion templates allow for simple incorporation of any water-soluble gel building block given the confinement of these entities within the emulsified droplets along with the easily tuneable sizes of the droplets that ultimately template the size of the nanogel. However, the particle size distribution achieved is typically broader than other approaches to nanogel formation (i.e. precipitation). Given that particle size is strongly correlated with biological transport, it is important to develop a process that achieves adequate monodispersity for the targeted biological application.

3.1.2 - Nanoparticle Nasal Tissue Penetration

To re-iterate nanoparticle discussion points from Chapter 1, nanoparticles have superior tissue penetration abilities, greater binding, adsorption and drug loading compared to macro-scale drug delivery platforms [30, 31]. More specifically, nanoparticles in the size range of 50-100nm are effective in BBB penetration from systemic circulation [32] but

suffer from short circulation times [33], thus minimizing contact time between particles and brain tissue and still resulting in relatively poor brain transport. IN delivery of nanoparticles alleviates some of these concerns but suffers from other limitations. Larger particles (~200nm) are more likely adhere to the nasal mucosa following spray-based delivery but are less likely to penetrate and travel through nerve pathways from the nose to the brain [10]. On the other hand, smaller nanoparticles (<50nm) can readily transport through neural pathways across the BBB but have lower inertia and are thus are more likely to be drained down the nasal cavity following spray-based administration. The surface chemistry of nano-based dosages also have a strong effect on this transport, with mucoadhesive surfaces providing great adherence to nasal tissue and thus retention in the nose but decreasing effective transport across nasal epithelium [32]. Ideally, larger particles that could be well-maintained in the nose upon spray but break down into smaller nanoparticles that can then penetrate across the nasal mucosa and transport to the brain would balance these competing effects to develop a more effective IN drug delivery platform.

Size-tunable nanoparticles for drug delivery have been previously reported [34], with different mechanisms demonstrated to achieve the desired tunability of nanoparticles for tissue penetration. Stimuli-responsive clustered nanoparticles for tumour targeting have been reported to breakdown from a 100nm nanocluster (to allow for enhanced blood circulation) to 5nm pro-drug dendrimers (to allow for enhanced tumor penetration) upon reaching the acidic tumour extracellular pH ~6.5-7.2 [35]. Nanoparticles that swell upon pH triggering to release drugs (via the increase in porosity and thus increased diffusion rates)have also been widely reported, with one specific example demonstrating a 10-

fold diameter increase following a pH change from 7.4 to 5 [36]. Other common nanoparticle formulations make use of reversible crosslinks including disulfide bonds that can be easily cleaved (ex. using dithiothreitol or glutathione, which is upregulated in tumour environments [37]), and imine bonds which can be broken down over time via hydrolysis [38].

However, for IN delivery, most existing nanocluster designs are limited by nanoparticle release that is either too rapid (promoting washout) [34] or too slow (limiting therapeutic value), or release particles too large to cross the BBB or too small such that they suffer from rapid target clearance [39]. Development of a nano-carrier that has size switching properties, coupled with appropriate surface chemistry for tunable mucoadhesion, offers potential to address these delivery limitations. Such a formulation would ideally consist of small nanoparticles (<50nm) combined to form a nanocluster (NC) that would be: (1) in the size range of 150-200nm; (2) mucoadhesive to promote immobilization of the formulation to the mucus layer; (3) degradable to allow the release and penetration of nanoparticles across the BBB upon exposure to a local microenvironment; and (4) slow releasing to facilitate extended drug efficacy following a single dose.

3.2 Experimental Objectives

The objective of this project was to address some of the biological limitations associated with intranasal drug delivery via nanoparticle drug carriers. This project builds on the bulk hydrogel hydrophilic drug delivery platform described in chapter 2 to fabricate SNP-CHO/CMC W/O nanoemulsion-templated nanogels, with the ultimate goal of further decreasing drug dose concentrations while increasing sustained release profiles by leveraging the size-tunable nanoparticle advantage. General emulsion strategies, nanoemulsion optimization parameters (precursor/surfactant quantities, concentrations and relevant formulation time points), template-based nanocluster formation (cross-linking within emulsion droplets), and nanocluster degradation profiles are investigated. Nanoclusters are characterized for stability in aqueous and organic phases utilizingdynamic light scattering (DLS), nanoparticle tracking analysis (NTA), and transmission electron microscopy (TEM). We aim to fabricate aqueous suspended SNP-CHO/CMC nanoclusters of size ~200nm that can be well-maintained in the nasal cavity following spray but can degrade and release the highly penetrative SNPs over time.

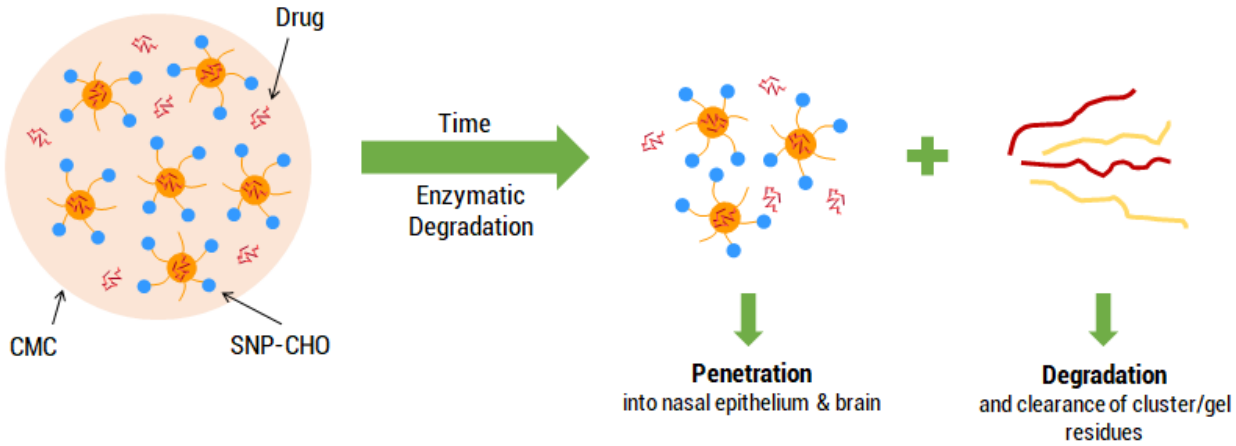

Figure 3-2. Schematic depicting the overarching goal of the project outlined in Chapter 3.

3.3 Materials

Experimental grade starch nanoparticles (SNPs) were supplied by EcoSynthetix Inc. [Burlington, ON, Canada] and used as received. O-carboxymethyl chitosan (CMC) was obtained from Bonding Chemical [Katy, TX, USA] and used as received.

Polyglycerol polyricinoleate (PGPR) 4175 was obtained from Paalsgaard [Morris Plains, NJ, USA] and Span 80 was obtained from MilliporeSigma [Oakville, ON, Canada] and used as received.

Fractionated coconut oil (medium chain triglycerides, MCT) was obtained from Voyage Soap and Candle [Surrey, BC, Canada] and used as received.

Double barrel syringes (L-series) were obtained from MEDMIX [Rotkreux, Switzerland] and used as received.

Sodium periodate ($NaIO_4$), 99% from AK Scientific [California, USA], and diethylene glycol from MilliporeSigma [Oakville, ON, Canada], were used as received.

For all experiments, Millipore Milli-Q grade distilled de-ionized water (MQW, 18.2 MΩ/cm resistivity) was used.

3.4 Metholodology

3.4.1 - Aldehyde Functionalization of Starch Nanoparticles (SNP-CHO)

SNPs were functionalized with aldehyde groups following the same methodology outlined in Chapter 2, section 2.4.1.

3.4.2 - Equipment Setup

To target a W/O emulsion, excess organic (oil) phase was used in conjunction with a small volume of aqueous (water) phase dissolving/suspending all the pre-gel materials. The relative polymer, surfactant, and phase concentrations are outlined in section 3.4.3. Formation of W/O emulsions was pursued through use of mechanical shearing. Initially, the appropriate volumes and concentrations of surfactants were dissolved into the organic phase and mixed for 15 minutes at 300 RPM on a benchtop stirplate. Pre-gel polymers (SNP-CHO and CMC) were dissolved in MQW until complete dissolution (homogenous solution observed). Pre-gel solutions were loaded into individual chambers of a double barrel syringe and capped with a 16 gauge needle at the mixing end. An IKA T25 Digital Ultra Turrax homogenizer tip was submerged ¾ into the organic phase (within a 50mL Falcon Tube), the speed was set to 12,000 RPM, and the double barrel syringe was completely expelled drop-wise over the course of one minute into the organic phase. Following 10minutes of homogenization, the W/O emulsion was immediately placed on an icebath and sonicated at an amplitude of 45 for 2 minutes using a Q700A sonicating probe. The emulsion was left to rest on the bench for 30 minutes prior to characterization to allow for crosslinking within the nanogel phase.

3.4.3 - Emulsion Parameters

Two different organic phases were tested for W/O emulsion formation: chloroform or fractionated coconut oil. Chloroform-based emulsions utilized between 25-30mL of the organic phase, 0.25mL of PGPR, and 0.5mL of both (3 wt%)SNP-CHO-0.50 and (2 wt%)CMC. Fractionated coconut oil-based emulsions utilized between 25-32.5mL of the organic phase, between 0.25-0.5mL of PGPR, 1-2mL of Span 80, and 0.5mL of both(3

wt%)SNP-CHO-0.50 and (2 wt%)CMC. In cases in which ranges of compositions are indicated, these parameters were altered to achieve the targeted size and stability of the nanoclusters.

3.4.4 - Emulsion Templated Nanogel Formation& Kinetics

Pre-gel polymer concentrations were selected by their ability to form a gel within several minutes following the homogenization and sonication steps, thus reducing the potential for emulsion destabilization via creaming, Ostwald ripening, and other destabilization mechanisms specific to liquid dispersions. To identify an appropriate concentration, gelation kinetics measurements were performed as described in Chapter 2, section 2.4.2.2.

3.4.5 - Water Re-suspension Methods

Nanogels prepared using chloroform as the continuous phase were re-suspended in water using a step-wise evaporation technique. Following nanocluster formation, the W/O emulsion was stirred at 400 RPM on a stirplate under steady air flow. When 10mL of chloroform remained, 10mL of water was slowly added over a period of 5 minutes and stirring was continued under air flow to evaporate the remaining chloroform.

Nanogels prepared using fractionated coconut oil as the continuous phase were re-suspended using a vortex-centrifugation technique. Following nanocluster formation, 1mL of the W/O solution was centrifuged at 20,000 RPM for 10 minutes. The oil phase was decanted, and the pellet was re-suspended in 5mL of water using a table top vortex mixer at 5000 rpm for 3 minutes. The resulting solution was filtered with a 0.45um filter to remove residual oil droplets.

3.4.6 - Nanocluster Size Characterization

The mean diameters of both precursor SNPs and nanoclusters were determined using a 90° dynamic light scattering (DLS) system (Brookhaven, Long Island, NY, USA) and single nanoparticle tracking analysis (NTA 3.4) using a LM14 HS NanoSight microscope (Malvern Panalytical, Worcester, UK). Morphological examination of the nanoclusters was performed using a JEOL 1200EX TEMSCAM transmission electron microscope.

3.4.7 - Swelling and Degradation

The swelling and degradation of the nanoclusters was studied via DLS and NTA by tracking the particle size of the nanoclusters over a period of 30 days at room temperature (24°C) or within a shaking incubator at physiologically relevant temperature (37°C).

3.5 Results & Discussion

3.5.1 - Gelation Kinetics

The gelation times observed for different concentration combinations of CMC and SNP-CHO-0.5 are shown in Table 3-2. The combination of 2wt% CMC with 3wt% SNP-CHO-0.5 had a t_{gel}= ~30 minutes; considering the emulsification process lasted ~15 minutes followed by a 30 minute wait time to allow for gelation prior to characterization, a 30 minute gelation time is appropriate to ensure free flowing of the combination prior to emulsification but effective bulk gelation of the droplet prior to removal of the oil template. Increasing the CMC concentration resulted in gelation within ~13 minutes but required working with a much more viscous CMC solution that was harder to emulsify; lower concentrations of either CMC or SNP-CHO-0.5 resulted in excessively long gelation times that would not result in stable nanogel formation.

Table 3-2. Comparison of t_{gel} (s) for different gel formulations.

SNP-CHO-0.5 (wt%)	2wt% CMC	4wt% CMC
3	31 minutes	13.3 minutes
1	> 1hr	42 minutes
0.5	> 1hr	> 1hr

3.5.2 - Emulsion Formation

Chloroform emulsions were initially pursued for ease of organic phase evaporation post-W/O emulsion formation. Generally, the resulting suspensions presented as mildly translucent and were non-viscous. However, these emulsions offered challenges in terms of reproducibility as well as water re-suspension, with poor colloidal stability observed following the replacement of the chloroform continuous phase. Instead, coconut oil (HLB = 4-5) emulsions prepared using a combination of Span 80 (HLB = 4.3) and PGPR (HLB = 1.5-2) as surfactants generated more easily characterized emulsions. The resulting solutions also presented as mildly translucent and non-viscous but were much more readily re-suspended in water.

Figure 3-3. Image of a coconut oil nanoemulsion

3.5.3 - Nanocluster Characterization

3.5.3.1 - Starch Nanoparticles

The hydrodynamic diameter of SNP-CHO-0.5 in MQW was measured in order to provide a baseline size range for comparison against nanocluster formulations. A tri-modal intensity-based distribution with a polydispersity index (PDI) of 0.35 was observed, with peaks at ~40nm, ~100nm and ~350nm. A mean effective diameter of 193 nm ± 2, mean diameter by intensity of 228 nm ± 8 and mean diameter by number of 51 nm ± 28 were recorded. The tri-modal size distribution is likely attributed to aggregation of SNPs in water, as further filtration of samples with a 0.2μm filter produced a similar particle size distribution. (Fig. 3-4)

NTA analysis corroborated DLS size measurements, with a tri-modal concentration-based distribution depicting peaks at ~55 nm, ~100 nm and ~400 nm, with a mean diameter size of 185 nm ± 127.

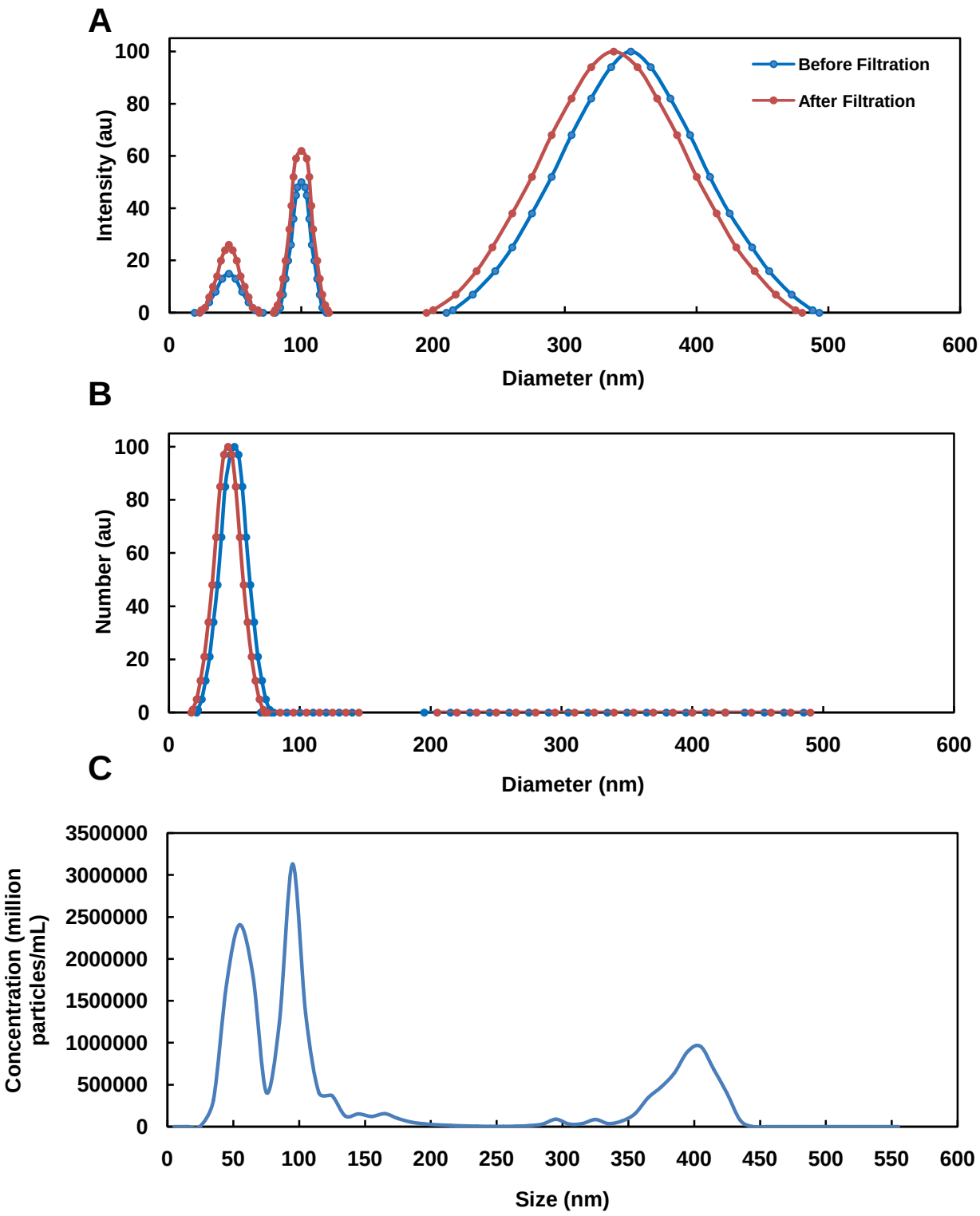

Figure 3-4. Size distribution of SNPs via DLS by intensity before and after filtration (A), by number before and after filtration (assuming refractive index = 1.45) (B) and by concentration via NTA (C).

3.5.3.2 - Organic (oil) Suspended Nanoclusters

As various emulsification parameters were manipulated (section 3.4.3), different size distributions were identified for both chloroform and coconut oil-based nanoclusters in their respective organic phases. Table 3-3 summarizes the size data for the resulting W/O emulsions prepared with different organic phases and surfactant concentrations.Note that only DLS sizing could be pursued for sizing nanoclusters in organic phases, as NTA and TEM techniques require aqueous solutions for accurate measurements.

Table 3-3. Mean diameters of emulsion-templated nanoclusters in both chloroform and fractionated coconut oil with varying volumes of surfactants and organic phases. CH denotes chloroform formulations, and CO denotes coconut oil formulations.

Sample ID	Chloroform Volume (mL)	Coconut Oil Volume (mL)	Span80 Volume (mL)	PGPR Volume (mL)	Effective Diam. (nm)	Mean Diam. By Intensity (nm)	PDI
CH-A	25	0	0	0.25	171± 21	163± 9	0.364
CH-B	30	0	0	0.25	185 ± 37	273± 32	0.381
CO-A	0	32.5	1	0.25	151 ± 8	182 ± 29	0.269
CO-B	0	32.5	2	0.5	173 ± 31	253 ± 47	0.276
CO-C	0	25	2	0.5	172 ± 6	229 ± 43	0.352

For chloroform emulsions with a fixed PGPR volume, increasing organic phase volume resulted in small increases in nanocluster size, although the effects were only observed in the mean diameter by intensity (which heavily weights the aggregate fraction) rather than the effective diameter; as such, this is likely more a reflection of the emulsion stability than significant differences in real particle sizes. For coconut oil emulsions, either increasing Span80 volume or decreasing organic phase volume generated larger

cluster sizes when PGPR volume was held constant. However, optimal emulsions (~150nm) were produced at the lower range of surfactant volumes with a high coconut oil volume.

3.5.2.3 - Aqueous (water) Re-suspended Nanoclusters

Following completion of the water re-suspension methods outlined in section 3.4.5., optimal nanocluster formulations were re-analyzed to assess for any differences in size. Table 3-4 shows the resulting particle size data for nanoclusters re-suspended in water as the continuous phase following organic phase removal. Note that CH-B nanoclusters were not re-suspended in water due to their high dispersity even in the organic phase.

Table 3-4. Mean diameters of selected nanoclusters following water re-suspension from both chloroform and coconut oil.

Sample ID	Effective Diam. (nm)	Mean Diam. By Intensity (nm)	PDI
CH-A	209 ± 9	226 ± 17	0.257
CO-A	183 ± 2	191 ± 5	0.072
CO-B	2895 ± 225	4152 ± 478	0.460
CO-C	265 ± 92	220 ± 34	0.839

Generally speaking, all nanoclusters increased in size once re-suspended in water, an expected phenomenon due to the high water retention ability of SNPs. Out of the four formulations tested, CO-A nanoclusters presented ideal sizes in the desired 150-200nm size range as outlined in section 3.2. CO-B nanoclusters presented data which may be considered an anomaly, as the formulation was prepared only once and suffered contamination resulting in excessively large diameters, while CO-C nanoclusters exceeded the targeted size range, resulting in exclusion of both formulations for further testing. While CH-A nanoclusters gave reasonable particle sizes, they were also no

longer pursed given that the re-suspension step was challenging to accurately reproduce, with very low particle counts often observed in DLS suggestive of particle losses during the re-suspension process. As well, to limit potential future biocompatibility issues, chloroform presents obvious concerns that coconut oil does not. TEM imaging performed on freshly water suspended CO-A nanoclusters (Fig. 3-5 C) confirms that the now aqueous-dispersed nanoclusters exhibited a spherical morphology, had particle sizes in the expected size range of 150-200nm, and maintained reasonably good monodispersity. NTA analysis further confirmed CO-A nanocluster size in the desired range for promoting mucosal adhesion, with a mean size of 184± 50 nm and a mode of 163 nm (Fig. 3-5 B). Furthermore, in comparison to the results obtained for SNPs alone (Fig. 3-4), it is clear that the emulsification/gelation process produced nanoclusters rather than simply regenerated free SNPs given the significantly higher particle sizes and significantly lower polydispersities (Table 3-3) observed with the nanoclusters compared to SNPs alone.

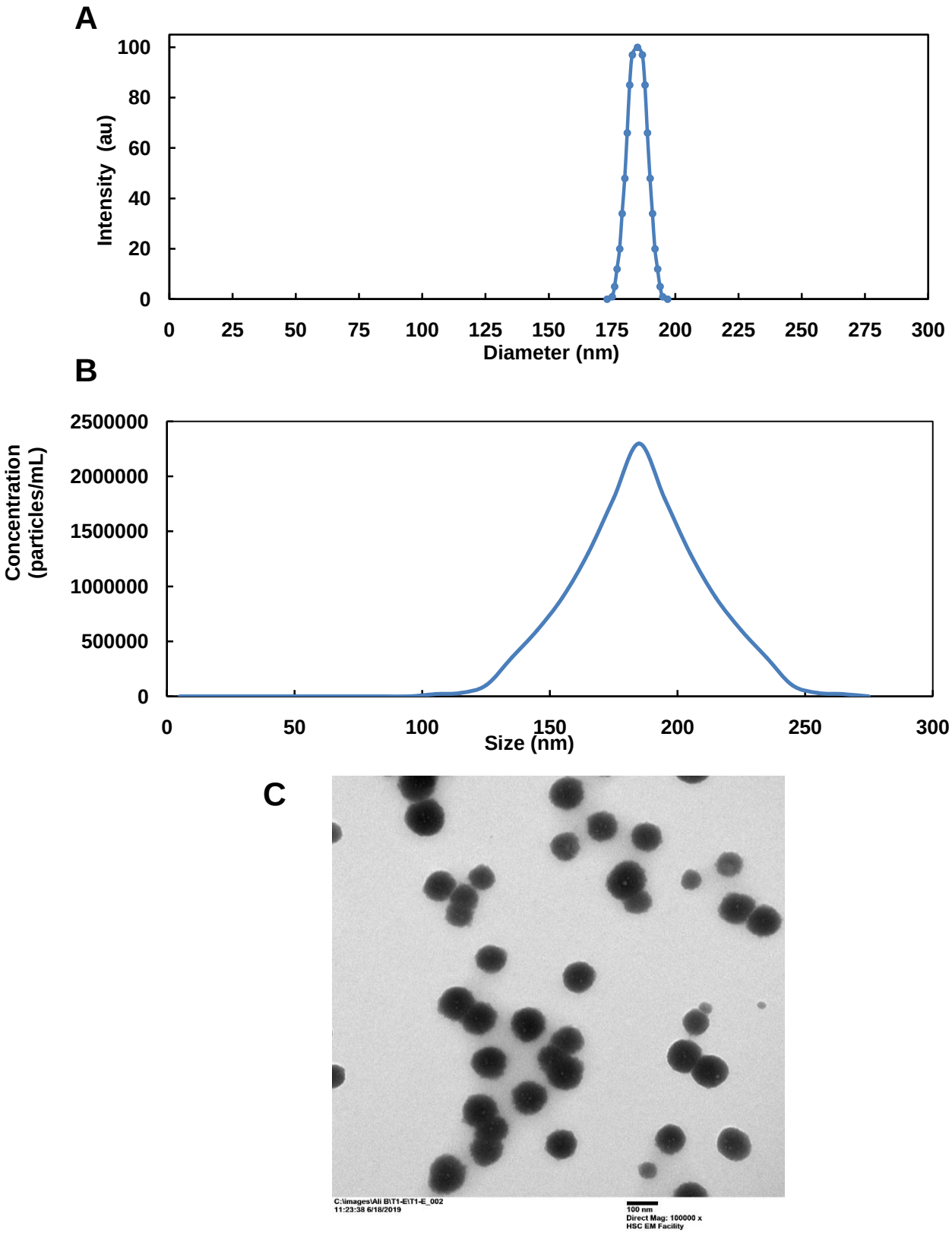

Figure 3-5. CO-A nanogel sizing via (A) intensity by DLS, (B) concentration by NTA and (C) TEM (100nm scale bar)

3.5.2.4 - Stability & Degradation of Nanoclusters

To assess for stability and degradation, CO-A nanocluster size in both coconut oil and water as the continuous phase was tracked via DLS over the course of 30 days at both room temperature (24°C, bench-top) and in physiological conditions (37°C, shaking incubator) (Fig. 3-6). Nanoclusters were observed to maintain their size in coconut oil for up to 30 days, suggesting high stability of the W/O emulsion over storage. At 24°C, water re-suspended nanocluster degradation via imine hydrolysis became apparent at day 4, represented by an overall size increase in the DLS measurement (Fig. 3-6 A, B). As the nanoclusters degrade, a fraction of the released SNPs and CMC begin to form aggregates that dominate the intensity sizing measurements in the resulting heterogenous solution; in turn, larger mean sizes are also accompanied by a greater range of particle sizes consistent with the release of a fraction of small SNPs that remain free, as evidenced by higher error values at the later time points and the broader particle size distributions observed that include a peak at lower sizes not observed in the nanocluster results (Fig. 3-6 A, B, C). Increased degradation was observed at each subsequent time point over the 30 day observation time. Re-suspended nanoclusters at 37°C also exhibited degradation starting at day 4, with an overall larger increase in size over 30 days in contrast to RT degradation and a higher intensity free SNP peak in the DLS data over time (Fig. 3-6 C).

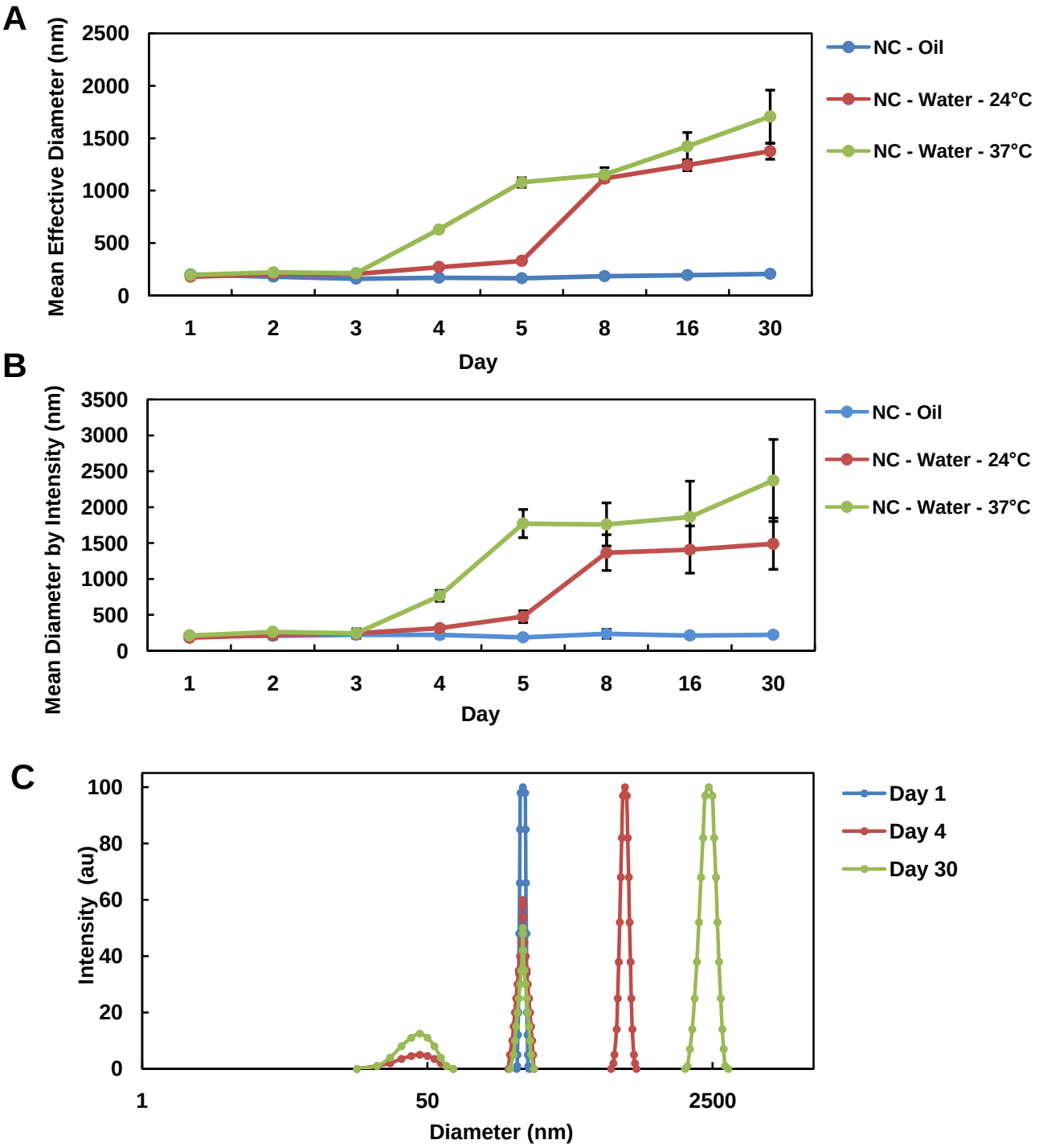

Figure 3-6. **(A)** DLS-based mean effective diameter (nm) and **(B)** DLS-based mean diameter by intensity (nm) of nanoclustersover the course of 30 days to track stability and degradation. (Blue) nanoclusters in coconut oil; (Red) nanoclusters re-suspended in water at room temperature (24°C); (Green) nanoclusters re-suspended in water and incubated at 37°C; **(C)** representative logarithmic intensity-weighted nanocluster particle size distributionsover the 30 day incubation time (37°C)

TEM images of CO-A nanoclusters revealed the morphology of the nanogels over a 10-day study period (Fig. 3-7). On day 1, nanoclusters exhibited the expected spherical shape and 150-200nm size range (Fig. 3-7 A), consistent with the as-prepared images shown in section 3.5.2.3. On day 10, room temperature degraded NCs showed substantially higherpolydispersity, with spherical particles observed between 50-350nm in size (Fig. 3-7 B). The smaller ~50nm particles are consistent with the sizes of free SNPs (Fig. 3-4), which implies degradation of the nanocluster to release free SNPs. It is important to note that nanoclusters in the starting size range of 150-200nm were still observed, indicating lack of complete degradation at day 10 for these formulations; however, the size of the remaining nanoclusters became significantly more irregular and some particle aggregates are observed, consistent with the large sizes measured utilizing DLS. For nanoclusters incubated at 37°C, similar results were observed on day 10 (Fig. 3-7 C), with a polydisperse sample containing a mixture of small (~50nm corresponding to released SNPs), normal (~150nm corresponding to the original NCs), and larger aggregates of particles (likely aggregates of released SNPs, consistent with their formation of aggregates in solution even following filtration in Fig. 3-4).

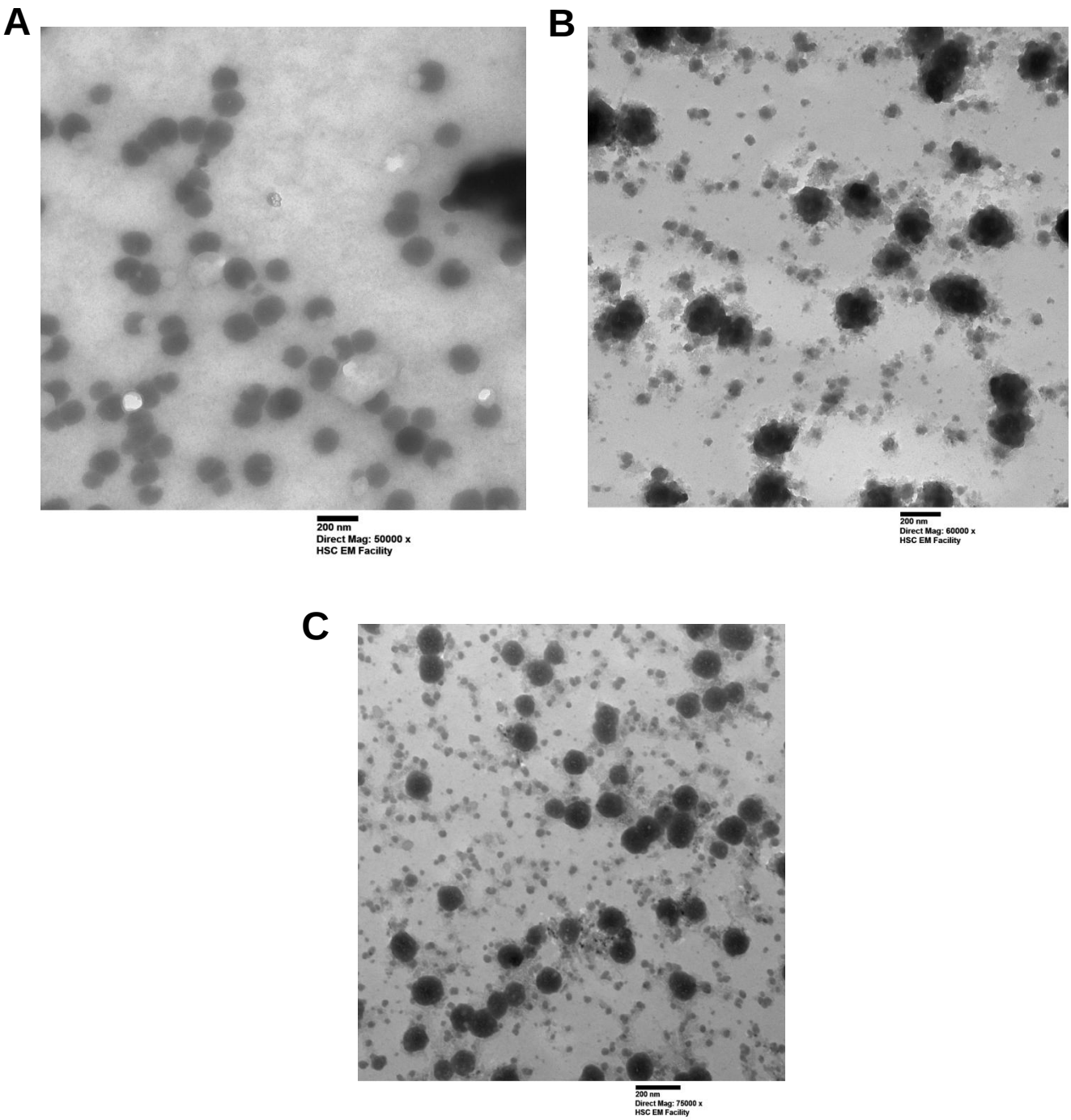

Figure 3-7. Representative transmission electron microscopy images (TEM) of the CO-A nanocluster degradation over time. (A) NCs on day 1 (24°C); (B) NCs on Day 10(24°C); (C) NCs on Day 10 (37°C)

NTA analysis of CO-A nanoclusters over the same degradation times reflected similar overall trends (Fig. 3-8 A). NCs incubated at both 24°C and 37°C experienced nanocluster breakdown on similar timescales, as evidenced by a general mean size increase and an increase in standard deviation over time suggesting growing polydispersity within the system consistent with the TEM results. Representative concentration-weighted particle size distributions show a similar trend (Fig. 3-8 B), whereby a single relatively monodisperse concentration peak at ~170-190nm is observed at day 1 (consistent with the initially prepared nanoclusters, Fig. 3-5) and a multi-modal concentration can be seen on day 10 (Fig. 3-8 B) more consistent with the SNP-only NTA result (Fig. 3-4). Thus, particle size analysis via multiple methods confirms the slow degradation of the nanoparticles and ultimate release of the highly penetrative SNPs over time, as desired for promoting good mucoadhesion (nanocluster) and good mucopenetration (SNPs) of the IN drug delivery vehicle.

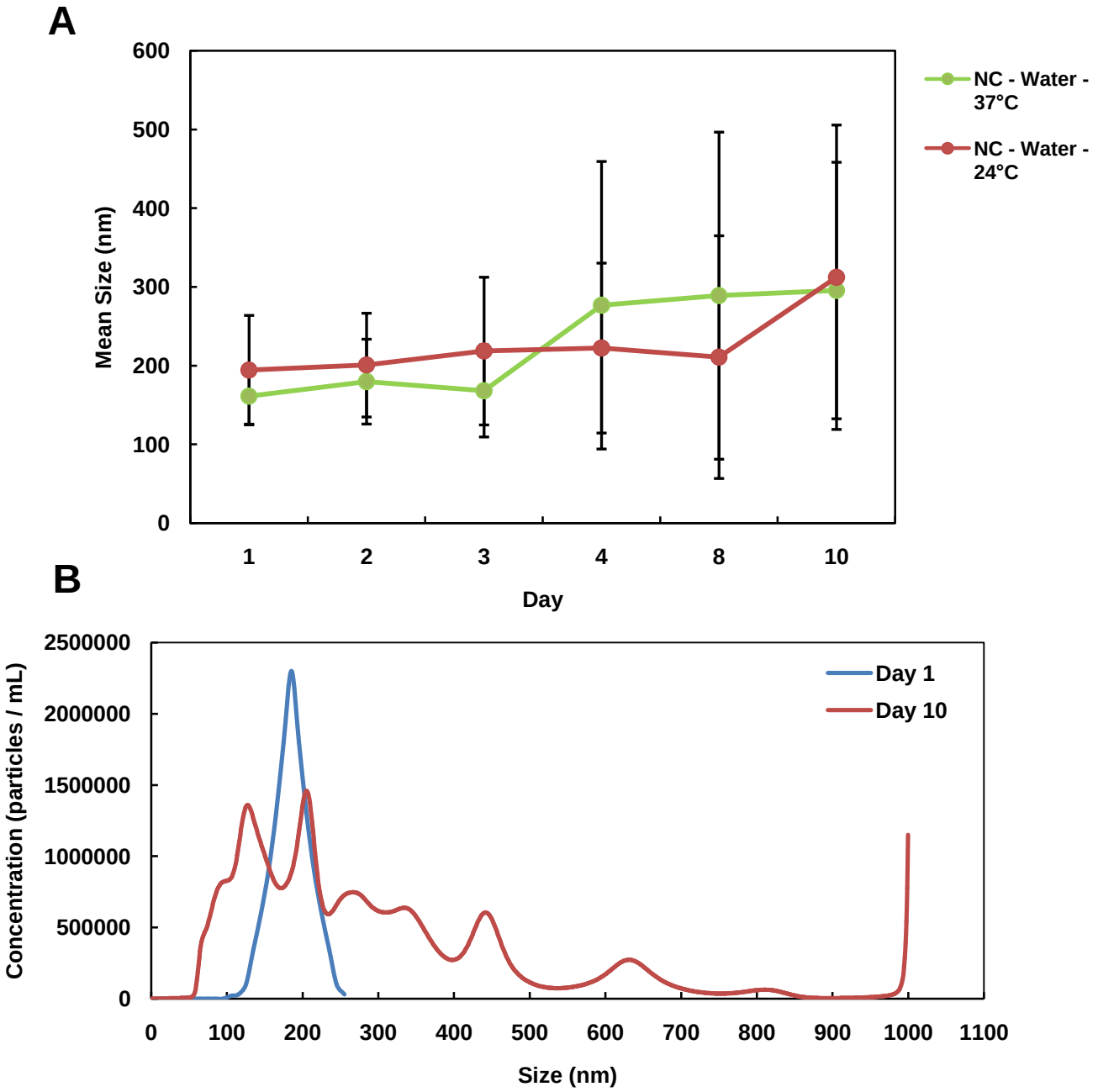

Figure 3-8. (A) Mean particle sizes from NTA analysis of NCs in water at both 24°C (green) and 37°C (red) over the period of 10 days. (B) Representative NTA particle size distributions for CO-A nanoclusters at Day 1 (blue) and Day 10 (red) during incubation at 37°C.

3.6 Conclusions

This chapter highlights the fabrication and stability of nanogel nanoclusters formed via inverse emulsion templating techniques. The primary goals were to create nanocluster gels between 150-200nm (which, based on both size and the CMC contained in the nanocluster, was anticipated to allow for intranasal mucoadhesion and prevention of rapid clearance) that could release of smaller SNPs (50nm) upon degradation to allow for tissue penetration into the brain.

As discussed in chapter 2, aldehyde functionalization of SNPs did not alter the desired size or morphology of the SNPs (50nm, spherical) that is essential to enable suitable tissue penetration and drug delivery characteristics. Two different organic phases were tested for optimal emulsion formation, of which coconut oil performed better than chloroform in terms of reproducibility, stability when transferred to an aqueous continuous phase, and targeted size ranges (~200nm). The use of both Span 80 and PGPR as emulsion stabilizers was found to be appropriate to creating stable nanoemulsion templates to enable *in situ* gelation via imine crosslinking, with the resulting nanoclusters demonstrating organic phase (coconut oil) stability for at least 30 days. This data suggests promise in terms of the long-term shelf storage value of these nanoclusters, which would then require simple re-suspension in aqueous media for drug delivery purposes. Upon re-suspension into water via centrifugation, nanoclusters continued to exhibit targeted sizes and morphology with only slight swelling consistent with the high hygroscopicity of the nanoclusters (as corroborated with DLS, NTA and TEM). Subsequently, nanoclusters were tested for degradation at both room temperature and physiological temperature in order to elucidate potential SNP

dissociation from the nanocluster complex, a major objective. Across all measurement and visualization techniques, clear evidence for nanocluster degradation was observed starting at the day 4 mark at both measured temperatures. DLS revealed nanocluster degradation via an expected increase in size because of SNP aggregation upon release, NTA demonstrated appearance of a multi-modal polydisperse solution consistent with SNP release, and TEM imaging confirmed the presence of free SNPs emerging over time, as desired for the use of SNPs as drug carrying tissue penetrators in the intranasal pathways pursued.

This platform builds on the same in situ-gelling hydrogel formulation described in Chapter 2 but packages the dynamic hydrogel in a nanoscale vehicle that itself offers benefits for IN delivery. The increase in surface area would provide for potentially greater mucosal adherence and avoids concerns about forming a continuous hydrogel in the nose that might impair other nasal/mucosal functions and/or may be more susceptible to sloughing off in the non-consolidated regions. Ease of sprayability is also expected to increase, as water re-suspended nanoclusters exhibit significantly decreased, if any, viscosity when compared to a bulk gel solution. The downside is that, while the nanoclusters are stable over long timescales in oil, practical use of the nanoclusters requires removal of that oil (via a relatively simple centrifugation/washing step) prior to use; this step would impede routine clinical use in a way that the sprayable hydrogels, whose precursor components could be stored in separate solutions in a double barrel syringe over long periods and applied directly to the nose without any further processing, would not. Ultimately, we aim to pursue biological testing of the

nanoclusters to identify what, if any, benefits are accrued via the nanoscale dimensions of the delivery vehicle.

3.7 References

[1] M. Ito, M. Uehara, R. Wakui, M. Shiota, and T. Kuroiwa, "Preparation Characteristics of Water-in-oil Emulsion Using Olive Oil as a Continuous Phase in Microchannel Emulsification," *Japan Journal of Food Engineering,* vol. 18, no. 2, pp. 103-111, 2017, doi: 10.11301/jsfe.17489.

[2] "Emulsions and Emulsification," *Particle Sciences: Drug Development Services,* vol. 9, 2009.

[3] S. N. Kale and S. L. Deore, "Emulsion Micro Emulsion and Nano Emulsion: A Review," *Systematic Reviews in Pharmacy,* vol. 8, no. 1, pp. 39-47, 2016, doi: 10.5530/srp.2017.1.8.

[4] L. Rashidi and K. Khosravi-Darani, "The applications of nanotechnology in food industry," *Crit Rev Food Sci Nutr,* vol. 51, no. 8, pp. 723-30, Sep 2011, doi: 10.1080/10408391003785417.

[5] S. K. I. A. B. F. Gibbs, "Encapsulation in the food industry: a review," *International Journal of Food Sciences and Nutrition,* vol. 50, no. 3, pp. 213-224, 2009, doi: 10.1080/096374899101256.

[6] B. A. Khan *et al.*, "Basics of pharmaceutical emulsions: A review," *African Journal of Pharmacy and Pharmacology,* vol. 5, no. 25, 2011, doi: 10.5897/ajpp11.698.

[7] J. M. Gutiérrez, C. González, A. Maestro, I. Solè, C. M. Pey, and J. Nolla, "Nano-emulsions: New applications and optimization of their preparation," *Current Opinion in Colloid & Interface Science,* vol. 13, no. 4, pp. 245-251, 2008, doi: 10.1016/j.cocis.2008.01.005.

[8] M. C. Bonferoni *et al.*, "Nanoemulsions for "Nose-to-Brain" Drug Delivery," *Pharmaceutics,* vol. 11, no. 2, Feb 17 2019, doi: 10.3390/pharmaceutics11020084.

[9] K. Bouchemal, S. Briancon, E. Perrier, and H. Fessi, "Nano-emulsion formulation using spontaneous emulsification: solvent, oil and surfactant optimisation," *Int J Pharm,* vol. 280, no. 1-2, pp. 241-51, Aug 6 2004, doi: 10.1016/j.ijpharm.2004.05.016.

[10] H. S. Mahajan, M. S. Mahajan, P. P. Nerkar, and A. Agrawal, "Nanoemulsion-based intranasal drug delivery system of saquinavir mesylate for brain targeting," *Drug Deliv,* vol. 21, no. 2, pp. 148-54, Mar 2014, doi: 10.3109/10717544.2013.838014.

[11] C. Lovelyn and A. A. Attama, "Current State of Nanoemulsions in Drug Delivery," *Journal of Biomaterials and Nanobiotechnology,* vol. 02, no. 05, pp. 626-639, 2011, doi: 10.4236/jbnb.2011.225075.

[12] C. Charcosset, I. Limayem, and H. Fessi, "The membrane emulsification process—a review," *Journal of Chemical Technology & Biotechnology,* vol. 79, no. 3, pp. 209-218, 2004, doi: 10.1002/jctb.969.

[13] C. Solans, P. Izquierdo, J. Nolla, N. Azemar, and M. Garciacelma, "Nano-emulsions," *Current Opinion in Colloid & Interface Science,* vol. 10, no. 3-4, pp. 102-110, 2005, doi: 10.1016/j.cocis.2005.06.004.

[14] J. R. Kanicky, J. Lopez-Montilla, S. Pandey, and O. D. Shah, "Surface Chemistry in the Petroleum Industry," *Handbook ofApplied Surface and Colloid Chemistry.,* 2001.

[15] E. Ruckenstein, "Microemulsions, Macroemulsions, and the Bancroft Rule," *Langmuir,* vol. 12, pp. 6351-6353, 1996.

[16] *The HLB system: a guide to time-saving emulsifier selection*. ICI Americas Inc, 1980.

[17] K. Shinoda, "The comparison between the PIT system and the HLB-value system to emulsifier selection," *International Congress of Surface Activity,* vol. 2, no. International Congress of Surface Activity, Barcelona, Spain. Vol 2, 275-283 (1969), pp. 275-283, 1969.

[18] D. G. R. Dongmei Lu, "Mixed Composition Films of Spans and Tween 80 at the Air-Water Interface," *Langmuir,* vol. 16, pp. 107-8112, 2000.

[19] F. Y. Ushikubo and R. L. Cunha, "Stability mechanisms of liquid water-in-oil emulsions," *Food Hydrocolloids,* vol. 34, pp. 145-153, 2014, doi: 10.1016/j.foodhyd.2012.11.016.

[20] M. Tabibiazar and H. Hamishehkar, "Formulation of a Food Grade Water-In-Oil Nanoemulsion: Factors Affecting on Stability," *Pharmaceutical Sciences,* vol. 21, no. 4, pp. 220-224, 2015, doi: 10.15171/ps.2015.40.

[21] J. Bastida-Rodríguez, "The Food Additive Polyglycerol Polyricinoleate (E-476): Structure, Applications, and Production Methods," *ISRN Chemical Engineering,* vol. 2013, pp. 1-21, 2013, doi: 10.1155/2013/124767.

[22] S. Ding *et al.*, "A new method for the formulation of double nanoemulsions," *Soft Matter,* vol. 13, no. 8, pp. 1660-1669, Feb 22 2017, doi: 10.1039/c6sm02603f.

[23] J. H. Yao, K. R. Elder, H. Guo, and M. Grant, "Theory and simulation of Ostwald ripening," *Phys Rev B Condens Matter,* vol. 47, no. 21, pp. 14110-14125, Jun 1 1993, doi: 10.1103/physrevb.47.14110.

[24] S. Kokal, "Crude-Oil Emulsions: A State-Of-The-Art Review," *Society of Petroleum Engineers Productions & Facilities,* 2005.

[25] R. Pelton and T. Hoare, "Microgels and Their Synthesis: An Introduction," *Microgel Suspensions: Fundamentals and Applications,* 2011.

[26] K. Landfester, M. Willert, and M. Antonietti, "Preparation of Polymer Particles in Nonaqueous Direct and Inverse Miniemulsions," *Macromolecules,* vol. 33, no. 7, pp. 2370-2376, 2000.

[27] E. M. Ahmed, "Hydrogel: Preparation, characterization, and applications: A review," *J Adv Res,* vol. 6, no. 2, pp. 105-21, Mar 2015, doi: 10.1016/j.jare.2013.07.006.

[28] P. Marizza *et al.*, "Synthesis and characterization of UV photocrosslinkable hydrogels with poly(N-vinyl-2-pyrrolidone): Determination of the network mesh size distribution," *International Journal of Polymeric Materials and Polymeric Biomaterials,* vol. 65, no. 10, pp. 516-525, 2016, doi: 10.1080/00914037.2015.1129964.

[29] L. Klouda and A. G. Mikos, "Thermoresponsive hydrogels in biomedical applications," *Eur J Pharm Biopharm,* vol. 68, no. 1, pp. 34-45, Jan 2008, doi: 10.1016/j.ejpb.2007.02.025.
[30] W. H. Jong and P. J. Borm, "Drug delivery and nanoparticles: Applications and hazards," *International Journal of Nanomedicine,* vol. 3, no. 2, pp. 133-149, 2008.
[31] J. K. Patra *et al.*, "Nano based drug delivery systems: recent developments and future prospects," *J Nanobiotechnology,* vol. 16, no. 1, p. 71, Sep 19 2018, doi: 10.1186/s12951-018-0392-8.
[32] Y. K. Katare *et al.*, "Intranasal delivery of antipsychotic drugs," *Schizophr Res,* vol. 184, pp. 2-13, Jun 2017, doi: 10.1016/j.schres.2016.11.027.
[33] W. Gao, Y. Zhang, Q. Zhang, and L. Zhang, "Nanoparticle-Hydrogel: A Hybrid Biomaterial System for Localized Drug Delivery," *Ann Biomed Eng,* vol. 44, no. 6, pp. 2049-61, Jun 2016, doi: 10.1007/s10439-016-1583-9.
[34] C. Wong, T. Stylianopoulos, and J. Cui, "Multistage nanoparticle delivery system for deep penetration into tumor tissue," *Proceedings of the National Academy of Sciences,* vol. 108, no. 6, pp. 2426–2431, 2011, doi: 10.1073/pnas.1103909108.
[35] J. Li and D. J. Mooney, "Designing hydrogels for controlled drug delivery," *Nat Rev Mater,* vol. 1, no. 12, Dec 2016, doi: 10.1038/natrevmats.2016.71.
[36] A. H. Colby, Y. L. Colson, and M. W. Grinstaff, "Microscopy and tunable resistive pulse sensing characterization of the swelling of pH-responsive, polymeric expansile nanoparticles," *Nanoscale,* vol. 5, no. 8, pp. 3496-504, Apr 21 2013, doi: 10.1039/c3nr00114h.
[37] I. S. Harris *et al.*, "Glutathione and thioredoxin antioxidant pathways synergize to drive cancer initiation and progression," *Cancer Cell,* vol. 27, no. 2, pp. 211-22, Feb 9 2015, doi: 10.1016/j.ccell.2014.11.019.
[38] J. Zhang, X. Jiang, Y. Zhang, Y. Li, and S. Liu, "Facile Fabrication of Reversible Core Cross-Linked Micelles Possessing Thermosensitive Swellability," *Macromolecules,* vol. 40, pp. 9125-9132, 2007.
[39] G. Hu, X. Chun, Y. Wang, Q. He, and H. Gao, "Peptide mediated active targeting and intelligent particle size reduction-mediated enhanced penetrating of fabricated nanoparticles for triple-negative breast cancer treatment," *Oncotarget,* vol. 6, no. 38, pp. 41258-41274, 2015.

4. Conclusions & Recommendations

This thesis aimed to synthesize and apply starch nanoparticle-carboxymethyl chitosan hydrogels for the IN delivery of therapeutics. In reviewing the main objectives, formulations were successfully fabricated that were easily sprayable, retained in the nasal cavity, demonstrated nanoparticle release over time, and provided sustained drug release for symptom alleviation.

Bulk imine-hydrogel properties were studied in Chapter 2. Gels were fabricated to form rapidly (<5 mins), degrade over the course of one week, and be readily sprayed using commercially-available nasal atomizers. The application of PAOPA-loaded gels through the IN route demonstrated negative symptom relief (via behavioural testing) for up to 3 days (with effects persisting through at least five days) using a 0.5mg/kg drug dose in induced schizophrenic *in vivo* models, half the dose required to achieve efficacy for one day in an intraperitoneal injection. Mucoadhesion and nanoparticle penetration abilities were confirmed through a biodistribution assay of fluorescently labelled SNPs, showing that gels maintained nasal residency while SNPs could be transported into the brain over the same 3 day time points observed via behavioural testing.

Formulation of degradable SNP-CMC nanocluster nanogels was studied in Chapter 3. An inverse nanoemulsion templating strategy was optimized to generate ~150-200nm diameter nanocluster nanogels using the same imine chemistry described in Chapter 2. The nanocluster hydrogels were stable in the organic coconut oil phase for up to 30 days, while nanogels began to degrade in aqueous media by day 4. Utilizing DLS, NTA

and TEM, release of SNPs from the nanoclusters over time was observed, which was consistent with one of the primary goals in fabricating a degradable nanogel that can adhere to the nose but release small and highly penetrative nanoparticles over time when applied in a biological context.

Moving forward, additional studies regarding the IN bulk hydrogel delivery system may elucidate some of the mechanisms at work. The selected PAOPA dosage (0.5mg/kg) was based on a preliminary study in which a range of doses were tested. While it was observed that a 1mg/kg dose resulted in greater negative symptoms than the schizophrenic model alone (MK-801), it is possible that an intermediate dosage (i.e. 0.75mg/kg) may potentially extend symptom alleviation past the 3 day time point currently observed with the 0.5mg/kg dose without re-inducing the negative symptoms. Other behavioural tests may be employed to corroborate the social interaction conclusions, such as the locomotor activity test that looks to study the hyperactivity also commonly associated with schizophrenia and easily modelled using MK-801 [1]. It would also be beneficial to conduct an *in vitro* drug release study using high performance liquid chromatography (HPLC) to assess the release kinetics of PAOPA from the bulk gels and from the released SNPs over time. Additionally, other hydrophilic APDs may also be loaded into these bulk gel formulations for applications in treating different brain disorders. One such example is the use of levodopa (L-DOPA) for treatment of Parkinson's disease, which currently suffers from high gut microbiome degradation through oral routes [2]. The hydrogel platforms developed in this work may allow for similar benefits in L-DOPA delivery i.e. drug dosage reduction and extension of

symptom alleviation following a single dosage. Finally, utilization of the aforementioned nebulizer for the delivery of these gels intranasally should be further explored (ideally in larger mammals) to elucidate how a potentially differing deposition onto the mucosal layer as a function of spraying conditions affects retention and degradation.

Supplementary studies are also required to study the application of the nanocluster nanogels developed in Chapter 3 in the targeted PAOPA delivery application. Although *in vitro* results suggest minimal cytotoxicity with our polymer precursors, it would be important to confirm that the entirety of the nanogel (with the potential for lingering surfactants and/or organic phase) is also cytocompatible. Following this, nanogel drug loading must be explored via passive means (allowing hydrophilic drugs to be entrapped within SNPs as they swell and imbibe water) or active means (using SNP surface chemistry to tether drugs). HPLC should also be employed to reveal drug release profiles from these nanogels *in vitro*. Application of these nanogels *in vivo* may then be accomplished using similar models for the bulk hydrogels, either through pipetting the nanocluster nanogel into the nose or (ideally) using the same nebulizers used in Chapter 2. If developed properly, this nanocluster nanogel system would provide even greater therapeutic relief compared to the bulk gel system because of improved retention due to the increased surface area of the nanoclusters and greater control over drug loading within nanoparticles.

Ultimately, these hydrogel-based intranasal drug delivery platforms offer a unique, tuneable, and functional controlled release system for hydrophilic antipsychotic

medication. Long term, we anticipate this strategy will lower required drug doses and ultimately improve clinical outcomes in treating mental illness.

4.1 References

[1] S. Liljequist, K. Ossowka, M. Graboswki-Anden, and N. Anden, "Effects of NMDA Receptor Antagonist, MK-801, on locomotor activity and on the metabolism of dopamine in various brain areas of mice," *European Journal of Pharmacology,* vol. 195, pp. 55-61, 1991.

[2] S. P. van Kessel *et al.*, "Gut bacterial tyrosine decarboxylases restrict levels of levodopa in the treatment of Parkinson's disease," *Nat Commun,* vol. 10, no. 1, p. 310, Jan 18 2019, doi: 10.1038/s41467-019-08294-y.

5. Appendix

Appendix 1. Raw biodistribution assay results, showcasing fluorescence of different tissues for adult male Sprague-Dawley rats which received F-SNP-CHO

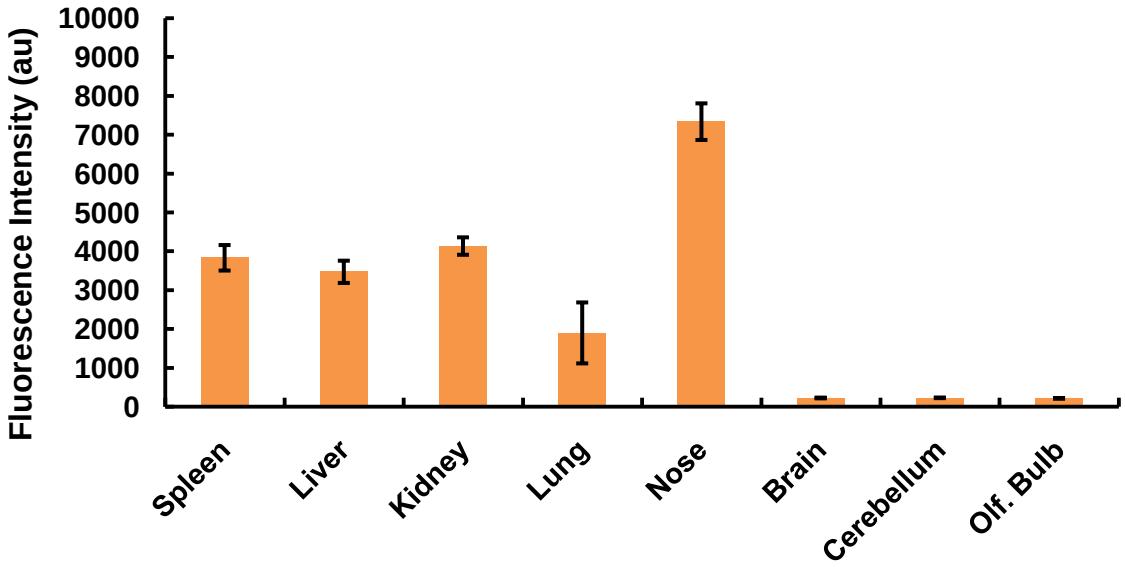

Appendix Figure 1. Fluorescence of untreated background tissue for adult male Sprague-Dawley rats

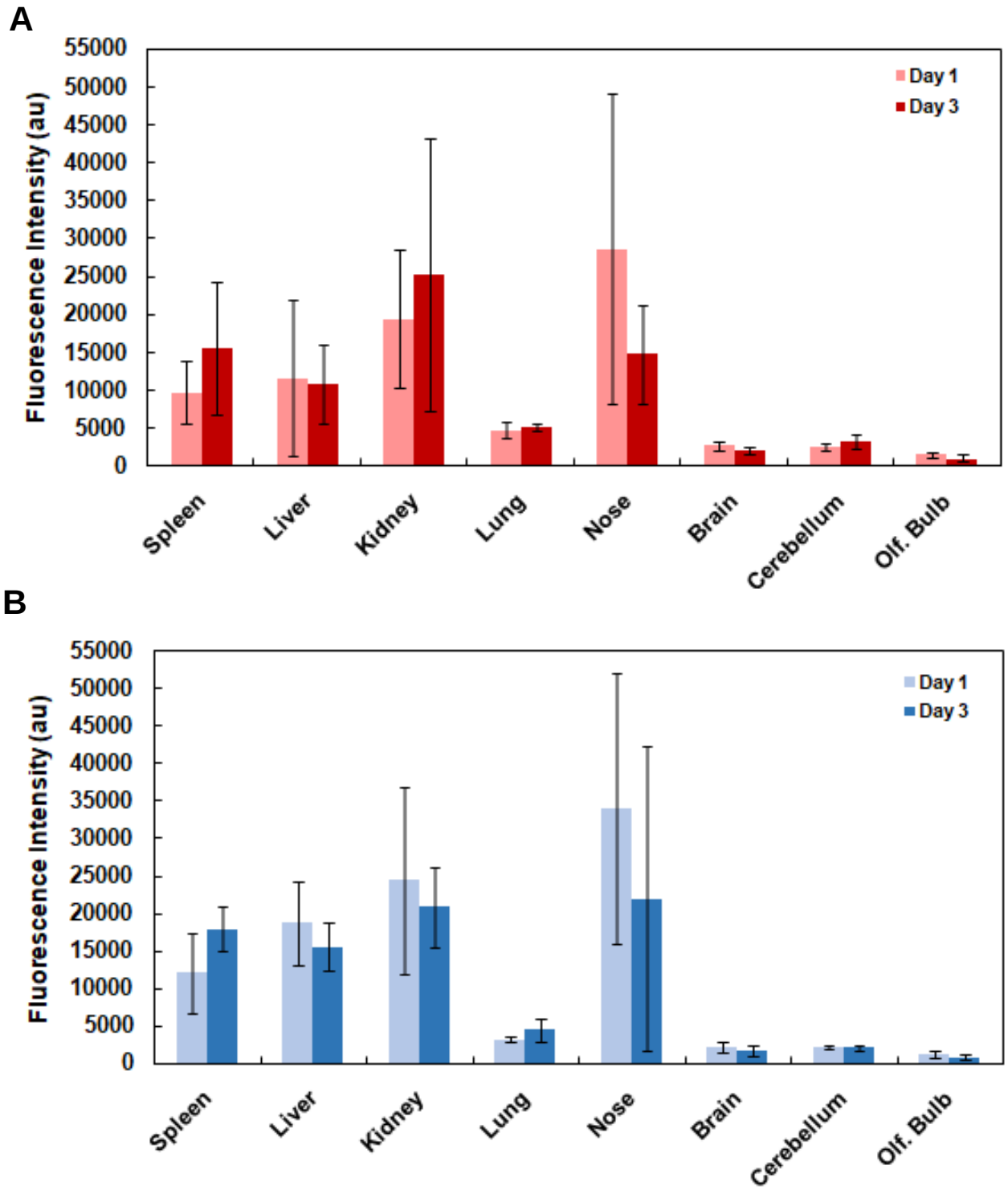

Appendix Figure 2. Biodistribution of SNP-CHO particles fluorescence for each organ 1 day (light series) or 3 days (dark series) after IN administration for (A) 2wt% CMCS/35wt% SNP-CHO-0.25 hydrogel and (B) 4wt% CMCS/35wt% SNP-CHO-0.25 hydrogel.